JIMMA UNIVERSITY
SCHOOL OF POSTGRADUATE STUDIES
JIMMA INSTITUTE OF TECHNOLOGY
SCHOOL OF CIVIL AND ENVIRONMENTAL ENGINEERING
DEPARTMENT HYDRAULICS AND WATER RESOURCES ENGINEERING
MASTERS OF SCIENCE PROGRAM IN HYDRAULIC ENGINEERING

Development of Rainfall Intensity-Duration-Frequency (IDF) Curve under Changing Climate: Case study in Omo-Gibe Basin, Ethiopia

A Thesis Submitted to Graduate Studies of Jimma University in Partial fulfillment of the requirements for the Degree of Master of Science in Hydraulic Engineering

By: Wozader Wolde Kachama

March, 2018

Jimma, Ethiopia

JIMMA UNIVERSITY
SCHOOL OF POSTGRADUATE STUDIES
JIMMA INSTITUTE OF TECHNOLOGY
SCHOOL OF CIVIL AND ENVIRONMENTAL ENGINEERING
DEPARTMENT HYDRAULICS AND WATER RESOURCES ENGINEERING
MASTERS OF SCIENCE PROGRAM IN HYDRAULIC ENGINEERING

Development of Rainfall Intensity-Duration-Frequency (IDF) Curve under Changing Climate: Case study in Omo-Gibe Basin, Ethiopia

A Thesis Submitted to Graduate Studies of Jimma University in Partial fulfillment of the requirements for the Degree of Master of Science in Hydraulic Engineering

By: Wozader Wolde Kachama

Advisor: Fiseha Behulu (Ph.D.)

Co-Advisor: Mamuye Busier (Assistant Prof.)

March, 2018

Jimma, Ethiopia

Declaration

I, the undersigned declared that this thesis is my own original work and that it has not been presented and will not be presented by me to any other university for similar or any degree award. And all sources of materials used for this thesis have been appropriately acknowledged. Any copying and publication of this research for commercial purposes or any financial gain is not allowed without my written permission.

Wozader Wolde Kachama ....
Email: wozwolde@gmail.com *Signature* *Date*

Advisor:

Fiseha Behulu (Ph.D.)  February 26, 2018
Signature *Date*

Co-Advisor:

Mamuye Busier (Assistant Prof.) ....
Signature *Date*

Approval Page

As member of the Board of Examiners of the M.Sc. Thesis Open Defense Examination, we certify that we have read, evaluated the thesis prepared by Wozader Wolde Kachama and examined the candidate. We recommend that the thesis be accepted as fulfilling the requirement for the degree of Master of Science in Hydraulic Engineering

Approved by Board of Examiners

1 Dr. Ing. Kassa Tadele (Ph.D.)	.....	.....
External Examiner	Signature	Date
2 Mr. Tolera Abdisa	.....	.....
Internal Examiner	Signature	Date
3 Mr. Andualem Shigute	.....	.....
Chairperson	Signature	Date

Final approval and acceptance of the thesis is contingent upon the submission of final copy of the thesis to council of Graduate studies (CGS) through the departmental or school graduate committee (DGC or SGC) of the candidate.

Dedication

This Work is dedicated to my beloved family

Abstract

One means of adaptation to climate change is through assessment of rainfall Intensity-Duration-Frequency (IDF) curve developed from historical datasets. However, the representativeness of IDF curves for the future time period remains to be the most challenging issue in view of climate change. IDF curves are commonly developed either at national or basin level in a given watershed. Such curves are not readily available for Omo-Gibe River Basin. Thus, the aim of this research is to evaluate the impact of climate change on rainfall IDF relation in Omo-Gibe River Basin. Long term historic daily rainfall time series data of 34 year (1980-2013) of 18 stations were used as an input. Other geospatial datasets like DEM, land use land cover and soil data were utilized in this study as a proxy inputs. In order to evaluate the climate change impact, the most recent data from Coordinated Regional Climate Downscaling Experiment (CORDEX) data of the fifth Intergovernmental Panel on Climate Change scenarios were used as additional source of data. In order to overcome missing data issues of observation, nearest neighbor (NN) method of interpolation was applied. The completed datasets were further passed through rigorous quality controlling process including data consistency check and outlier tests. The CORDEX data were thoroughly evaluated and appropriate bias correction using power transformation method was undertaken. The bias correction was implemented between historical run of CORDEX data of the same period with observed data. Trend analysis was also carried out for observed data; and future projection was made for a mid-21st century. Extrapolation of values for larger return periods from extracted extreme data were undertaken based on the well fitted empirical distribution function and disaggregation was made to get the required short duration rainfall data. Accordingly, the log Pearson type-III, Gumbel's and Log Normal distributions were applied to all stations. Goodness of fit test using Kolmogorov-Smirnov (K-S), Anderson-Darling (A-D) and Chi-square confirmed the appropriateness of the selected distribution. The spatial distribution of rainfall over the basin is not uniform and varied with topography. According to output from 42 stations, the central western part of the basin received mean annual rainfall as high as up to 2000 mm; whereas, the southern low land region received mean annual rainfall below 675mm. Historical rainfall examination of annual and annual maximum had shown declining trends when averaged over the total basin. However, rainfall projection from 18 stations for (2040-2069) from RCP 2.6, RCP 4.5, RCP 8.5 scenarios has shown insignificant decline with annual mean of (968.9-1675.6); (973.6-1784) and 935.9-

1868.5) mm respectively; while for baseline period (1046.1-1891.2)mm. From comparative evaluation, it is found that projected mean monthly rainfall pattern over the basin doesn't show much difference from the observed data. However, there is a probable expectation for a little bit decrements of rainfall in months of December-March over the majority of the basin. Besides, under changing climate conditions; RCP 2.6 scenario projection shows the difference falls in (40-73) %; and (31-41) % for RCP 4.5 scenario projection, which is moderate except Bonga and Wolaita Sodo stations where the changes is non-significant. Furthermore, RCP 8.5projection scenario has shown a substantial change (21-57) % except a tremendous change as high as up to its double value particularly in south western part of the basin. Therefore, it is a best to consider the changing climate condition during design of infrastructures over the basin than the conventional ways.

Key Words: *Bias correction, Climate Change, IDF Curve, Omo-Gibe River basin, Rainfall*

Acknowledgment

First of all, I would thank my Lord for his usual presence in my way of life. Thank you God for your grace given up on any challenges I have been encountered in my study life.

My special thanks is to my advisor Fiseha Behulu (Ph.D.) for his usual guidance. I appreciate his motivation, encouragement, friendship approach and commitment to make my thesis work to be fruitful. Frankly speaking, I have enjoyed under his supervision. Thank you Dr. anymore and may God bless you. My gratitude also goes to my Co-Advisor Mamuye Busier (M.Sc.) for his motivation and review of my work and valuable comment on my paper.

Next, I would give thanks to National Meteorology Agency (NMA) and Ministry of Water, Irrigation and Electricity (MWIE) for their contribution in giving raw data with free of charge. But, Service in (MWIE) should be highly acknowledged.

Due credit is also given to Aksum university and Ethiopian Road Authority for their financial support during my study leave and sponsoring the program respectively. My appreciation also goes to academic staff of Jimma Institute of Technology and my relatives who take part a role in my stay at Jimma University.

Finally, I would like to extend my deepest appreciations to those who take care of my life includes my family, w/ro Algaynesh W/Mariam with her family in my Jimma life, beloved sister Mariam Datiko and others for their best encouragement and in depth pray to accomplish this study.

Table of Content

List of Tables

List of Figures

Acronyms

amsl	above mean sea level
CDF	Cumulative Distribution Function
CMIP5	Coupled Model Inter-comparison Project Phase 5five
CORDEX	Coordinated Regional Climate Downscaling Experiment
CRGE	Climate Resilient Green Economy
CV	Coefficient of Variation
DEM	Digital Elevation Model
ECDF	Empirical Cumulative Distribution Function
EPCC	Ethiopian Panel on Climate Change
ERA	Ethiopian Road Authority
EV-I	Extreme value Type-I
GCM	General Circulation Model
GEV	Generalized Extreme Value
GHG	Greenhouse Gases
GOF	Goodness of Fit
GTP	Growth and Transformation Plan
HSG	Hydrologic Soils Groups
IDF	Intensity-Duration-Frequency
IPCC	Intergovernmental Panel on Climate Change
ITCZ	Inter-tropical Convergence Zone
MoFED	Ministry of Finance and Economic Development
MoWIE	Ministry of water, irrigation and electricity
NAPA	National Adaptation Program Action in Ethiopia
Net-CDF	Network Common Data Form
NMA	National Meteorology Agency
NN	Nearest neighbor
NRCS	Natural Resources Conservation Service
RCM	Regional Climate Model

RCP	Representative Concentration Pathways
RSCZ	Red Sea Convergence Zone
SCS	Soil Conservation Service
SRES	Special Report on Emissions Scenarios
STJ	Subtropical Jet
TEJ	Tropical Easterly Jet
USAID	United States Agency International Development
WCRP	World Climate Research Program

1 Introduction

1.1 Background

Ethiopia has huge water potential with 12 major river basins contributing a total estimated annual surface flow of approximately 124 billion m^3 and groundwater resources potential estimated about 12-30 billion m^3 of water (MoWR, 2011)). This shows that it has abundant water resources, but they have yet to contribute more than a fraction of their potential to achieving the national economic and social development goals. Because of the uneven distribution of those resources, and the limited financial and technical capacity, Ethiopia has repeatedly suffered from drought and the aridity of much of its lands. Very little has been done to date in harnessing the country's water resources to boost national economic and social development.

In addition to the limitations of infrastructure development, there is emerging challenges due to climate change. Currently, Ethiopia is implementing a Climate Resilient Green Economy (CRGE) initiative with the objective to protect the country from the adverse effects of climate change and to build a green economy (EPCC 2015). Alongside adaptation, the country has committed itself to work on mitigation of climate change (reducing greenhouse gas emissions) as expressed in its climate resilient green economy strategy and the five-year development plan, known as Growth and Transformation Plan (GTP) (MoFED, 2010)

According to Ethiopian Panel on Climate Change (EPCC) report, the nation is making remarkable progress in the development of water recourses infrastructure as a means of building sustainable and climate resilient green economy and as a measure of both adaptation to and mitigation of climate change. It is widely recognized that, in the face of climate change, adaptation (i.e. adjustment in natural or human systems to moderate harm in response to expected change) is a key mechanism for reducing negative impacts of current and future changes (Kiparsky *et al.*, 2012).

At the time of planning of any hydraulic structure, maximum flood intensity that is likely to occur at a given point of interest is an important parameter to be analyzed. Statistical analysis is to be carried out for calculating such maximum flood intensity. Hydraulic structures such as dams are designed and constructed such that they are able to discharge their design flood safely.

This design flood is same as probable maximum flood. This probable maximum flood (PMF) is estimated from probable maximum precipitation (PMP) that may occur in a given region (Jahnvi *et al.*, 2014). The manifestation on of climate change impact on water resources can be felt in several ways. Increased frequency and intensity of rainfall will produce increased soil erosion and sedimentation. Flooding will damage infrastructure, cause loss of lives and property as well as affect water quality as large volume of water polluted with contaminants is transported to water bodies (EPCC, 2015).

Information on quintiles of extreme rainfall of various durations is needed in the hydraulic design of structures that control storm runoff, such as flood detention reservoirs, sewer systems etc. Such information in engineering hydrology usually expressed as a relationship between intensity-duration-frequency (IDF) of extreme rainfall. The establishment of such relationships goes back to the 1930s (Bernard, 1932). Since then, different forms of relationships have been constructed for several regions of the world

Increased industrial activity during the last century and a half has increased concentration of carbon dioxide in Earth's atmosphere. This has in turn initiated large scale atmospheric processes resulting in change of global temperature and precipitation (among other variables). Changes in Earth's climate system can disrupt the delicate balance of the hydrologic cycle and can eventually lead to increased occurrence of extreme events (such as floods, droughts, heat waves, summer and ice storms, etc.). For municipalities, changed frequency of extreme events (such as intense rainfall, heavy winds and/or ice storms) are of particular importance as adequate procedures, plans and management strategies must be put in place to deal with them (Mehdi *et al.*, 2006).

Many scientific research conducted on climate change impact including (IPCC) report indicated that there is a change in future meteorological parameters (maximum temperature minimum temperature and precipitation) in different time horizon. One way of reducing vulnerability to adverse impacts of climate change is to anticipate their possible effects, and adapt; the other is to actually reduce the rate of carbon dioxide released into the atmosphere. Reducing climate change vulnerability means that decision makers and stakeholders need to understand its effects, and develop suitable measures to deal with them in the future. The report by (Mehdi *et al.*) outlines a

number of important points regarding why decision makers need to consider climate change. The main point is that "even small shifts in climate system will have potentially large ramifications for existing infrastructure". Further, the report states that climate change "will affect large and small, urban and rural, and have positive and negative consequences for the various type of infrastructure, health and education"

In most water resources planning and management systems, time-invariant hydrological processes, where the past is assumed representative of the future is considered. However, such assumption of stationarity is no longer valid due to the natural variability and anthropogenic induced changes in the climate system (Wagesho et al., 2013). A recent study by (Milly and C.D.), also claims the need to review existing methodologies to account for the non-stationary behavior of climatic variables.

Since rainfall characteristics are often used to design water structures, reviewing and updating rainfall characteristics (i.e., Intensity–Duration–Frequency (IDF) curves) for future climate scenarios is necessary (Mirhosseini et al., 2013).

1.2 Statement problem

Precipitation is primary component of the hydrologic cycle and its quantity is influenced by other factors like wind, temperature altitude. It is a main cause for hydrological problems including flood disasters that brings damages to agricultural land, residential area and water related infrastructures. Unless those hydraulic structures are properly planned and designed, their damaging effect leads to socio economic problems and many loss of life.

There is a sacristy of recorded observed flow data from Ethiopian context; and there is no adequate and reliable flow data in the country. This become a major problem and challenge for engineers in planning and designing of any water resource infrastructures. According to (Berhanu *et al.*), there are about 470 operational hydrological gauging stations, which cover only 40% of the country. Their finding also argues that; the existing gauge coverage's are very little by any standard and a lot of hydrologic information of river basins are being estimated using models that may not be verified with observed data. To cover the ungauged section of the country, engineers are using rainfall–runoff methods. However, there is still unreliable rainfall–runoff methods that address the climatic and topographic variability of the country. Moreover,

flow estimation by Rainfall-Runoff relationship requires knowledge of several site specific rainfall intensity-duration-frequency relationships in addition to catchment characteristics.

Ethiopian Road Authority (ERA) in its Drainage Design Manual had developed the IDF curves for different hydrological regions displaying similar rainfall patterns. However, such approaches overlook the rainfall variability over a large area such as watershed. Moreover, the representativeness of such IDF curves for the future time period remains to be the most challenging issue in view of climate change.

1.3 Research Objective

1.3.1 General Objective

– The main objective of this research is to evaluate the impact of climate change on a rainfall intensity-duration- frequency relation in Omo-Gibe River basin

1.3.2 Specific Objective

- To examine the trends and spatial variability of rainfall experienced over the basin for the last three decades
- To generate a future representative daily based rainfall data series for Omo-Gibe River basin under changing climate condition
- To comparatively evaluate the extreme storms between observed and projected period over the basin
- To develop a set of IDF curve from observed data series of a basin for different representative station
- To develop IDF curve from projected rainfall for future time considering bias corrected climate model output data

1.4 Research Question

The key questions addressed in this study in order to meet the above objectives were;

- What seems the trend of observed rainfall over the last three decades and what possible image could it reflect under the impact of climate change for a future over the basin?
- What looks spatial variability of rainfall over the basin and would it have effect on IDF curve?
- Does impact of climate change affect intensity-duration-frequency of rainfall over the basin?

1.5 Significance of the study

The result of this study will be useful to estimate the intensity of a given storm even the under impact of climate change for a required return period; given that duration of the event which equal to time of concentration. It will assist planning and design of water resource projects, flood plain mapping, flood control urban drainage networks, highway and culvert design of Omo-Gibe basin. The output the study could fully assist particularly those engineers who use rational formula and event based models for discharge estimation for a specific catchment over Omo-Gibe basin.

1.6 Scope of the study

This study tried to evaluate the impact of climate change on rainfall intensities over Omo-Gibe basin. Therefore, it is subjected to comparison between rainfall patterns of baseline period with projected climate at mid-21st century. The study is limited in addressing the evaluation of other climate parameters like mean, maximum and minimum temperature over the basin.

2 Literature Review

2.1 Overview of Climate Change

Climate is often described by the statistical interpretation of precipitation and temperature data recorded over a long period of time for a given region or location (NAPA, 2007). Africa is one of the region's most vulnerable to weather and climate variability (IPCC, 2007). Due to its low adaptive capacity, projected climate change may lead to severe impacts on many vital sectors such as agriculture, water management, and health. It is very challenging for climate models to replicate the multitude of physical processes and the complexity of their feedbacks, which span multiple temporal and spatial scales, over such a large and heterogeneous continent (Dosio *et al.*, 2014).

According to the IPCC, there is 95% scientific certainty that human activities are responsible for these increased greenhouse gas concentrations. The primary sources of emissions are fossil fuel emissions and changes in land use, such as deforestation, to make room for agricultural expansion to meet food requirements for a growing population. These greenhouse gases do not only stay in the atmosphere, they are also absorbed by the oceans (IPCC, 2014)

The IPCC's Special Report on Managing the Risks of Extreme Events and Disasters to Advance Climate Change Adaptation (IPCC, 2012) indicates that there will likely be more heavy rainfall eastern Africa with high certainty and more extremely wet days by the mid-21st century. There will also likely be an increase in the frequency of hot days in the future (high confidence), although a decreasing dryness trend over large areas is also projected (medium confidence).

According in to (NAPA) report, for the IPCC mid-range (A1B) emission scenario indicated that, the mean annual temperature will increase in the range of 0.9 -1.1 °C by 2030, 1.7 - 2.1 °C by 2050 and 2.7-3.4 °C by 2080 over Ethiopia as compared to the 1961-1990 normal. Also a small increase in annual precipitation is expected over the country. Accordingly, the report summarized the major adverse impacts of climate change the country had been experienced. Some of them were food insecurity arising from occurrences of droughts and floods; outbreak of diseases such as malaria, dengue fever, water borne diseases (such as cholera, dysentery)

associated with floods and respiratory diseases associated with droughts; land degradation due to heavy rainfall; damage to communication, road and other infrastructure by floods.

Local scale impacts of climate change in Ethiopia are common. As per (NMA), report, the 2006 main rainy season (June-September), Diredawa flood caused a lot of negative impacts. Among others, more than 250 people died, about 250 people were unaccounted for and more than 10,000 people became homeless which is estimated in the order of tenth of millions of dollars in terms of loss of life and property. Similarly, more than 364 people died, and more than 6000 people were displaced due to flooding of about 14 villages in South Omo. Other situations also occurred in West Shewa due to which more than 16,000 people were displaced.

2.2 Climate model

i. General Circulation Model

General Circulation Models (GCMs) are the major tools that project future climate change information. GCMs are numerical models that can represent physical processes in the atmosphere, ocean and land surface; therefore can simulate the responses of the global climate to increasing greenhouse gas concentrations (Moss *et al.*, 2010; Taylor *et al.*, 2012).

The spatial resolution of GCMs is generally coarse, with a grid size of about 100–500 kilometers in which each modeled grid cell is homogenous. In particular, in mountainous regions, fine-scale information needs to be incorporated into coarse GCM projections for hydrologic modeling because of the altitude-dependence of precipitation and temperature that are usually not represented by GCMs (Seager and Vecchi, 2010). Therefore, direct use of GCM outputs in regional water resources impact assessment studies is restricted (Arpita and Mujumdar, 2015).

Simulation results of GCMs for future projection of climate change impact on precipitation needs validation against historical precipitation observations prior to any use for local impact studies of climate change (Tabari et al., 2015). When GCM results are validated based on observations, sometimes large biases are observed, especially for extreme precipitation values (Tabari *et al.*, 2015; Van Pelt *et al.*, 2012; Van Haren *et al.*, 2013).

ii. Regional Climate Model

Regional Climate Model (RCM) is similar to a GCM in its principles but with high resolution. RCMs take the large-scale atmospheric information supplied by GCM output at the lateral

boundaries and incorporate more complex topography, the land-sea contrast, surface heterogeneities, and detailed descriptions of physical processes in order to generate realistic climate information at a spatial resolution of approximately 20–50 kilometers(USAID, 2014). Atmospheric fields (e.g., surface pressure, wind, temperature, and humidity) simulated by a GCM are fed into the vertical and horizontal boundaries of the RCM. Most RCMs capture the main climatologically features of precipitation but with different levels of accuracy. Locally specific data and physics-based equations are then used to process this information and obtain regional climate outputs. The primary advantage of RCMs is their ability to model atmospheric processes and land cover changes explicitly (USAID, 2014)

2.3 Downscaling approaches

Downscaling, or regionalization, is the term given to the process of deriving finer resolution data (e.g., for a particular site) from coarser resolution GCM or RCM data set (Abdella K.M., 2013)

Statistical downscaling involves the establishment of empirical relationships between historical large-scale atmospheric and local climate characteristics. Once a relationship has been determined and validated, future large-scale atmospheric conditions projected by GCMs are used to predict future local climate characteristics. In other words, large-scale GCM outputs are used as predictors to obtain local variables or predictands (USAID, 2014). This approach relies on the critical assumption that the relationship between present large scale circulation and local climate remains valid under different forcing conditions of possible future climates (Zorita and von Storch, 1999). However, it is unknown whether present-day statistical relationships between large- and regional-scale variables will be upheld in the future climate system.

Dynamical downscaling is one of the techniques that transfer information from GCMs to finer scales by applying a higher-resolution regional climate model (RCM) over a limited area with initial and boundary conditions taken from a driving GCM (Yang *et al.*, 2010). Dynamical downscaling relies on the use of a regional climate model (RCM), similar to a GCM in its principles but with high resolution. RCMs take the large-scale atmospheric information supplied by GCM output at the lateral boundaries and incorporate more complex topography, the land-sea contrast, surface heterogeneities, and detailed descriptions of physical processes in order to generate realistic climate information at a spatial resolution of approximately 20–50km (USAID,

2014). Since the RCM is nested in a GCM, the overall quality of dynamically downscaled RCM output is tied to the accuracy of the large-scale forcing of the GCM and its biases (Seaby *et al.*, 2013).

Compared to GCMs, RCMs are more reliable at reproducing relevant meso-scale patterns of local precipitation, and so the topographic effects on precipitation can be much better represented at a regional scale (IPCC, 2007). Moreover, RCMs usually provide an improved description of surface features (topographical, land cover, etc.) and more complex description of atmospheric processes compared to GCMs (Tabari *et al.*, 2015).

It becomes evident that climate change will increase the frequency and intensity of extreme events (IPCC 2013). Therefore, the impacts of climate change on hydrological extremes such as heavy precipitation events have to be considered when designing and optimizing water infrastructures (Tabari *et al.*, 2015).

For the reason of lack of general climate projections based on Regional Climate Downscaling tools, Africa was selected as the first target region for the World Climate Research Program CORDEX (Coordinated Regional climate Downscaling Experiment) (Giorgi *et al.*, 2009). CORDEX aims to foster international collaboration in order to generate an ensemble of high-resolution historical and future climate projections at regional scale, by downscaling different Global Climate Models (GCMs) participating in the Coupled Model Inter-comparison Project Phase 5 (CMIP5) (Taylor *et al.*, 2012).

Globally, there has been a marked increase in the number of RCM simulations. However, finding from different researches indicated that only few of them are participating in simulation of African climate domain regardless of their reliability. Assessment on the performance of CORDEX regional climate models in simulating East African rainfall indicated that, only four RCMs (CRCMP5, RACMO, RegCM3, RCA) among the ten models of CORDEX-Africa captured the shape of the monthly rainfall distribution and the annual rainfall anomaly with high spatial correlations together with consistency in reproducing spatial patterns of rainfall. However, they overestimated the mean monthly rainfall amount of Jun- September (ENDRIS *et al.*, 2013). On the other hand, Assessment was carried on rainfall accuracy of eight independent

GCMs at a wide range of time scales over the Upper Blue Nile basin which is dynamically downscaled by RCA regional climate model (Haile and Rientjes, 2015). The finding shows that, MPI-ESM-LR climate model performed best in many aspects. It also argued that, the performance of the models differs subject to the performance measures used for evaluation. Therefore, multi-models' simulations was recommended in order to capture different aspects of the Upper Blue Nile basin rainfall. Other fifteen selected GCMs from CMIP5 were also comparatively evaluated over upper blue Nile River Basin; and MPI-ESM-MR found to be the best model in capturing rainfall pattern (Bokke *et al.*, 2017).

2.4 An overview of RCPs

Previously, the GCMs' simulations of climate variables were based on three emission scenarios (SRES: A1B, A2, and B1) from the Coupled Model Inter-comparison Project Phase 3 (CMIP3). The Fourth Assessment Report (AR4) of IPCC was supported by CMIP3 and the outputs of climate models included in CMIP3 have been the basis of climate change impact studies conducted by the research community around the world (IPCC, 2007; Taylor *et al.*, 2012). The outputs of climate models from CMIP3 provided comprehensive multi-model impact assessment for climate change projections during the 21st century, based on the IPCC Special Report Emission Scenarios (SRES), i.e., A1B, A2, and B1 (Moss *et al.*, 2010). With the release of the Fifth Assessment Report (AR5) of IPCC based on Phase 5 (CMIP5), a new set of GCM simulations was made freely available to the research community. CMIP5 climate models produce a comprehensive set of outputs with the inclusion of new emission scenarios, known as Representative Concentration Pathways (RCPs) (Moss *et al.*, 2010; Taylor *et al.*, 2012) Generally, CMIP5 includes more than 50 sophisticated climate models (GCMs) from more than 20 modeling groups and a set of new forcing scenarios (Taylor *et al.*, 2012). The Integrated Assessment Models (IAMs) were used by the Integrated Assessment Modeling Consortium (IAMC) to produce the RCPs by considering various components such as demographics, economics, energy, and climate (IPCC, 2013). The four RCP's, namely RCP 2.6, RCP 4.5, RCP 6.0, and RCP 8.5, are defined by their total radiative forcing, which is a cumulative measure of all anthropogenic emissions of GHG's from all source expressed in Watts per square meter, by 2100. The four RCP's were chosen to represent a broad range of climate outcomes from various possible socio-economic policies and technological interventions (IPCC, 2013).

The word “representative” signifies that each of the RCPs represents a larger set of scenarios in the literature. In fact, as a set, the RCPs should be compatible with the full range of emissions scenarios available in the current scientific literature, with and without climate policy. The words “concentration pathway” are meant to emphasize that these RCPs are not the final new, fully integrated scenarios (i.e. they are not a complete package of socio-economic, emission and climate projections), but instead are internally consistent sets of projections of the components of radiative forcing that are used in subsequent phases. The use of the word “concentration” instead of “emissions” also emphasizes that concentrations are used as the primary product of the RCPs, designed as input to climate models (Van Vuuren *et al.*, 2011b).

2.5 RCM bias correction

RCMs have difficulty in accurately simulating convective precipitation, which is a major concern for tropical regions. Most RCMs also do not accurately simulate extreme precipitation a systematic bias that can worsen as the resolution is increased. Statistical bias corrections often need to be performed to better match the model output to the observations (Brown *et al.*, 2008).

RCMs perform better in regions with temperate climate conditions than tropical regions, since tropical rainfall is often predominantly convective in nature and occurs at a sub daily time scale (Lenderink and Meijgaard, 2008). RCM biases can be introduced by incorrect boundary conditions provided by reanalysis data or by a GCM, and by systematic model errors, such as the errors resulting from the imperfect parameterization of some climate processes (Ehret *et al.*, 2012). That means a twentieth century simulated climate projected from a model, is not the same as the climate of the twentieth century coming from observations (Mirhosseini *et al.*, 2012). Hence, climate model outputs have to be post-processed to match the observed climate (Christensen *et al.*, 2008; Maraun, 2013)

Table 2.1 some of bias correction methods and their descriptions

S.N	Bias correction Methods	Description of Methods	References
1	Delta Method	Sometimes referred to as the direct method in the scientific literature. The long-term mean changes are calculated and added to the observation records. The delta method removes biases in the mean but not the coefficient of variance of the modeled precipitation. The variance in future climate is kept the same as under present climate, which will likely not be true. This means that it does not account for potential future changes in climate dynamics, e.g., the number of dry vs. wet days does not change.	(Fang *et al.*, 2015; Raty *et al.*, 2014 ; Sarr *et al.*, 2015; Wetterhall, 2012; Teutschbein and Seibert, 2012)
3	Linear Scaling Approach	Precipitation is typically corrected with a multiplier term on a monthly basis. The linear scaling approach used to reduce the biases of precipitation, has a correct estimation of mean but a slight underestimation of the 90th percentile and standard deviation. All events are adjusted with the same correction factor. It is furthermore not able to correct frequencies.	(Fang *et al.*, 2015; Yekambessoun NTcha MPo, 2017; Teutschbein and Seibert, 2012)
3	Quantile-Mapping Methods	The quantile matching adjusts all moments of the probability distribution function (PDF) of any variable of the model by using the PDF of observations, integrating both PDFs to cumulative distribution functions (CDFs) and construct a transfer function. It corrects most of the statistical characteristics and has the narrowest variability ranges. However, it main drawback is its stationarity assumption that, the same correction algorithm applies to both current and future climate conditions	(Piani *et al.*, 2010; Stepanek *et al.*, 2016; Yekambessoun NTcha MPo, 2017; Mirhosseini *et al.*, 2012 ; Teutschbein and Seibert, 2012)
4	Nonlinear (power transformation)	While linear scaling accounts for a bias in the mean, it does not allow differences in the variance to be corrected. Therefore, a nonlinear correction in an exponential form, $a * P^b$; can be used to specifically adjust the variance statistics of a precipitation time series and monthly mean. They perform much better than the previous approaches in terms of correcting several statistical characteristics and in terms of the variability range.	(Biniyam and Kemal, 2017; Lenderink *et al.*, 2007; Teutschbein and Seibert, 2012)

2.6 Rainfall Variability in Ethiopia

Rainfall distribution is extremely variable both in space and time (EPCC, 2015) . Rainfall in Ethiopia is the result of multi-weather systems that include Subtropical Jet (STJ), Inter-tropical Convergence Zone (ITCZ), Red Sea Convergence Zone (RSCZ), Tropical Easterly Jet (TEJ), and Somali Jet (NMA, 1996). The intensity, position, and direction of these weather systems lead the variability of the amount and distribution of rainfall in the country. This variability is reflected in the uneven distribution of surface and groundwater resources of the country (EPCC, 2015). Thus, the rainfall in the country is characterized by seasonal and inter-annual variability (Camberlin P., 1997; Shanko D. and Camberlin P., 1998; Conway D., 2000; Seleshi Y and Zanke U, 2004). Further, some investigation realized that the spatial distribution of rainfall in Ethiopia is significantly influenced by topographical variability of the country (NMA, 1996; Camberlin P., 1997); and seasonal changes in the atmospheric pressure systems that control the prevailing winds (Reda *et al.*, 2014). This makes the rainfall system more complex over the total country.

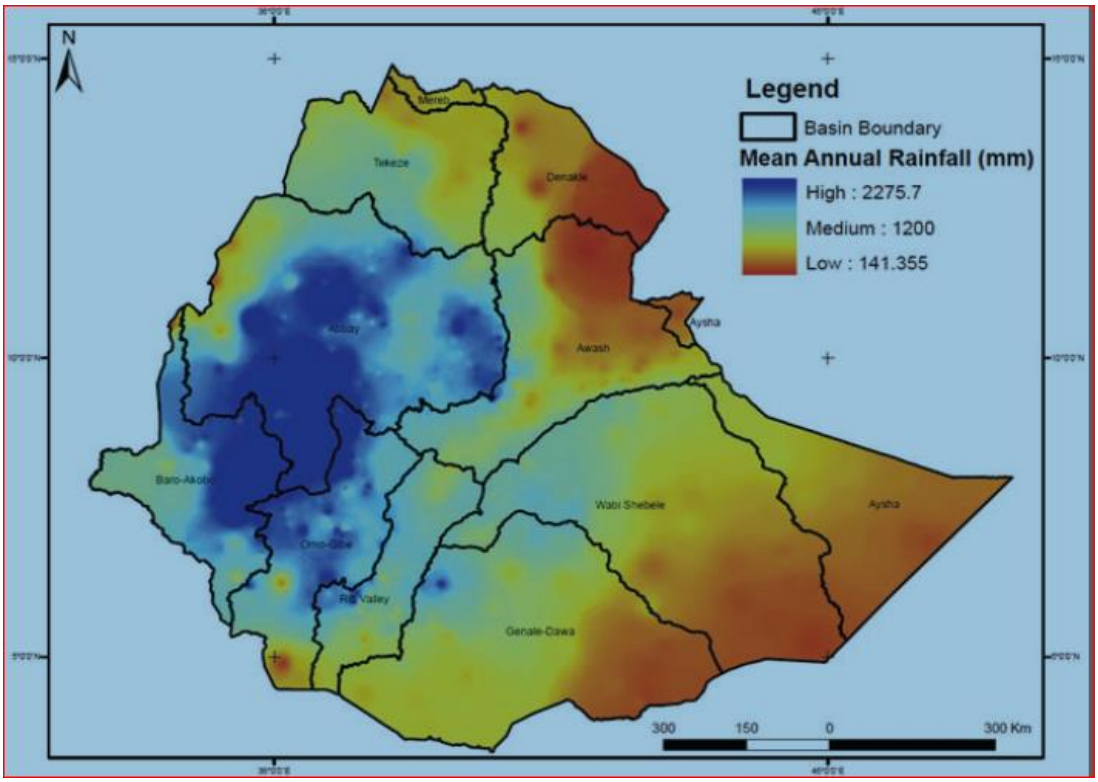

Figure: 2.1 Spatial variability of the mean annual rainfall in Ethiopia, *(Source: Berhanu et al., 2014)*

2.6.1 Spatial Variability of Rainfall

The water resources of Ethiopia are governed strongly by the amount and distribution of rainfall. The distribution of rainfall over the country is highly variable (EPCC, 2015). The regional and global change of the weather systems and the topographic variation along with the seasonal cycles are responsible for the spatial variability of rainfall in the country. Looking into the rainfall variability of the country by river basins, the eastern flowing river basins (Wabishebele and Genale-Dawa) receive low to medium rainfall, whereas those that flow to the west (Abay, Baro-Akobo, Omo-Gibe, and Tekeze) receive a mean annual rainfall in the range of medium to high (Berhanu *et al.*, 2014).

2.6.2 Temporal Rainfall Variability

Seasonal rainfall in Ethiopia is driven mainly by the migration of the ITCZ, tropical upper easterlies, and local convergence in the Red Sea coastal region (Conway D., 2000). The exact position of the ITCZ changes over the course of the year, oscillating across the equator from its northernmost position over northern Ethiopia in July and August, to its southernmost position over southern Kenya in January and February lead the inter-annual variability of rainfall in the country (McSweeney *et al.*, 2012). Most of the area in Ethiopia receives one main wet season (called "Kiremt")from mid-June to mid-September (up to 350 mm per month in the wettest regions), when the ITCZ is at its northernmost position. Parts of northern and central Ethiopia also have a secondary wet season of erratic, and considerably lesser, rainfall from February to May (called the "Belg"). The southern regions of Ethiopia experience two distinct wet seasons, which occur as the ITCZ passes through this to its southern position. The March to May "Belg" season is the main rainfall season yielding 100–200 mm of rainfall per month, followed by a lesser rainfall season in October to December called "Bega" (around 100 mm of rainfall per month). The easternmost corner of Ethiopia receives very little rainfall at any time of the year (McSweeney *et al.*, 2012).

2.7 Rainfall data quality controlling and its characteristics.

Many practical applications like extreme value analysis and hydrological modeling have no tolerance to missing values. Preprocessing of raw data sets by infilling their missing values is thus a necessary procedure (Pappas *et al.*, 2014). At small scales, the use of measurements from individual rain gauges might be appropriate. However at larger scales, it is required to draw special attention to the appropriate representation of the spatial precipitation

patterns, which are usually interpolated from point measurements. There is a wide range of interpolation methods are available on literatures, ranging from simple techniques to more complex and computationally intensive approaches. (Boke A. S., 2017) comparatively evaluate most commonly used five spatial interpolation techniques and recommended Nearest Neighbor (NN), Inverse distance weighting average (IDWA) and Modified inverse distance weighting average (MIDWA interpolation methods to be comparatively used over Ethiopia.

The principal characteristics of rainfall events are its intensity, duration and frequency or recurrence interval. Therefore, their precise measurements are essential inputs for the purpose of water resource planning and engineering design and usually expressed graphically into the Intensity-Duration-Frequency curve (Kewtae Kim 2007).

2.8 Frequency Distribution Models

A probability distribution is a function representing the probability of occurrence of a random variable. By fitting a distribution to a set of hydrologic data, a great deal of the probabilistic information in the sample can be compactly summarized in the function and its associated parameters (Chow *et al.*, 1987).

Annual maxima and magnitudes above certain threshold or partial duration series of rainfall data are commonly applied as input for IDF analysis (Ben-Zvi, 2009). The intensity duration frequency analysis starts by gathering time series records of different durations. After time series data is gathered, annual extremes are extracted. The annual extreme data is then fit to a probability distribution in order to estimate rainfall quantities. The fit of the probability distribution is necessary in order to standardize the character of rainfall across stations with widely varying lengths of record (Prodanovic and Simonovic, 2007).

There are different distribution functions for IDF analysis: Extreme Value Type I, i.e., Gumbel (EV-I) distribution, Generalized extreme value (GEV) distribution, Gamma distribution, Log Pearson III distribution, Lognormal distribution, Exponential distribution [(Koutsoyiannis *et al.*, 1998; Nguyen *et al.*, 2007), recommend Gumbel distribution function and GEV distribution function to be used for IDF analysis. (Prodanovic and Simonovic, 2007) used Gumbel's distribution in constructing IDF curves in two different studies, whereas (Overeem *et al.*, 2008;

Hassanzadeh *et al.*, 2014), used the GEV distribution to construct IDF curves due to the superiority of the distribution in describing upper tail behavior.

Ethiopia has been statistically analyzed by using three methods of distribution analysis namely; Generalized Extreme Value, Log Pearson-III and Gumbel's Methods. The goodness of fit (GOF) tests measures the compatibility of a random sample with a theoretical probability distribution function. In other words, these tests show how well the distribution being selected fits to the data. Different GOF criteria's namely; Kolmogorov-Smirnov(K-S), Chi-Squared (Shrestha *et al.*, 2017; ERA, 2013), Anderson-Darling(A-D) (ERA, 2013) tests are used for best fitting probability distribution selection. The selection of the best fit method is based on the ranks given by the three criteria (ERA, 2013).

2.9 Construction of Future IDF Curves

IDF curve presents the probability of a given rainfall intensity and duration expected to occur at a particular location (Mirhosseini *et al.*, 2012). Changes in extreme rainfall events can lead to a revision of standards for designing civil engineering infrastructures. It can also lead to reconstruction and/or upgrade of existing infrastructures. Current design standards are based on historic climate information which is assumed stable (Mirhosseini *et al.*, 2012).

Using the statistical analyses, rainfall intensity-duration curves have been developed for commonly used design frequencies. The rainfall intensity (I) is the average rainfall rate depth in mm for duration equal to the time of concentration for a selected return period. Once a particular return period has been selected for design and a time of concentration calculated for the catchment area, the rainfall intensity can be determined from Rainfall-Intensity-Duration curves (ERA, 2013).

2.10 IDF Curve of ERA Manual

The rainfall intensity (I) is the average rainfall rate in mm/hr for duration equal to the time of concentration for a selected return period. Once a particular return period has been selected for design and a time of concentration calculated for the catchment area, the rainfall intensity can be determined from Rainfall-Intensity-Duration-frequency curves.

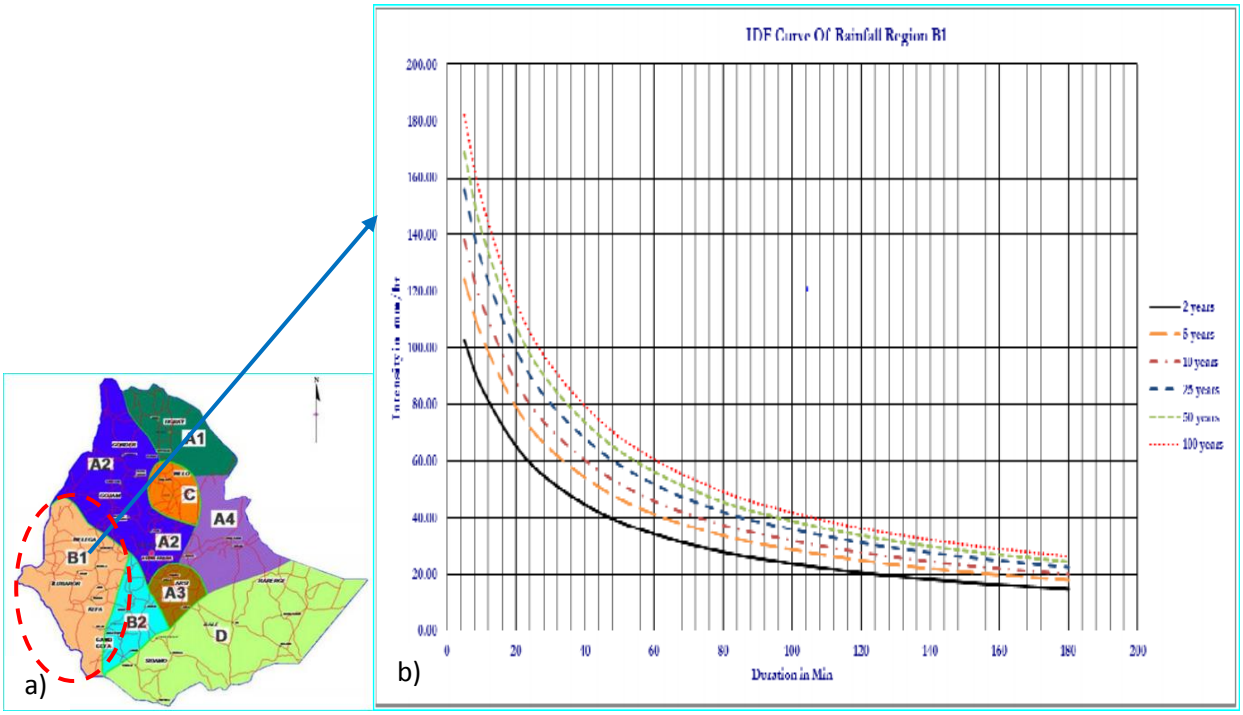

Figure: 2.2 a) Hydrological regions displayed similar rainfall pattern; b) IDF curve developed for regions including majority of Omo-Gibe basin *(Source: ERA, 2013)*.

According to (ERA) manual, some of common ways in peak flow estimation for design of road drainage structures in Ethiopia are Rational Method; NRCS Runoff Curve Number Methods; Statistical analysis of stream data and Regional regression equations. Each method may have their respective application and limitations. However, rational method which is highly common for small watershed with area up to 0.5km^2 relays up on the application of IDF curve.

3 Methodology

3.1 Description of the Study Area

3.1.1 Location

The study area, Omo -Gibe river basin, is geographically located between of 4^0 25' to 9^0 22' North and 35^0 23' to 38^0 22' East in the south west of Ethiopia. The Omo-Gibe River basin covers a total area of about 77,826.93 Km^2. General course direction of the Omo-Gibe River basin is north-south direction towards Lake Turkana. It is filled with alluvial and lacustrine sediments of recent origin associated with the Great Rift Valley even if there are some important tributaries from different directions. The basin is between Baro-Akobo Basin in the West and Rift valley basin in the South East and Blue Nile Basin in the northwest with small area of Awash Basin in the northeast border and Lake Turkana in Kenya which forms its most southern boundary.

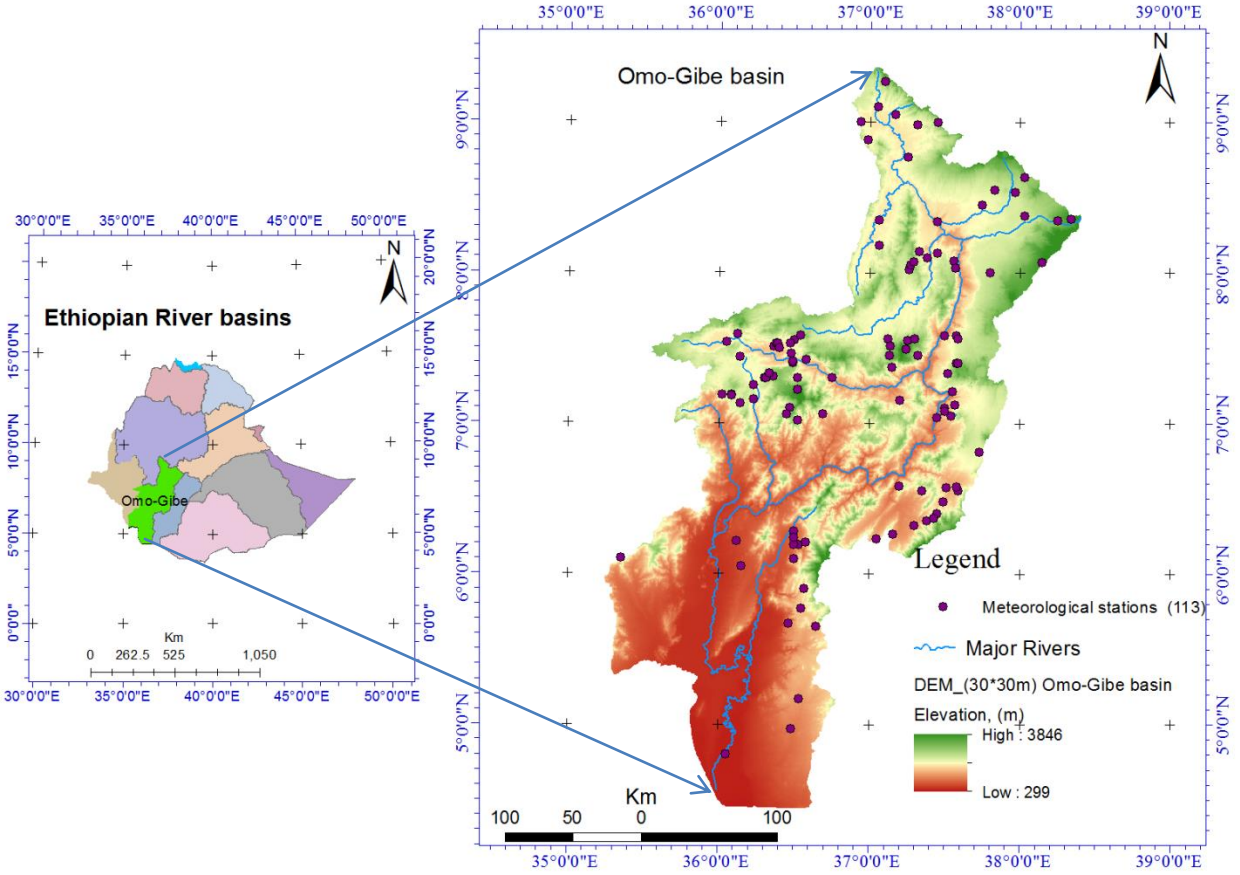

Figure: 3.1: Location of the study area *(Source: MoWIE)*

3.1.2 Topography

The topography of the basin is more of it seems a complex topography. The northern part of the basin is characterized by variety of mountains to hilly terrain in the gorges of Main River. The northern and central half of the basin lies at an altitude greater than 1500m masl with maximum elevation of 3360m amsl (located between Gilgel-Gibe and Gojeb tributaries), and the plains of the lower Omo lies between 400-500 masl (Richard Woodroofe & associates, 1996). As shown in the figure below, the central part of the basin is dominated by mountain ranges and has relatively steep slope as compared to the northern and southern part of the basin. As shown in the figure below, the southern part of the Omo-Gibe basin is relatively flat. Generally, the topography of the basin ranges within elevation as high as up to 3846m amsl in the northern part and as low as up to 299m amsl in the southern part of the basin.

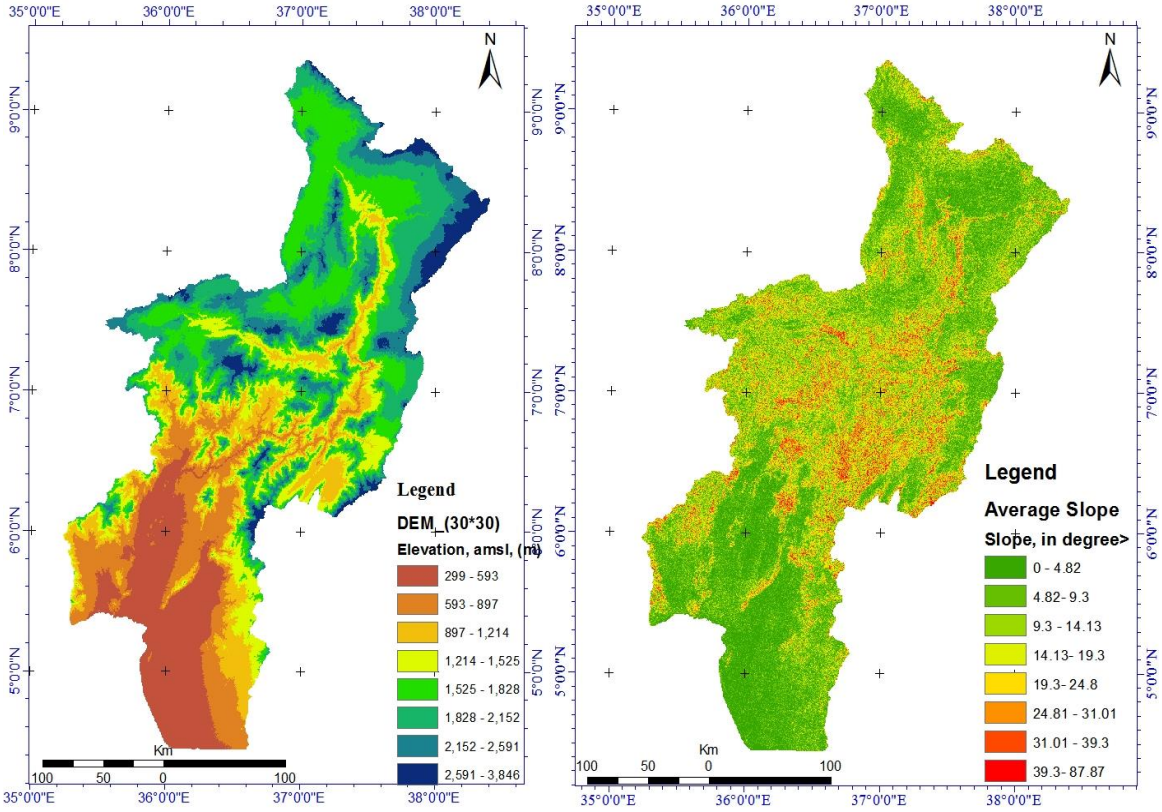

Figure: 3.2 Elevation Ranges and average slope of the basin

3.1.3 Climate

Ethiopia has two seasons of tropical climate. The first is the dry winter season that occurs between October and April and the second is the rainy season that spans of the time window of May to September (the summer months). According to different studies, it was indicated that climate of Omo-Gibe River basin varies from a hot arid climate in the southern part of the floodplain to a tropical humid one in the highlands that include the extreme north and north-western part of the Basin. Intermediate between these extremes and for the greatest part of the basin, the climate is characterized by sub-humid. The climate is classifiable as tropical humid in the highlands that include the areas surrounding Jimma and around the headwaters of the Gojeb River. For the rest and greatest part of the watershed, the climate is classified as a tropical sub-humid which is intermediate between the tropical humid and the hot arid.

3.1.4 Land Use land cover

In a very broad term, the Omo-Gibe basin is composed of complex natural features. Most of the northern catchments of the Omo-Gibe Basin are under moderately and extensive cultivation with increased land pressure, meaning the expansion of cultivated areas in to increasingly marginal lands at the expense of wood lands. The main gorges of the basin are relatively covered by bushed shrub-bed grass land and relatively unpopulated and support a cover of open wood-land and bush-land with grasses, the central western region of the basin is dominated by dense and distributed mixed high forest, wooden land, dens shrub land and wooded grass land. Deforested areas are now confined to areas too steep and inaccessible to farm. The south and lower part of the basin is more sparsely populated with a greater population of open grass land and open wooden and shrub land.

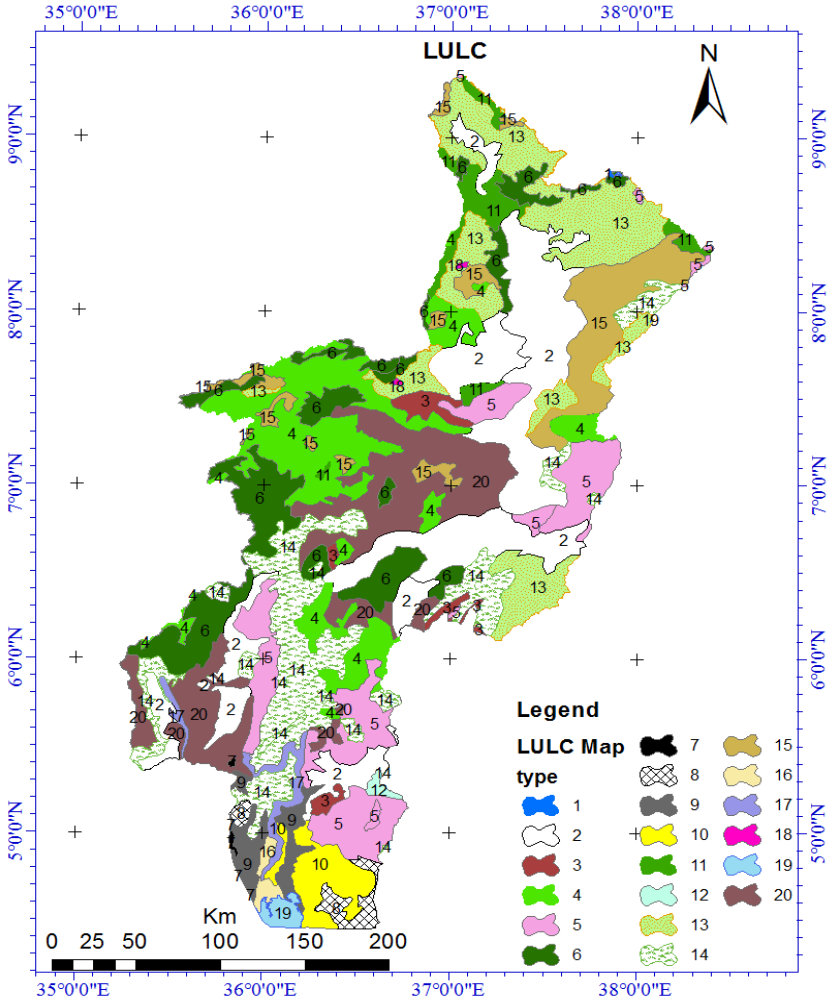

Figure: 3.3 Land use land cover (LULC) distribution pattern of Omo-Gibe basin (Explanation of numbered values are given in Table 3.1). *(Source: MoWIE)*

Table: 3.1 Percentage ratio of land use land cover of study area

S.N	Land Cover	Area (Km^2)	Area Ratio (%)
1	Afro-Alpine Heath Vegetation	8.90	0.01
2	Bushed Shrubbed Grassland	14019.54	18.04
3	Dense Bushland	1005.68	1.29
4	Dense Mixed High Forest	8831.06	11.36
5	Dense Woodland and dense shrub land	7109.75	9.15
6	Disturbed High Forest	7404.06	9.53
7	Exposed Rock Surface	69.59	0.09
8	Exposed Rock Surface with Scat. Grass Veg	811.38	1.04
9	Exposed Sand Soil Surface	1400.09	1.80
10	Exposed Sand Soil Surface With Scat, Scrub& Grass	1866.08	2.40
11	Intensively Cultivated	1762.33	2.27
12	Lowland Bamboo Bushland	163.25	0.21
13	Moderately Cultivated	9244.10	11.89
14	Open Grassland and Open Wooden Land	8474.75	10.90
15	Perennial Crop Cultivation	5039.89	6.48
16	Perennial Swamp	356.64	0.46
17	Riparian Woodland Or Bush land	886.88	1.14
18	State Farm	40.69	0.05
19	Water Body	420.38	0.54
20	Wooded Grassland	8809.79	11.33

3.1.5 Soil Type

Shape file of soil map of Ethiopia which was collected from Ministry of Water, Irrigation and Electricity was extracted for the study area and analyzed. The resulted map shows that the basin is characterized by different soil types. Majority of the western and some of central eastern regions of the basin are dominated by dystric cambisols, orthic Acrisols and Lithosols. But, the lower region of the basin is dominated by Eutric Fluvisols.Whereas the northern highland region of the basin is characterized by Pellic verti soil. The other major soil type with their corresponding area coverage is discussed briefly on table.

Table: 3.2 Major soil type distribution of the basin

S.N	Major soil type	Area (km^2)	Area ratio
1	Chromic Cambisols	2900.79	3.73
2	Chromic Luvisols	3239.5	4.17
3	Chromic Vertisols	6601.25	8.50
4	Dystric Cambisols	17742.4	22.84
5	Eutric Cambisols	2197.03	2.83
6	Eutric Fluvisols	8321.31	10.71
7	Eutric Nitosols	3410.92	4.39
8	Lake	397.543	0.51
9	Lithosols	10344.6	13.32
10	Marsh	345.736	0.45
11	Orthic Acrisols	15231.42	19.61
12	Orthic Luvisols	971.5077	1.25
13	Orthic Solonchaks	396.425	0.51
14	Pellic Vertisols	5204.69	6.70
15	Rendzinas	48.3075	0.06
16	Stone Surface	337.797	0.43

Soil properties influence the relationship between runoff and rainfall since soils have differing rates of infiltration. Permeability and infiltration are the principal data required to classify soils into Hydrologic Soils Groups (HSG). Based on infiltration rates, the Soil Conservation Service (SCS) has divided soils into four hydrologic soil groups as follows.

Group A: Sand, loamy sand or sandy loam: Soils having a low runoff potential due to high infiltration rates. These soils primarily consist of deep, well-drained sands and gravels.

Group B: Silt loam or loam: Soils having a moderately low runoff potential due to moderate infiltration rates. These soils primarily consist of moderately deep to deep, moderately well to well drained soils with moderately fine to moderately coarse textures.

Group C*:* Sandy clay loam, Soils having a moderately high runoff potential due to slow infiltration rates. These soils primarily consist of soils in which a layer exists near the surface that impedes the downward movement of water or soils with moderately fine to fine texture.

Group D: Clay loam, silty clay loam, sandy clay, silty clay or clay: Soils having a high runoff potential due to very slow infiltration rates. These soils primarily consist of clays with high swelling potential, soils with permanently-high water tables, soils with a clay pan or clay layer at or near the surface, and shallow soils over nearly impervious parent material.

Ethiopian Road Authority (2013) uses Ethiopian soil map prepared by Ministry of Agriculture based on soil permeability and infiltration rates which is classified in to four hydrological soil groups based on Soil Conservation Service (SCS) classification criteria. Accordingly, shape file of the soil map was used to extract hydrological soil group of Omo-Gibe basin. Reclassification for the study area was done based on ERA (2013) drainage design manual. The result indicated that the study area is composition of two hydrological soil groups (Group B and Group D) as shown in table3.4. The spatial distribution of hydrological soil groups of the basin was shown on figure 3.4 b). Accordingly, majority of the hydrological soil group of Omo-Gibe basin is under group B. But some part of the basin particularly, area near by deep gorge of the main river is under category of Group D

Table: 3.3 Hydrological soil groups Omo-Gibe basin and their area coverage

S.N	Hydrological Soli Group	Area (km^2)	Percentage Ratio[1]
1	B	54411.27523	70.04
2	D	22882.40151	29.45

[1] About 0.52% of the basin is covered by a lake

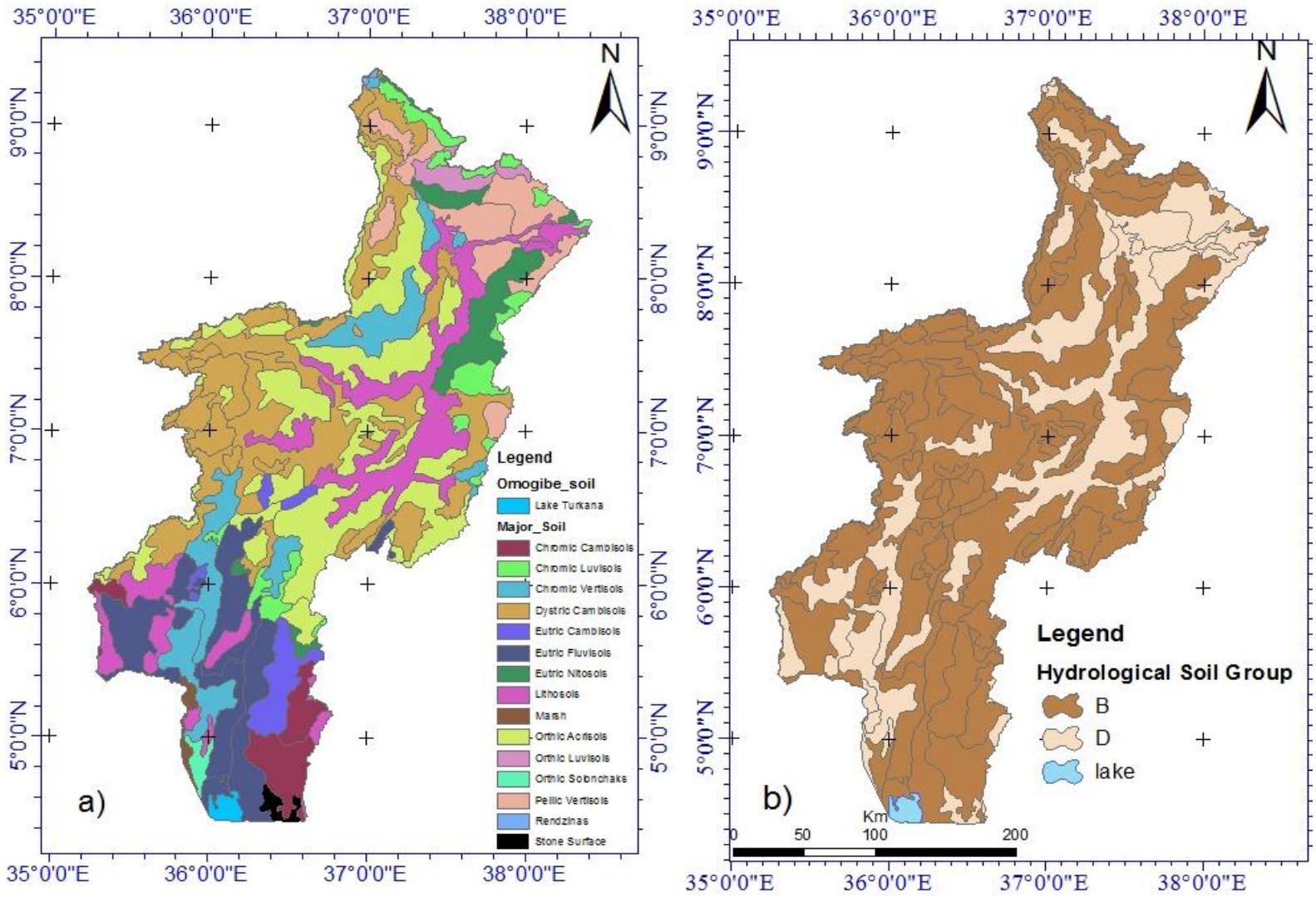

Figure: 3.4 Major soil group (a) and hydrological soil group (b) distributed over the basin *(Source: MoWIE)*

3.2 Data Sources and Descriptions

3.2.1 Meteorology Data

There are about 112 meteorological stations with in the basin randomly dispersed over the basin. However, most of them are class-IV (collect only rainfall) and class-III (Collects rainfall and air temperature). Moreover, they had been established in recent time so that they had a recorded data of less than 10 years.

Records of daily meteorological data were collected from National Meteorology Agency (NMA) which is responsible for the measurement, control, and storage of meteorological data of the total country. Data of 42 gauging stations scattered over and nearby the basin were selected and collected which have relatively reliable and long year's data and the detail descriptions of them were presented as follows.

Table: 3.4 descriptions of stations used for mean annual rainfall computation

S.N	Station Name	class	longitude	latitude	Elevation (M) amsl	Location (Sub-basin)	Years of records
1	Ejaji	1	37.3167	8.9833	1731.1	Omo-Gibe	1987-2013
2	Shambu	1	37.1167	9.5667	2464.9	Abay	1987-2013
3	Woliso/Giyon/	1	37.9667	8.5333	2064.3	Omo-Gibe	1987-2013
4	Ameya Gindo	4	37.45	8.34	2100	Omo-Gibe	1987-2013
5	Arjo	1	36.5	8.75	2565	Abay	1987-2013
6	Nekemte	2	36.4633	9.0833	2080	Abay	1987-2013
7	Hosana	1	37.52	7.33	2200	Omo-Gibe	1987-2013
8	Imdibir	1	37.56	8.08	2100	Omo-Gibe	1987-2013
9	Jinka	1	36.55	5.7667	1373	Omo-Gibe	1987-2013
10	Konso	1	37.4333	5.3333	1431	Rift valley	1987-2013
11	Tercha	1	37.2	6.58	0	Omo-Gibe	1998-2013
12	Wolaita sodo	1	37.73	6.81	1854	Omo-Gibe	1987-2013
13	Arba Minch	2	37.55	6.05	1220	Rift Valley	1987-2013
14	Angacha	3	37.55	7.21	2100	Omo-Gibe	1987-2013
15	Bulki(Mindre)	3	36.5	6.19	2300	Omo-Gibe	1987-2013
16	Butajra	3	38.22	8.09	2000	Rift Valley	1987-2013
17	Dimeka	3	36.5333	5.1667	1115	Omo-Gibe	1987-2013
18	Hana	3	36.1167	6.2167	586	Omo-Gibe	2006-2015
19	Omorate	3	36.05	4.8	365	Omo-Gibe	2006-2015

S.N	Station Name	class	longitude	latitude	Elevation (M) amsl	Location (Sub-basin)	Years of records
20	Wolkite	3	37.45	8.13	2000	Omo-Gibe	1987-2013
21	yaya otena	3	37.32	7.45	1545	Omo-Gibe	1987-2013
22	Bele	4	37.35	6.55	1200	Omo-Gibe	1987-2013
23	Dara Malo	4	37.16	6.13	1320	Omo-Gibe	1988-2013
24	Dinke	4	37.3	6.32	1620	Omo-Gibe	1988-2013
25	Gubre	4	37.5	7.1	1800	Omo-Gibe	1988-2013
26	Gunchire	4	37.57	8.03	2070	Omo-Gibe	1988-2013
27	Kako	4	36.65	5.65	1409	Omo-Gibe	1988-2013
28	Turmi	1	36.4833	4.9667	934	Omo-Gibe	1986-2000
29	Zenga	4	36.58	6.21	1620	Omo-Gibe	1987-2013
30	Aman	1	35.34	6.57	1192	Baro--kobo	1999-2011
31	Chida	1	36.47	7.1	1659	Omo-Gibe	1987-2013
32	Gatira	1	36.12	7.59	2358	Omo-Gibe	1987-2013
33	Limu Genet	1	36.57	8.04	1766	Abay	1987-2013
34	Masha	1	35.28	7.45	2282	Baro-Akobo	1987-2013
35	Sokoru	1	37.25	7.55	1928	Omo-Gibe	1987-2013
36	Jimma	2	36.49	7.4	1718	Omo-Gibe	1987-2013
37	Asendabo	3	37.13	7.45	1764	Omo-Gibe	1987-2013
38	Bonga	3	36.3	7.3	1779	Omo-Gibe	1987-2013
39	Shebe	3	36.31	7.3	1813	Omo-Gibe	1987-2013
40	Abelti	4	37.38	8.1	1968	Omo-Gibe	1987-2013
41	Kumbi	4	37.29	8.07	1930	Omo-Gibe	1987-2013
42	Metesso	4	36.52	7.02	2283	Omo-Gibe	1987-2013

3.2.2 Digital Elevation Model (DEM)

Digital elevation model (DEM) was obtained from Shuttle Radar Topographic Mission (SRTM) freely downloaded from (http://srtm.usgs.gov). Then, an Arc Map 10.1 package was used for extraction of study area and further analysis.

3.2.3 Shape file:

It is one of the most common Arc GIS file format which stores a set of thematically associated data considered to be a unit. A shape file usually represents a single layer, such as soils, streams, roads, or land use. Features in a shape file format are stored as points, arcs, and polygons. They have a variety of file extensions: .shp, .shx, .dbf and sometimes others. However, data collected

from MoWIE (Ethiopian Land use Land cover, Soil, River Basin) for this study were only with .shp file extension.

3.2.4 Climate model data sets

Coordinated Regional Climate Downscaling Experiment (CORDEX) data were used for future climate projection. CORDEX is an international effort supported by the World Climate Research Program (WRCP), aimed at producing a set of climate change projections covering different regions of the world with multiple RCMs and several emission scenarios. These regional climate projections were based on (CMIP5) projects. There are about 10 RCM participated over African domain. For this study, dynamically downscaled outputs by the recent version of the Rossby Centre Regional Climate Model—RCA4 were used. The model was developed in Swidish Meteorological and Hydrological institute (SMHI). Spatially, the RCA4 simulations cover the CORDEX-Africa domain at resolution of 0.44° × 0.44° (~50 km × 50 km) for the 1951–2100 time period which is divided into two: historical (1951–2005) and scenario (2006–2100) periods. Spatial emissions are provided as separate files in Net-CDF format. It is a fine scale (approximately 50 km × 50 km) climate projection readily available to users in a grid format. The data are based on Representative Concentration Pathways (RCPs) scenario which is four greenhouse gas concentration (not emissions) trajectories adopted by the IPCC for its fifth Assessment Report (AR5) in 2014. It is consistence sets of projections of only the components of radiative forcing that are meant to serve as input for climate modeling. It supersedes Special Report on Emissions Scenarios (SRES) projections published in 2000. Detail characteristics of realizations (RCP's) were summarized in appendix 7.5

3. 3 Selection of representative stations for the basin

Omo-Gibe basin is one of Ethiopian basin with inadequate and well organized set of meteorological data. Most of meteorological stations over the basin are with poor data sets which were found to be a challenge for the study to consider the whole meteorological stations. Therefore, the following factors were mainly considered as a selection criteria.

- **Temporal resolution of data**: implies for the availability of very fine time resolution of adequate and reliable data (daily, monthly and annual time series data availability)
- **Spatial resolution of data:** implies the consideration of topography and distance between each station. This was just for the sake of representation of the whole basin.
- **Variability of Rainfall:** Spatial variation of rainfall over the basin

Accordingly, eighteen (18) stations were selected for further analysis. For climate change impact evaluation, data series of dynamically downscaled RCM outputs in grid format were used.

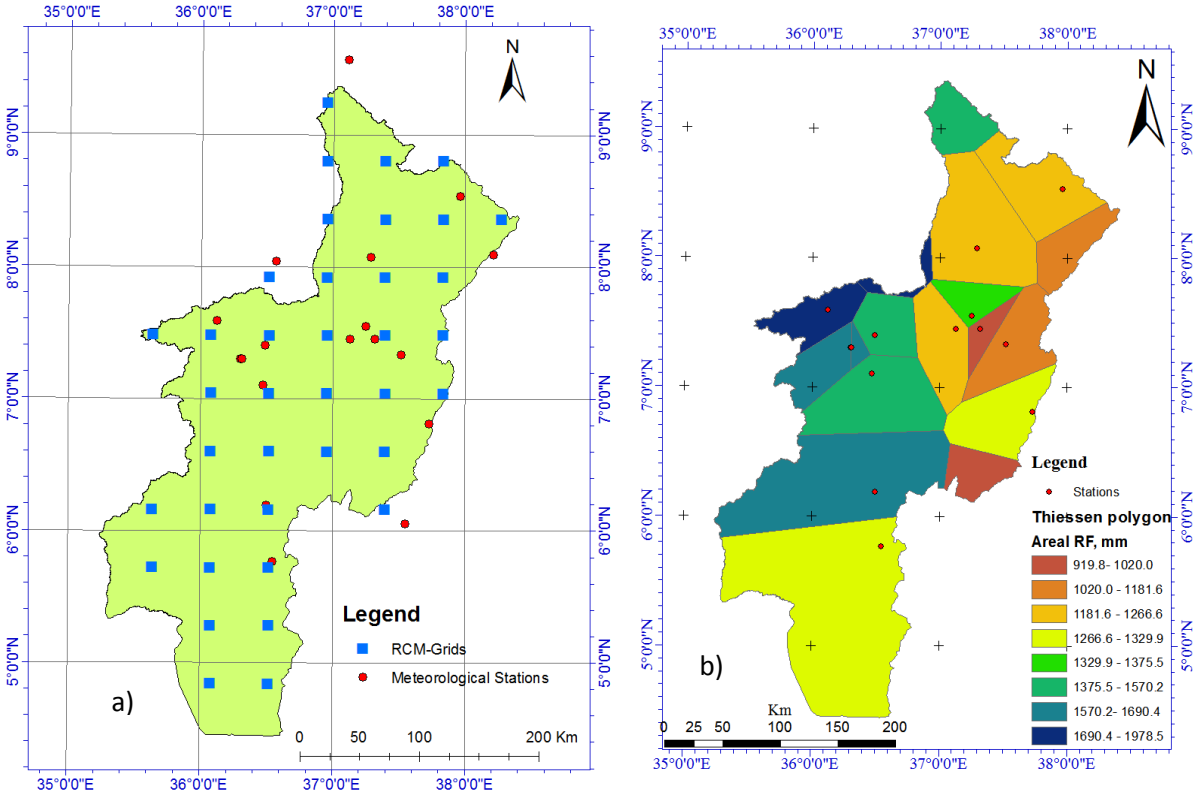

Figure: 3.5: a) Map showing meteorological stations and RCM grid points over the basin; (b) Thiessen polygon map established for representative stations

Table: 3.5 Representative stations and Corresponding RCM grid points

S.N	Station	Description of corresponding RCM out puts				Area, km^2 of each polygon
		Grid Code	Latitude	Longitude	Elev. (m)	
1	Arbaminch	GP[2]111208	6.16	37.40	1637.79	1900.4
2	Asendabo	GP110211	7.48	36.96	1815.11	3598.5
3	Bonga	GP108210	7.04	36.08	1575.54	2501.2
4	Bulki (Mindre)	GP109208	6.16	36.52	1196.30	11879.8
5	Butajira	GP112212	7.92	37.84	2084.56	2493.9
6	Chida	GP109210	7.04	36.52	1597.84	6207.5
7	Gatira	GP108211	7.04	36.08	1575.54	2618.3
8	Hosana	GP111210	7.04	37.40	1660.39	3820.6
9	Jimma	GP109211	7.04	36.52	1597.84	2471.3
10	Jinka	GP109207	5.72	36.52	1017.39	17961.0
11	Kumbi	GP111212	7.92	37.40	1916.55	7499.3
12	Limu Genet	GP109212	7.92	36.52	1938.00	588.0
13	Sokoru	GP111212	7.92	37.40	1916.55	1675
14	Shambu	GP110215	9.24	36.96	1907.67	2382.8
15	Shebe	GP109211	7.48	36.52	1857.95	354.8
16	Woliso Giyon	GP112213	8.36	37.84	2115.13	4706.6
17	Wolita Sodo	GP112210	7.04	37.84	1785.02	4199.8
18	Yayaotana	GP111211	7.48	37.40	1839.43	973.8

3.4 Preparation of data

3.4.1 Filling Missed data

For a missed data interpolation, Nearest Neighbor (NN) method was applied. NN interpolation method finds the closest subset of input samples to a query point and applies weights to them based on proportionate areas to interpolate a value. In other word NN method relays on the use of sampling point nearest to the missed point in estimating values where data gap exist. In principle, sampling points nearest to the missing point are considered in such a way that perpendicular bisectors are drawn between sampling points so as to form polygons. If these polygons are designated by V_i, V_2, $V_3 \ldots V_n$ and assuming points located in each of the polygons will have equal weight. The theoretical formulation of NN method according to (Li and Heap),

$$Z_o(x_o) = \sum_{i=1}^{n} \mu_i * Z(x_i) \qquad 3.1$$

$$\mu_i = \begin{cases} 1 & \text{if } x_i \in V_i \\ 0 & \text{otherwise} \end{cases}$$

[2] GP refers to Grid Point

Where: Z_o = estimated value of an attribute or variable at point of interest xo,

z = observed value at the sampled point (xi);

μ = weight assigned to the sampled point;

n = number of sampling points used for estimation;

x_i = represents geographic coordinate (x, y) at location i.

As shown on figure 3.1, the densities of raingauge stations over the basin are very poor besides of randomly distribution characteristics of existing stations. On the other hand, there is very diverse climatological pattern over the basin. High sacristy of data in existing stations over the basin also hinder the consideration of recommended threshold (radius of influence) in deciding neighboring stations for a given target point. Therefore, due to those constraints, NN interpolation method was adopted for this study. In doing so, special attention was also given to rainy season (Jun to September) as well as (March to May) as it is a period with high probability occurrence of maximum rainfall.

3.4.2 Outlier test

Outliers are data points which depart significantly from the trends of remaining data. For annual maximum daily based data series, the outlier tests were conducted for those 18 representative stations of both observed and projected data series of the basin according to (Water Resources Council) equation

$$\left.\begin{aligned} X_H &= \overline{X} + K_n S_x \\ X_L &= \overline{X} - K_n S_x \end{aligned}\right\} \qquad 3.2$$

Where, X_H =High outlier threshhold in log units

X_L =Low outlier threshhold in log units

S_x= standrad deviation of X

K_n = Value for Sample size n

Graghical approach's was adopted for demonestration of existance of both high and low outliers in the data series. Accordingly, treatments for detected outlier values were carried out based on events of the same period of nieghboring stations. Because, outliers significantly affect the maginitude of statistical parametrs computed from the data series.

3.4.3 Checking Consistency of the data

Data consistency for each station with respect to other neighboring stations, were checked by establishing Double Mass Curve. This was achieved by plotting cumulative annual maximum rainfall for stations as ordinate and cumulative annual maximum rainfall of base stations as abscissa. Data consistency for a given station was evaluated by determining the correlation coefficient (R^2) between observed and predicted data. The evaluations were made for both baseline and projected period data series and presented graphically in section 4.1.2.

$$R^2 = \left(\frac{\sum_{i=1}^{n} \left(O_i - \overline{O}\right)\left(P_i - \overline{P}\right)}{\sqrt{\sum_{i=1}^{n} \left(O_i - \overline{O}\right)^2} \sqrt{\sum_{i=1}^{n} \left(P_i - \overline{P}\right)^2}} \right)^2 \qquad 3.3$$

Where O_i observed and P_i predicted values

3.5 Fitting a Probability Distribution

Probability distribution fitting was carried out just to define which particular distributions would automatically fit to a given set of data series. The annual maximum daily data series were extracted for the eighteen stations and were fitted to the most commonly used distribution functions namely; Gumbel, Log-Pearson type-III and Log normal distributions. The reliability of best fit probability distribution function was made based on Goodness of Fit (GOF) test criteria in terms of Kolmogorov-Smirnov (K-S), Anderson-Darling (A-D) and Chi-square criteria. This way of selecting fitting probability distributions was adopted because of fitting process relays on computations of fitness parameters based on sample data. This would assist to rank the fitted distributions according to quality of fit over the raw data. GOF tests measures the compatibility of a random sample with a theoretical probability distribution function. Moreover, the reliability of selected best fit probability distribution with a set of observed data was shown graphically by quintile- quintile (Q-Q) plot for visual demonstration.

3.5.1 Kolmogorov-Smirnov (K-S) Test

This test is used to decide if a sample comes from a hypothesized continuous distribution. It is based on the empirical cumulative distribution function (ECDF). Assume that we have a random sample $x_1, ...,x_n$ from some distribution with CDF $F(x)$. The empirical CDF is denoted by;

$$F_n(x) = \frac{1}{n}\,[Number\ of\ observations \leq x] \qquad 3.4$$

The Kolmogorov-Smirnov statistic (D) is based on the largest vertical difference between the theoretical and the empirical cumulative distribution function:

$$D = \max_{1 \leq i \leq n} \left(F(x_i) - \frac{i-1}{n}, \frac{1}{n} - F(x_i) \right) \qquad 3.5$$

3.5.2 Chi-Squared Test

The Chi-Squared test is used to determine if a sample comes from a population with a specific distribution. This test is applied to binned data, so the value of the test statistic depends on how the data is binned.

The data can be grouped into intervals of equal probability or equal width. Each bin should contain at least 5 or more data points, so certain adjacent bins sometimes need to be joined together for this condition to be satisfied. Although there is no optimal choice for the number of bins (k), there are several formulas which can be used to calculate this number based on the sample size (N)

$$K = 1 + \log_2 N \qquad 3.6$$

The Chi-Squared statistic is defined as;

$$x^2 = \sum_{i=1}^{K} \frac{(O_i - E_i)^2}{E_i} \qquad 3.7$$

Where O_i is the observed frequency for bin i, and E_i is the expected frequency for bin i calculated by;

$$E_i = F(x_2) - F(x_1) \qquad 3.8$$

Where F is the CDF of the probability distribution being tested, and x_1, x_2 are the limits for bin i.

3.5.3 Anderson-Darling Test

The Anderson-Darling procedure is a general test to compare the fit of an observed cumulative distribution function to an expected cumulative distribution function. This test gives more weight to the tails than the Kolmogorov-Smirnov test. The Anderson-Darling statistic (A^2) is defined as;

$$A^2 = -n - \frac{1}{n}\sum_{i=1}^{n}(2i-1) * \left[\ln F(x_i) + \ln(1 - F(x_{n-i+1}))\right] \quad 3.9$$

The fitting of observed data with respect to the best selected fitting function was presented as quantile-quantile (Q-Q) plot; which is a graph of the input (observed) data values plotted against the theoretical (fitted) distribution quantiles. Both axes of this graph is in units of the input data set (i.e. millimeters). The Q-Q plot helps to judge by visual inspection, which type of the distribution functions were appropriately fitted to the data.

$$F^{-1}(F_n(x_i) - \frac{0.5}{n} \quad 3.10$$

Where: $F^{-1}(x)$ — inverse cumulative distribution function (ICDF)

$F_n(x)$ — empirical CDF; n — sample size.

Some of the common probability distribution for fitting hydrological data with their corresponding equations for probability density function and equations for parameters in terms of the sample moments are;

a. Lognormal Distribution

If the random variable Y = log X is normally distributed, then X is said to be log normally distributed. Chow (1954) reasoned that this distribution is applicable to hydrologic variables formed as the products of other variables since if $X = X_1, X_2, X_3, \ldots X_n$;

Then $Y = \log X = \sum_{i=1}^{n} \log X_i = \sum_{i=1}^{n} Y_i$ which tends to the normal distribution for large n provided that the X_i- are independent and identically distributed. Its probability density function is given as;

$$f(x) = \frac{1}{x\sigma\sqrt{2\pi}} \exp\left(-\frac{(y - \mu_y)}{2\sigma_y^{\,2}}\right); x > 0 \quad 3.11$$

Where, $y = \log x$; $\mu_y = \overline{Y}$; and $\sigma_y = \delta_y$

b. Log-Pearson Type III Distribution

If log *X* follows a Pearson Type III distribution, then *X* is said to follow a Log-Pearson Type III distribution. This distribution is the standard distribution for frequency analysis of annual maximum floods in the United States (Benson, 1968), As described previously, the Log-Pearson Type III distribution was developed as a method of fitting a curve to data. Its use is justified by the fact that it has been found to yield good results in many applications (Ven Te. Chow),

Its probability density function is given as;

$$f(x) = \frac{\alpha^{\beta}(y-\gamma)^{\beta-1}e^{-\alpha(1-\gamma)}}{x\Gamma(\beta)}; \log x \geq \gamma \qquad 3.12$$

$$\alpha = \frac{\delta_y}{\sqrt{\beta}}$$

Where, $\beta = \left[\frac{2}{C_s(y)}\right]^2$; and $y = \log x$ and assuming $C_s(y)$ is positive

$$\gamma = \overline{Y} - \delta_y\sqrt{\beta}$$

Where α , β and γ are the scale, shape and location parameters of the distribution and y= log(x), assuming the skeweness $C_s(y)$ is positive.

c. Gumbel's extreme value distribution

Gumbel Type I distribution, also known as the Extreme Value Type I distribution, is a two parameter distribution. One parameter is the most probable value of the distribution and the second is a measure of dispersion. Gumbel extreme value distribution has been widely used in hydrology and meteorology for prediction of flood peaks, maximum rainfall and wind speed (Chow *et al*., 1988). Analyzing data for the largest or smallest observations from sets of data became the basis for using the Gumbel (Extreme Value) Type I distribution. According to his theory of extreme events, the probability of occurrence of an event equal to or larger than a value xo is:

$$f(x) = \frac{1}{\sigma}\exp\left(-\frac{(x-\mu)}{\sigma} - \exp\left(-\frac{x-\mu}{\sigma}\right)\right); -\infty < x < \infty \qquad 3.13$$

Where; $\sigma = \frac{\sqrt{6}\delta_x}{\pi}$

$\mu = \overline{X} - 0.5772\sigma$

The parameter μ is the mode of the distribution (point of maximum probability density). A *reduced variate y* can be defined as;

$y = \frac{x-\mu}{\sigma}$; Solving the reduced variate and yields

$f(x) = \exp(-\exp(-Y))$; Solving for Y;

$$y = -\ln\left[\ln\left(\frac{1}{F(x)}\right)\right] \qquad 3.14$$

3.6 Computation of Extreme Values (X_T) Using Frequency Factors

Calculating the magnitudes of extreme events by probability distribution function method is recommended for those which are invertible. Calculating the magnitudes of extreme events requires that the probability distribution function be invertible, that is, given a value for *T* *or* $F(X_T) = \frac{T}{T-1}$, the corresponding value of X_T can be determined. Some probability distribution functions are not readily invertible, including the Normal and Pearson Type III distributions, and an alternative method of calculating the magnitudes of extreme events is required for these distributions (Chow et al., 1987). The magnitude X_T of a hydrologic event may be represented as the mean $\overline{X}$ plus the departure ΔX_T of the variate from the mean.

$$X_T = \overline{X} + \Delta X_T \qquad 3.15$$

The departure may be taken as equal to the product of the standard deviation δ and a *frequency factor* K_T, *that* is, $\Delta X_T = K_T\delta$, the departure and the frequency factor K_T are functions of the return period and the type of probability distribution to be used in the analysis. Therefore, it can be expressed as

$$X_T = \overline{X} + K_T\delta \qquad 3.16$$

$$\delta = \sqrt{\frac{\sum(x-\bar{x})^2}{N-1}} \qquad 3.17$$

$$\overline{X} = \frac{\sum_{i=1}^{n} X_i}{n} \qquad 3.18$$

For the Extreme Value Type I distribution,(Chow, 1953) derived the expression for frequency factor K_T;

$$K_T = -\frac{\sqrt{6}}{\pi}\left\{0.5772 + \ln\left[\ln\left(\frac{T}{T-1}\right)\right]\right\} \qquad 3.19$$

For Log-Pearson Type III Distribution: For this distribution, the first step is to take the logarithms of the hydrologic data, y = log *x*. Usually logarithms to base 10 are used. The mean $\overline{Y}$, standard deviation, δ and coefficient of skewness C_s are calculated for the logarithms of the data. The frequency factor depends on the return period *T* and the coefficient of skewness C_s. When $C_s \neq 0$, K_T is approximated by (Kite, 1977).

$$K_T = z + (z^2 - 1)k + \frac{1}{3}(z^3 - 6z)k^2 - (z^2 - 1)k^3 + zk^4 + \frac{1}{3}k^5 \qquad 3.20$$

$$\text{Where, } k = \frac{C_s}{6}$$

$$C_S = \frac{n\sum_{i=1}^{n}\left(Y_i - \overline{Y}\right)^3}{(n-1)(n-2)\delta_y^3} \qquad 3.21$$

For Log-normal distribution, the mean $\overline{Y}$; standard deviation δ; and coefficient of skewness C_s are calculated for the logarithms of the data and for a case, C_s, the frequency factor is equal to the standard normal variable z.

$$K_T = Z = \frac{X_T - \overline{X}}{\delta}; \textit{For} \text{ normal distribution}$$

For Log normal distribution, the following formula can be used for determining the frequency factor (K_T=Z):

$$z = w - \frac{2.515517 + 0.802853w + 0.01032w^2}{1 + 1.432788w + 0.18926w^2 + 0.001308w^3} \qquad 3.22$$

Where, w is intermediate variable which can be calculated using the following formula.

$$w = \left[\ln\left(\frac{1}{p^2} \right) \right]^{1/2} \qquad 3.23$$

$$(0 < p \leq 0.5)$$

For the lognormal distribution, Log Pearson Type III procedure is applied except the frequency factor $K_T = Z$; for $C_s = 0$, that it is applied to the logarithms of the variables

After identifying the best fit type of probability distribution for a given annual maximum observed data, the extreme rainfall events (X_T) was calculated for a return period of 2, 5, 10, 25, 50 and 100 years

3.7 Calculating Intensity of Rainfall (*i*)

For a given calculated extreme rainfall depth of a given return period, the corresponding intensity of rainfall was computed by;

$$i = \frac{R}{d} \qquad 3.24$$

Where, R is rainfall depth in mm and d is duration in hr. However, raw data collected from NMA were on daily base time series. In order to get fine resolution time series of data in minutes for analysis, annual maximum daily data were disaggregated in to the required time series (5, 10, 20, 30, 60, 90, 120 minutes) by using the relation recommended by (ERA 2013) drainage design manual.

$$RR_t = \frac{1}{24}\left(\frac{(b+24)^n}{(b+t)^n} \right) \qquad 3.25$$

Where, RR_t= Rainfall ratio; $R_t : R_{24}$

R_t = Rainfall in a given duration‘t’ in hours

R_{24} = Rainfall in 24 hours

t = time in hours

Based on studies of a large number of gauges in East Africa, b = 0.3, n = 0.9 ($0.78 \leq n \leq 1.09$)

3.8 Development of IDF curve

After the expected probable rainfall intensities were determined for a commonly used different return periods (2, 5, 10, 25, 50, and 100) years by equation for short durations by equation (3.15), outputs from extreme value analysis had been used for IDF curve developments. The procedures were repeated for each type of station used for this specific study.

Areal mean precipitations were also determined from these representative stations by using already extracted annual maximum rainfall for each station. Thiessen polygon mean method was adopted for the mean areal (basin wide) rainfall determination as long as the method gives some weightage factor to various stations based on rational basis. Further, the method could give a chance for raingauge stations outside the catchment. IDF curve for this representative mean areal rainfall for the study area was also developed. Mean areal storm was determined by;

$$\overline{P} = \frac{\sum_{i=1}^{M} P_i A_i}{A} = \sum_{i=1}^{M} P_i \frac{A_i}{A} \qquad 3.26$$

Where, Areal ratio $\frac{A_i}{A}$ is called the weightage factor for each station.

3.9 Bias Correction and projection

Data from the three RCP scenarios were not directly used for the analysis as it may have systematic error introduced from considered boundary condition and downscaling steps. In order to enhance RCM output resolution to the desired level, bias correction was therefore applied to compensate any significant deviation from observed data. In this study, Power transformation method which was used by (Biniyam and Kemal, 2017) for impact of climate change study on rainfall and flood frequency on Hare watershed in southern rift valley of Ethiopia. It is a nonlinear approach by its nature and the relation is given by;

$$p^{*} = a\, p^{b} \qquad 3.27$$

Where; P^{*} is corrected daily data in the projection period; a & b are parameters obtained from calibration in the baseline period and then subsequently applied to the projection period; whereas, p is daily precipitation amount of scenario data which is uncorrected. The parameters

(a & b) were obtained by conducting simple optimization algorithm on coefficient of variation and mean of observed and simulated data. It was achieved by taking;

$$\left.\begin{array}{l} CV_{observed} = CV_{RCM\ uncorrected} \ldots\ldots\ldots *; \text{ to fix the value of b} \\ M_{observed} = M_{RCM\ uncorrected} \ldots\ldots\ldots\ldots **; \text{ to fix the value of a} \end{array}\right\} \quad 3.28$$

CV is coefficient of variation whereas M refers to mean and the detail procedure followed on spread sheet was attached on the appendix 7.5 section.

$$CV = \frac{\delta}{M} \quad 3.29$$

δ is standard deviation and computed by equation 3.17 and M is average of sample data and computed by equation 3.18. Observed data of (1980-2005) for a baseline period corresponding to CORDEX historical run data of the same period were used for computation of values for a & b. Since the rainfall distribution is not uniform throughout the year, the daily data series were organized month by month; i.e. bias correction was made on the monthly basis; so that the constants (a & b) were determined for each month per a single station. This was achieved by optimizing the mean and coefficient of variation of scenario data of the same period to observed data of baseline period. After bias correction was carried out, the mean and standard deviation of scenario data would equal to the corresponding value of observed data. As a result, coefficient of variation of both observed and scenario data get equal which indicates perfect match between observed and historical scenario data of climate model data series

After bias correction, the projection was made for mid-21st century by using data of a time slice ranges (2040-2069). This is because; IPCC in its (AR5) report adopted a period of 2046-2065 for mid 21stcentury climate change projection. Moreover, (Prodanovic and Simonovic, 2007) used a period (2040-2069) for mid-21st century development of Intensity-Duration-Frequency curve under impact of climate change for city of London. Data sets of three RCP scenarios (RCP2.6, RCP 4.5, and RCP 8.5) were used for the analysis after bias correction had been applied.

The detected bias associated with Raw RCM data with respect to corresponding observed data were computed on the monthly bases by;

$$Bias = \frac{(R_{RCM} - R_{gauge})*100}{R_{gauge}} \qquad 3.30$$

Where: R represents monthly rainfall data, mm

3.10 Validation of climate model data with observed data

After bias correction steps, the historical observed data were compared with historical data of RCM model. For performance evaluation of the model, attempt was carried out by computing the error by calculating mean relative error for each month per stations.

$$\text{Mean Relative Error} = \frac{1}{n}\sum_{i=1}^{n}\left(\frac{Z_o(x_i) - Z(x_i)}{Z(x_i)}\right) \qquad 3.31$$

Where, n is number of data points

Z_o is historical scenario data after optimization algorithm were carried out

Z is historical observed data

x_i is day of month i

Once data series of historical period were corrected, raw RCM model outputs under future climate were further bias corrected by equation 3.27 before any analysis was conducted. Then, similar procedures were followed to construct IDF curve of projected period.

Typical isoheytal line for the study area were established by using both observed and projected extreme data of 25, 50, 100 years return period for events assumed to have a duration of 20 minute to see a potential spatial change of rainfall intensities due to impact of climate change over the study area.

4 Results and Discussions

4.1 Analysis of rainfall data

4.1.1 Interpolation of missed data

Before any analyses were started, interpolation of sample data for non-recorded values was one critical step in data preparation. The result obtained through interpolation steps were tabulated as follows.

Table: 4.1 Summary of result of interpolation

S. N	Station	Variable	Total Obser.	Missed Obser.	before interpolation			After interpolation		
					Mean	Std. dev.	CV	Mean	Std. dev.	CV
	Col-1	Col-2	Col-3	Col-4	Col-5	Col-6	Col-7	Col-8	Col-9	Col-10
1	Arbaminch	Rainfall	12419	1585	2.527	6.877	2.72	2.481	6.967	2.81
2	Asendabo	"	12419	1311	3.284	7.437	2.26	3.258	7.477	2.29
3	Bonga	"	12419	1140	4.662	7.559	1.62	4.589	7.412	1.62
4	Bulki (Minder)	"	12419	1704	4.579	8.514	1.86	4.628	8.775	1.90
5	Butajira	"	12419	1399	3.023	7.353	2.43	2.955	7.251	2.45
6	Chida	"	12419	2181	4.247	8.509	2.00	4.079	8.507	2.09
7	Gatira	"	12419	1170	5.356	9.067	1.69	5.228	8.931	1.71
8	Hosana	"	12419	359	3.358	7.132	2.12	3.331	7.095	2.13
9	Jimma	"	12419	447	4.169	7.829	1.88	4.175	7.848	1.88
11	Jinka	"	12419	349	3.580	7.831	2.19	3.576	7.801	2.18
11	Kumbi	"	12419	896	3.459	8.010	2.32	3.389	7.932	2.34
12	Limu Genet	"	12419	2247	5.370	9.721	1.81	5.172	9.522	1.84
13	Sekoru	"	12419	221	3.816	7.516	1.97	3.801	7.508	1.98
14	Shambu	"	12419	1608	4.246	8.141	1.92	4.139	7.987	1.93
15	Shebe	"	12419	1667	4.310	7.713	1.79	4.379	7.677	1.75
16	Woliso Giyon	"	12419	1329	3.422	7.126	2.08	3.411	7.135	2.09
17	Wolaita Sodo	"	12419	281	3.514	8.264	2.35	3.494	8.300	2.38
18	Yayaotena	"	12419	195	2.834	7.187	2.54	2.826	7.167	2.54

The result shows statistical parameters such as mean, standard deviation and coefficient of variation of recorded data (before interpolation) and data after interpolation. When col-7 and col-10 are compared, they are somewhat similar. This shows that data after interpolations shows good agreement and well match with the nature of recorded data. Since, coefficient of variation

(CV) measures the dispersion of data points in a data series around the mean[3]. So that it is a useful statistics for comparing the degree of variation from one data series to another.

4.1.2 Checking Consistency of the data

The double mass curve which is the plot of the annual cumulative average rainfall data of the total Omo-Gibe basin with respect to annual cumulative rainfall data of each station. Accordingly, the graph of double mass curve plotted for Jimma and Jinka stations were as shown below. It was found that almost linear for all the considered stations with a coefficient of correlation R^2 ranges between (0.998-0.999). This indicated that the annual maximum observed data over the basin were consistent for all selected stations over considered period.

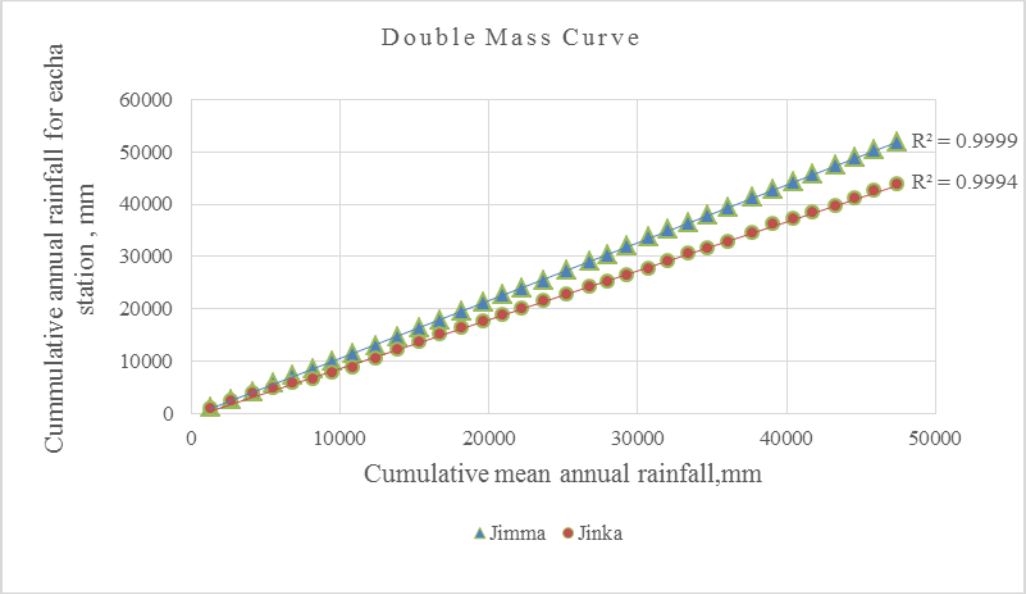

Figure: 4.1 Double Mass Curve analysis result for selected representative station

[3] https://www.investopedia.com/terms/c/coefficientofvariation.asp

4.1.3 Outliers test Result

Outlier test was conducted for annual maximum of both baseline and projected periods of 34 and 30 years' data series respectively. This was just to use well distributed sample data for frequency analysis or to remove data which much significantly depart from distribution of other sample data. For simple illustration, the following figure depicts outlier test results of Jimma station.

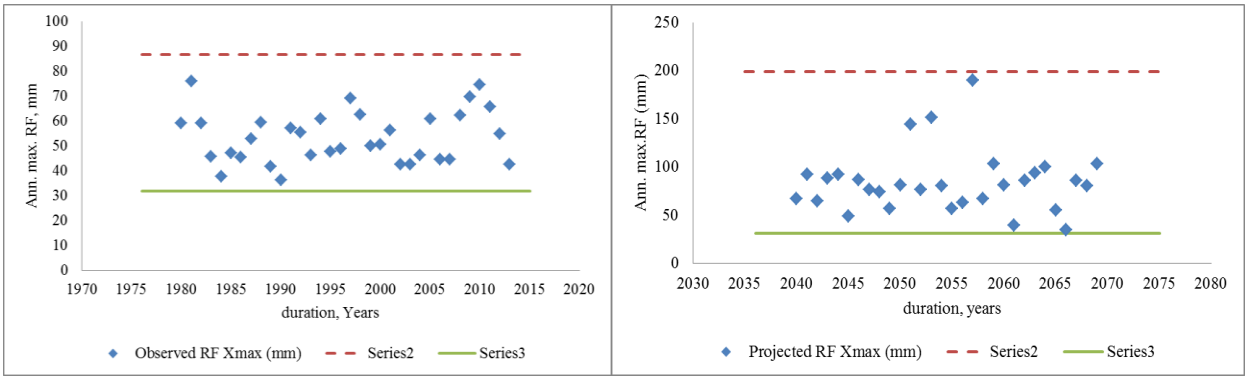

Figure: 4.2 Outlier test results of both baseline and projected period of Jimma station

Table: 4.2 Outlier test result for representative stations over study area

		Baseline Period (1980- 2013)				Projected Period (2040- 2069)				Remark
S.N	Station	Max	Min	X_H	X_L	Max	Min	X_H	X_L	
1	Arbaminch	79.00	56.00	81.00	50.50	172.29	34.46	172.89	24.26	No outliers
2	Asendabo	95.50	27.40	132.30	24.10	162.62	32.63	266.93	26.85	"
3	Bonga	65.500	28.00	79.15	25.79	85.77	32.15	101.32	24.65	"
4	Bulki(Minder)	93.50	35.20	113.81	30.29	208.34	32.89	291.86	21.60	"
5	Butajira	108.20	34.90	116.35	25.53	184.94	16.19	251.49	12.07	"
6	Chida	91.70	32.20	132.93	26.33	250.26	40.45	304.52	25.69	"
7	Gatira	80.50	38.80	83.89	34.69	137.46	36.93	140.06	33.28	"
8	Hosana	94.10	33.50	102.40	22.61	171.64	27.20	273.22	16.94	"
9	Jimma	75.90	36.30	86.63	31.74	189.92	34.37	194.34	29.58	"
10	Jinka	80.90	32.30	109.02	29.16	150.07	33.73	166.51	21.07	"
11	Kumbi	129.00	43.30	146.13	30.65	140.61	28.74	178.72	27.91	"
12	Limu Genet	93.70	35.50	106.99	34.04	149.77	36.94	152.74	31.76	"
13	Sokoru	72.70	31.60	87.69	26.74	112.61	26.11	156.91	21.16	"
14	Shambu	91.30	38.50	91.47	31.22	167.74	34.95	175.49	26.55	"
15	Shebe	108.00	34.00	112.17	24.51	151.48	31.31	170.28	25.17	"
16	Woliso Giyon	76.40	31.30	85.59	28.02	184.89	29.02	201.12	23.38	"
17	Wolaita Sodo	117.20	32.70	129.13	28.66	132.34	31.10	147.02	23.61	"
18	Yayaotena	110.50	36.30	129.64	23.55	170.84	33.21	199.98	26.45	"
Areal Precipitation		69.1	49.5	73.1	47.5	109.3	49	119.6	43.4	"

As it was shown in the above, outliers were carried out for data sets of baseline and projected period. In doing so, all data were inspected for both outliers. For detected value, events of the same period nearby stations were considered for treatments of the value. The test result indicated that, the most severe storm recorded over the basin were within a range of (65.5-129) mm and the most severe storm expected in a near future under the impact of climate change over the basin ranges between (85.77-250) mm. Accordingly, all data were examined for both upper and lower bounds and no outliers were detected in data being used for frequency analysis.

4.2 Rainfall characteristics over the basin

4.2.1 Temporal Rainfall Variability

Rainfall distribution in space and time by its nature is variable. As stated above, rainfall distribution pattern over Ethiopia is highly variable in spatial, seasonal and time. For figurative illustration of distribution pattern of rainfall, daily based hyetographs of some of the selected stations of a period (1980-2013) were presented here under the following.

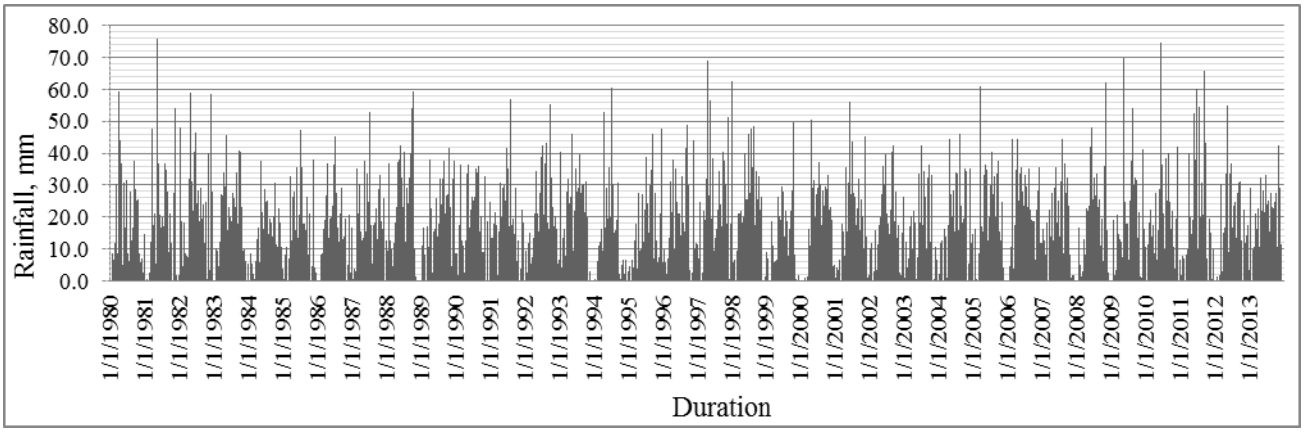

Figure: 4.3 Daily rainfall recorded in Jimma station for a period 1980-2013

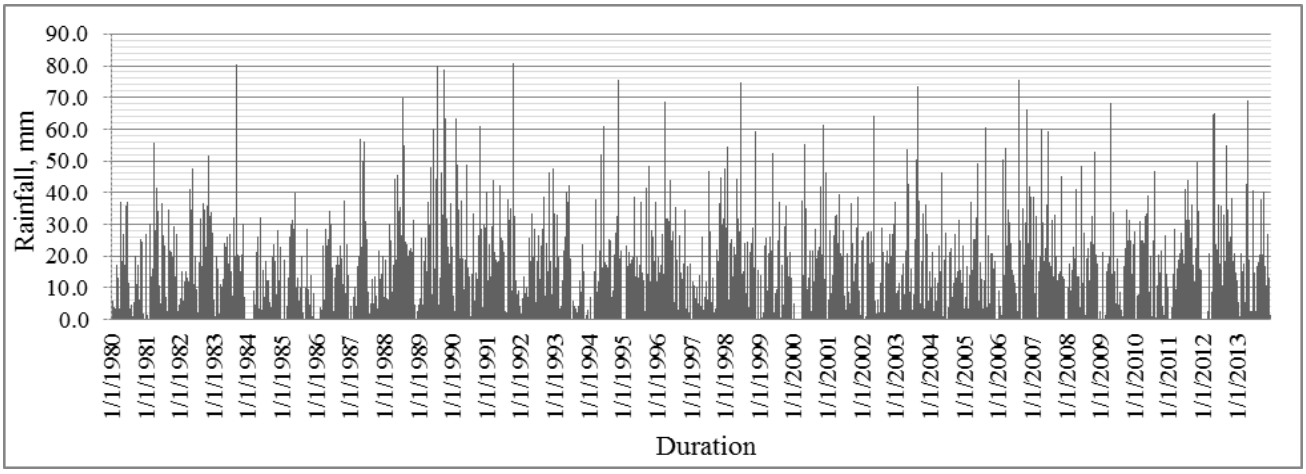

Figure: 4.4 Daily rainfalls recorded in Jinka station for a period 1980-2013

As indicated in the figure above, the timely variation of rainfall of the two stations is different as the gap between the bar graph is different for the two stations. The magnitude of the rainfall also shows variations for the two stations. However, the variability of rainfall with time, season and space over the basin could be clearly understood form mean monthly rainfall. For clear understanding, those stations which receive somewhat similar annual rainfall over the basin were categorized together and presented on the same graph as follows.

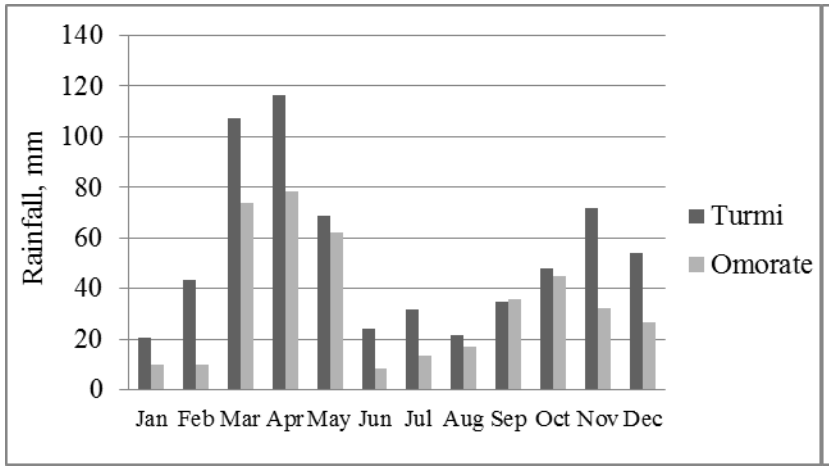

a) Mean monthly rainfall for stations with mean annual rainfall of 425.9-741.7mm

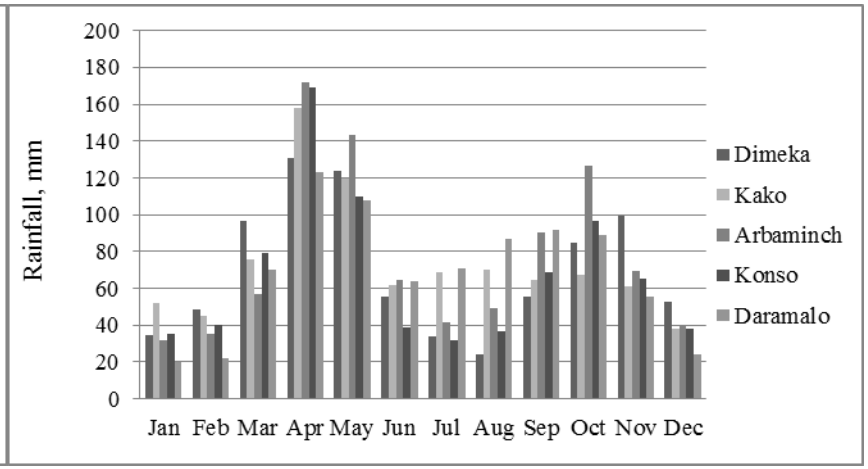

b) Mean monthly rainfall for stations with mean annual rainfall of 741.7-952.4 mm

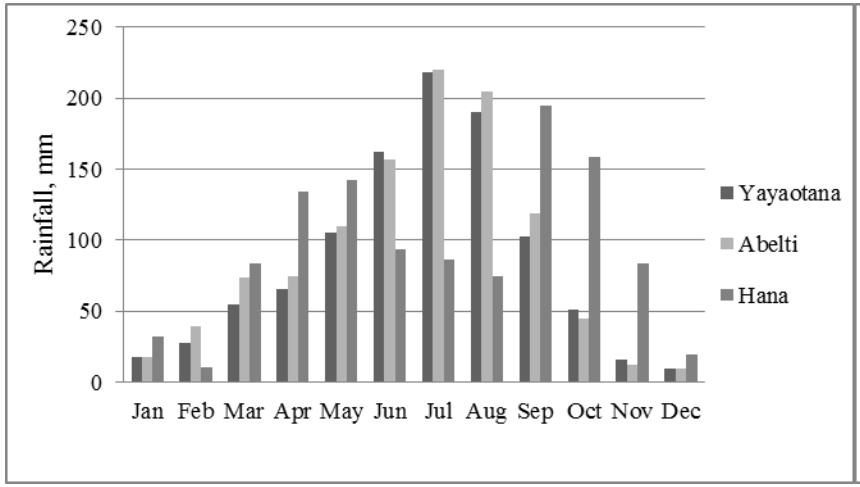

c) Mean monthly rainfall for stations with mean annual rainfall of 952.4-1144.4mm

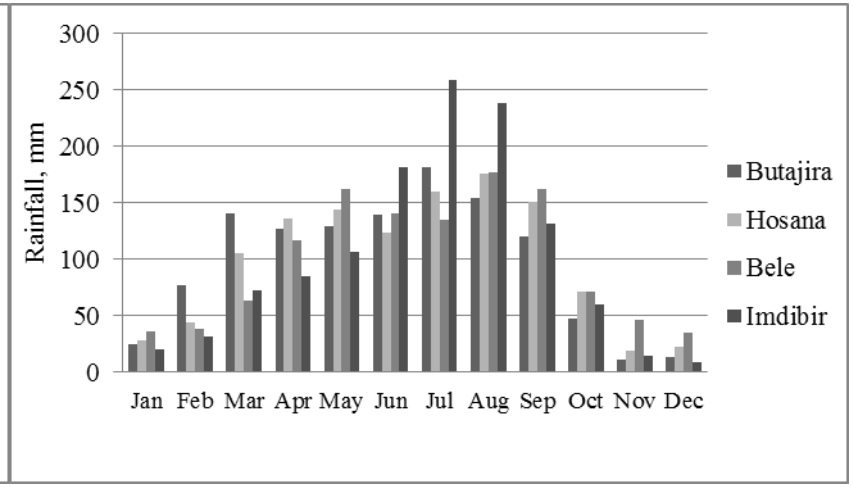

d) Mean monthly rainfall for stations with mean annual rainfall of 1144.4-1210 mm

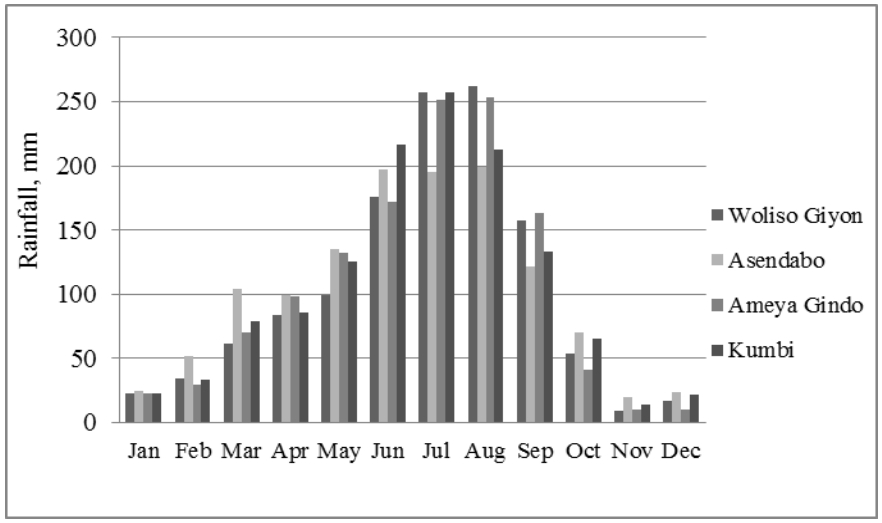

e) Mean monthly rainfall for stations with mean annual rainfall of 1210-1285.6 mm

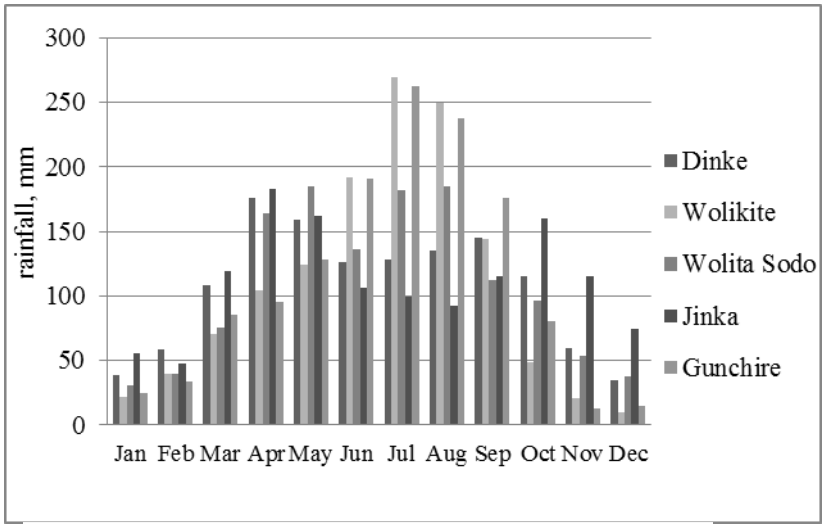

f) Mean monthly rainfall for stations with mean annual rainfall of 1280.6-1340 mm

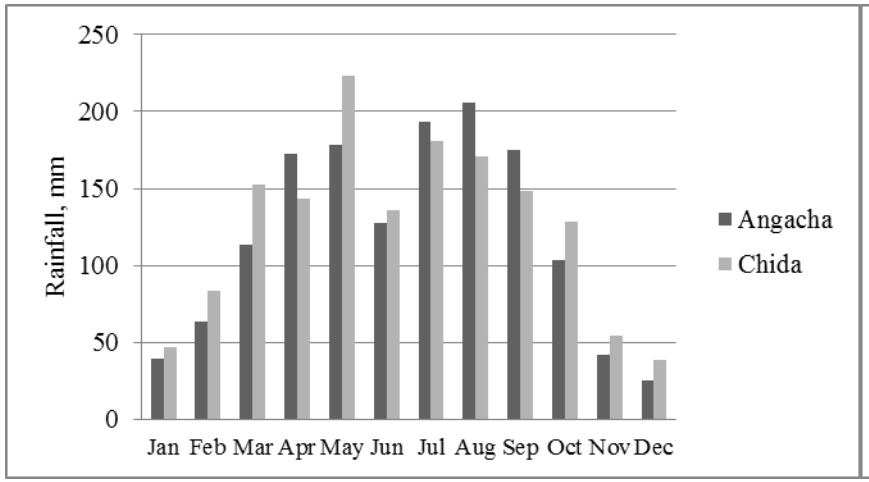

g) Mean monthly rainfall for stations with mean annual rainfall of 1385.9-1522.2 mm

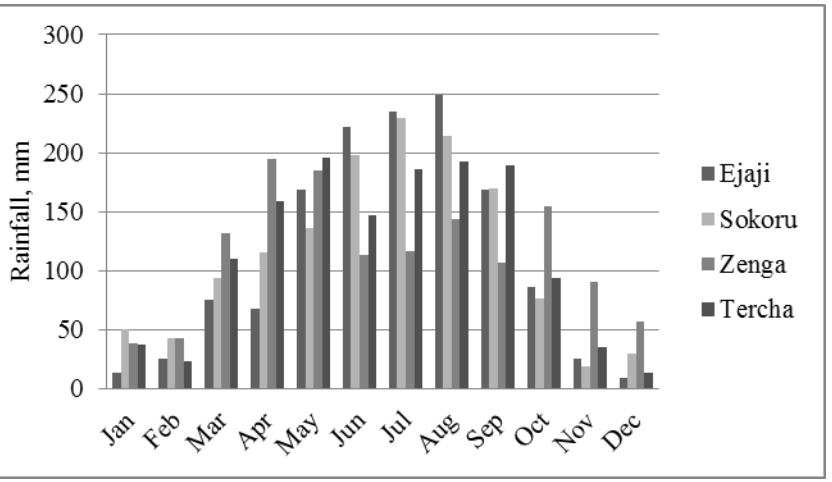

h) Mean monthly rainfall for stations with mean annual rainfall of 1340-1385mm

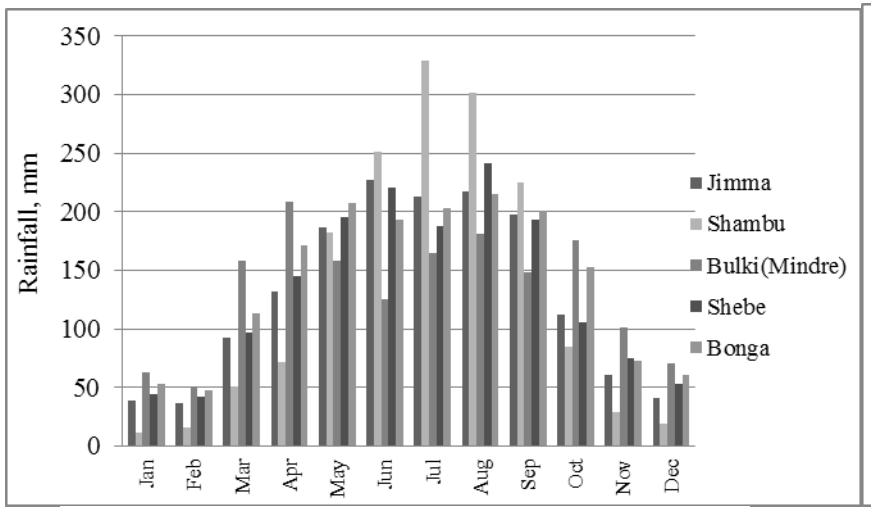

h) Mean monthly rainfall for stations with mean annual rainfall of 1522.2-1702 mm

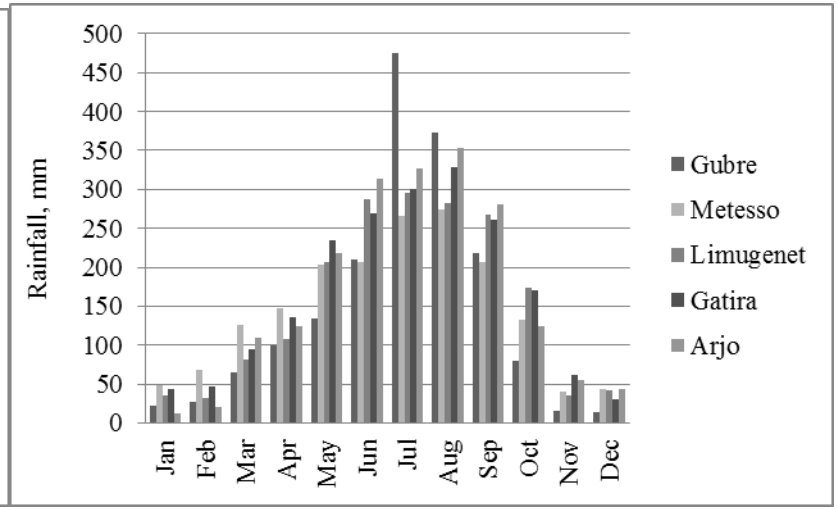

h) Mean monthly rainfall for stations with mean annual rainfall of 1702-2005.3 mm

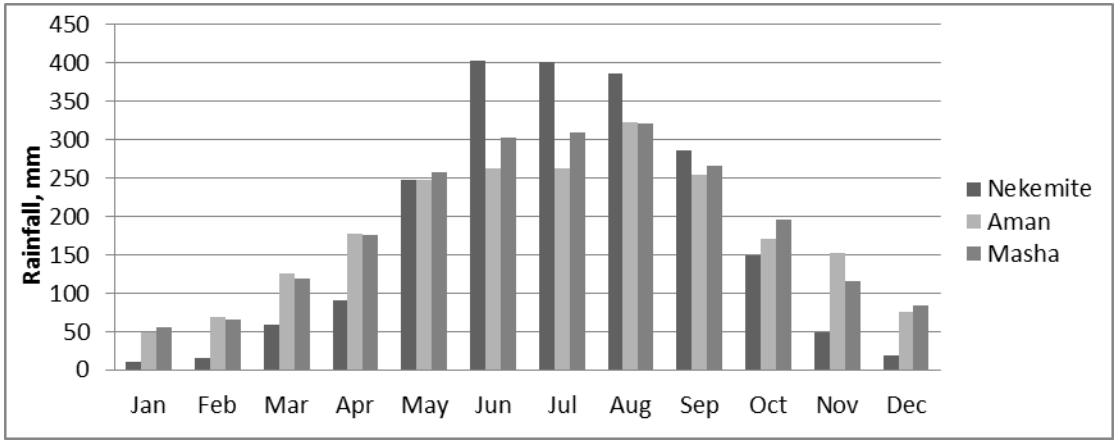

h) Mean monthly rainfall for stations with mean annual rainfall of 2005.3-2269.2 mm

Figure 4.5: Mean annual rainfall of stations relatively receive similar rainfall pattern

4.2.2 Spatial variability of rainfall over Omo-Gibe basin

A number of studies conducted over Ethiopia including (EPCC 2015) with regard to spatial variability rainfall indicated that spatial variation of rainfall is highly depending up on topography of the area. IDW average interpolation method was applied to show spatial variation of rainfall over the total basin in terms of mean annual precipitation.

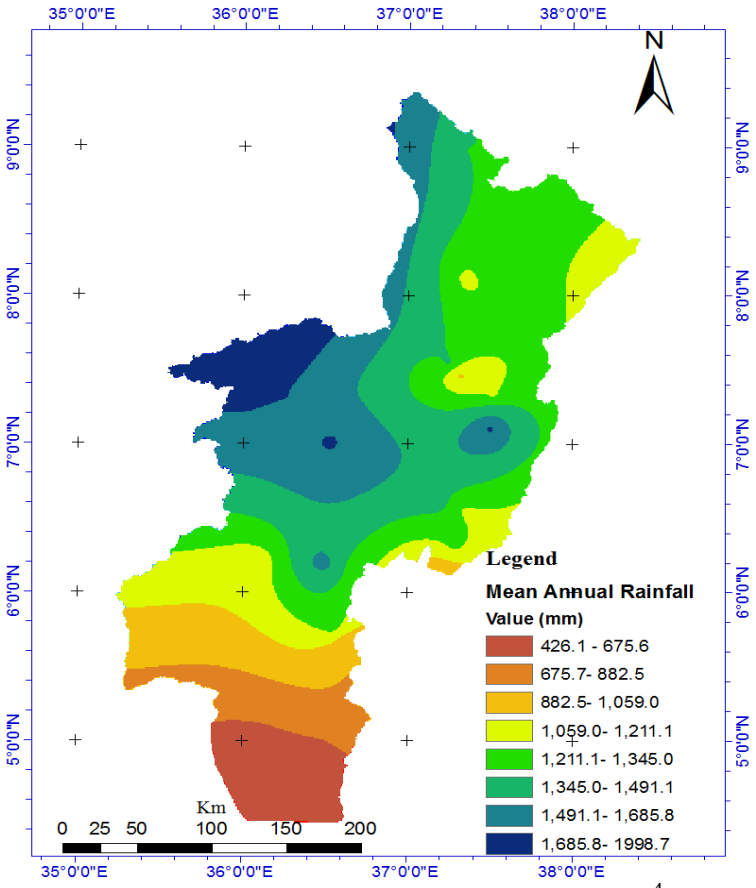

Figure: 4.6 spatial distribution of rainfall pattern over Omo-Gibe basin[4]

The result of the analysis as shown in figure 4.6 central western and North West highland regions of the study area received mean annual rainfall ranges between 1490-2000 mm. However, majority of the basin particularly, north eastern and most of central region of the basin received mean annual rainfall between 1211.1-1490 mm. Some of the southern low land region which is under category of hot arid region of the study area received mean annual rainfall less than 1000 mm. Generally, characteristics of rainfall distribution pattern and its spatial distribution over Omo-Gibe river basin varied with the variation of topography. As long as the

[4]Forty-two (42) stations were taken for the analysis to see the spatial distribution of rainfall over the total basin in terms of mean annual rainfall

examination of figure presented above revealed significant spatial variability, providing respective managements of water resources system is very important over the basin.

4.2.3 Rainfall characteristics of representative stations

For the total stations under consideration, attempt was made to summarize rainfall characteristic in terms mean annual rainfall observed for the last three decades. Besides, the most severe (maximum and minimum) rainfall magnitude in a observed annually was the corresponding maximum and minimum

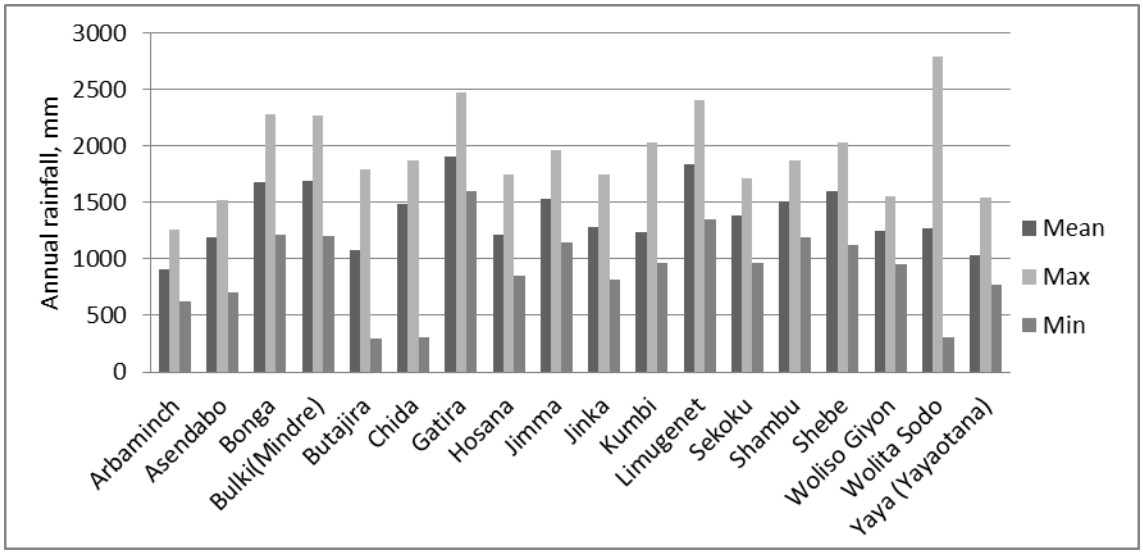

Figure: 4.7 annual rainfall characteristics of representative stations for study area

4.2.4 Rainfall variability and its trends over the study area

Rainfall variability for baseline period (1980-2013) of selected stations was examined by using historical observed data collected from NMA for 18 stations. As it can be seen from figure 4.7, Omo-Gibe basin has experienced both dry and wet years over the last 34 years. Years like 1984, 1985, 1987, 1999, 2000, 2004 and 2009 were dry while 1981, 1982, 1988, 1989, 1998, 2001 and 2006 were wet years. Generally, trend analysis of annual rainfall shows declining as shown below when averaged over total basin. Whereas, when it has been seen at a single station level, the trend analysis show both increasing for Limu Genet, Gatira, Jinka, Kumbi and decreasing trend for Hosana, Bulki (Minder), Woliso Giyon, Yayaotana.

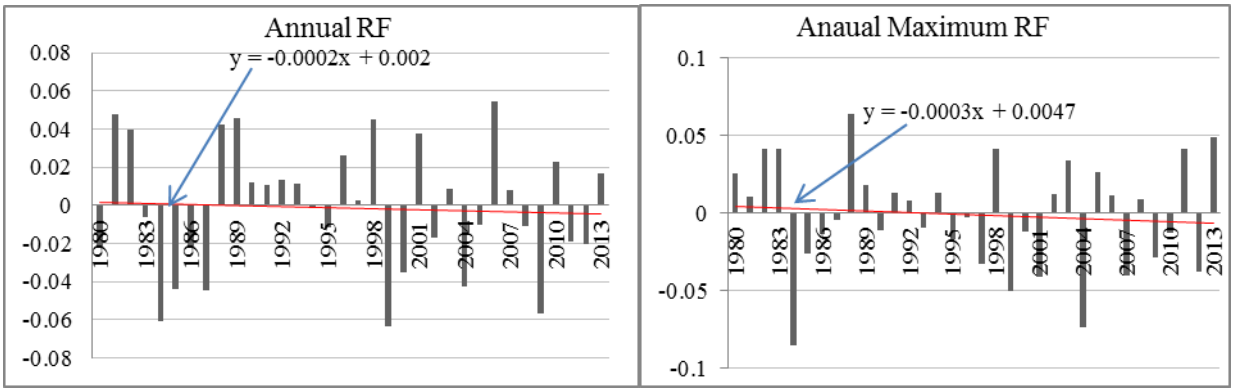

a) b)

Figure: 4.8 Year to year variability of annual rainfall and annual maximum of the basin & their corresponding trend expressed in normalized deviation

As shown in figure 4.8 b), annual maximum variability trend shows somewhat decreasing trend when viewed over total basin. The analysis result of 18 stations indicated that, the occurrence of severe storm for stations in the western and southern part of the basin shows increasing trend. Whereas, stations in the northern and central part of north east region of Omo-Gibe basin shows declining trend. Figure 4.9 shows part of the basin experienced increasing and decreasing trend of extreme rainfall for the last 34 years over the basin.

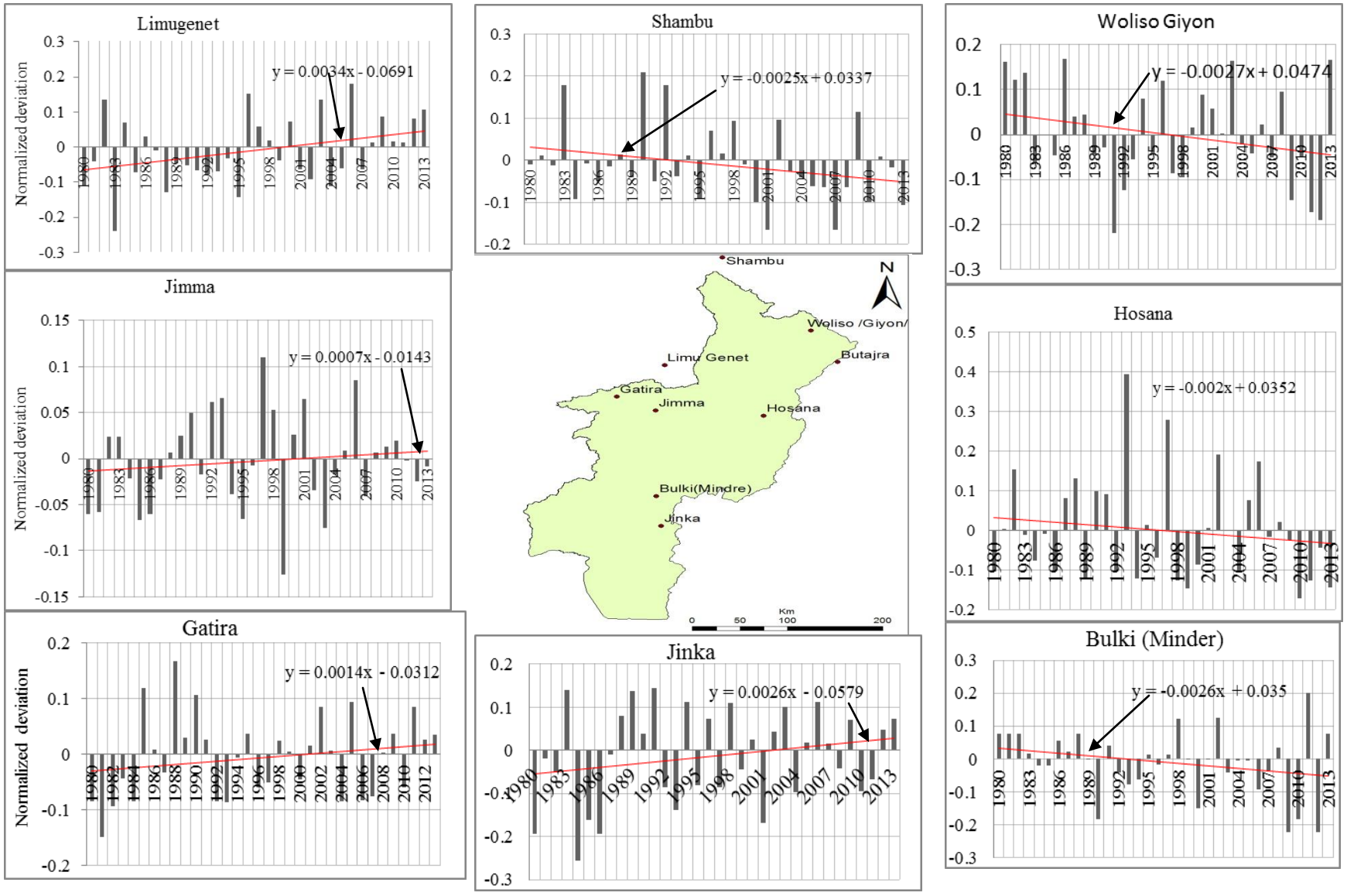

Figure: 4.9 Year to year variability and its trends of annual maximum rainfall of some of selected stations for Omo-Gibe basin expressed in normalized deviation

4.3 Comparison and selection of best fit Probability Distribution Functions

Frequency analyses of hydrologic and meteorological data use probability distributions to relate the magnitude of extreme events to their frequency of occurrence. In this research work, Extreme value Type-I (Gumble, Log pearson type III and Lognormal distribution were considered and the comparison was made based on Goodness of test result.

Test scores ranging from one to three (1-3) is awarded to each distribution type based on the criteria that the distribution with the highest total score is chosen as the best distribution type firstly, secondly and thirdly, respectively. In general, the distribution with highest statistic value was awarded a score of three (3), the next best is awarded two (2), and one (1). Three (3) point was given for the one with first rank; two (2) point was for the second rank and one (1) point was given for the one with the third rank. Then, the overall rank was based up on the total score earned form Kolmogorov S., Anderson D. Chi-squared (goodness of test) criteria. The overall ranking result which indicates the best-fit probability distribution types for each station was presented in Table 4.3 below.

Table: 4.3 Summary of Selection of fitting distribution function result for all station

Station	Distribution	Parameter	Goodness of Test						Total score	Rank
			Kolmogorov S.		Anderson D.		Chi-squared			
			Statistic	R	Statistic	R	Statistic	R		
Arbaminch	EV-I (Gumbel's)	σ=12.972 μ=52.845	0.09889	3	0.45964	3	0.81587	3	3	3
	Log Pearson-III	α=610.33 β=0.01104 γ=-2.676	0.09095	1	0.32751	1	0.14475	1	**9**	**1**
	Lognormal	σ=0.26875 μ=4.0637	0.09662	2	0.34055	2	0.75456	2	6	2
Asendabo	EV-I (Gumbel's)	σ=15.354 μ=50.558	0.09008	2	0.37199	2	0.8839	2	6	2
	Log Pearson-III	α=453.89 β=0.01529 γ=-2.906	0.08634	1	0.34526	1	0.91781	3	**7**	**1**
	Lognormal	σ=0.32086 μ=4.033	0.09157	3	0.3966	3	0.88189	1	5	3
Chida	EV-I (Gumbel's)	σ=14.487 μ=53.538	0.1562	3	0.92404	3	0.36926	1	5	3
	Log Pearson-III	α=66.883 β=-0.03784 γ=6.611	0.15229	2	0.80184	2	5.9119	2	6	2
	Lognormal	σ=0.30485 μ=4.0804	0.14917	1	0.78606	1	5.9459	3	**7**	**1**
Bonga	EV-I (Gumbel's)	σ=12.972 μ=52.845	0.09889	3	0.45964	3	0.81587	3	3	3
	Log Pearson-III	α=610.33 β=0.01104 γ=-2.676	0.09095	1	0.32751	1	0.14475	1	**9**	**1**
	Lognormal	σ=0.26875 μ=4.0637	0.09662	2	0.34055	2	0.75456	2	6	2
Bulki(Minder)	EV-I (Gumbel's)	σ=11.782 μ=53.732	0.12224	3	0.67658	3	1.7316	3	3	3
	Log Pearson-III	α=91.971 β=-0.0264 γ=6.4989	0.10753	1	0.42295	1	1.509	2	**8**	**1**
	Lognormal	σ=0.24924 μ=4.0727	0.11648	2	0.45697	2	1.0956	1	7	2
Butajira	EV-I (Gumbel's)	σ=14.188 μ=48.72	0.17472	2	0.72461	2	6.3872	3	5	2
	Log Pearson-III	α=8.3138 β=0.10054 γ=3.1624	0.14485	1	0.45948	1	3.8289	1	**9**	**1**
	Lognormal	σ=0.28559 μ=3.9982	0.19124	3	0.86831	3	6.2453	2	4	3
Gatira	EV-I (Gumbel's)	σ=7.4181 μ=50.424	0.11237	3	0.56031	3	3.6873	3	3	3
	Log Pearson-III	α=32.949 β=0.0294 γ=3.0191	0.09783	1	0.49632	1	3.4011	2	**8**	**1**

	Lognormal	σ=0.16628 μ=3.9879	0.10912	2	0.55848	2	1.6138	1	7	2
Hosana	EV-I (Gumbel's)	σ=14.641 μ=43.734	0.14145	3	0.95208	3	2.2246	2	4	3
	Log Pearson-III	α=3.155 β=0.16951 γ=3.3711	0.08995	1	0.26674	1	0.66843	1	**9**	**1**
	Lognormal	σ=0.29664 μ=3.9059	0.14001	2	0.88529	2	2.9821	3	5	2
Jimma	EV-I (Gumbel's)	σ=12.972 μ=52.845	0.09889	3	0.45964	3	0.81587	3	3	3
	Log Pearson-III	α=610.33 β=0.01104 γ=-2.676	0.09095	1	0.32751	1	0.14475	1	**9**	**1**
	Lognormal	σ=0.26875 μ=4.0637	0.09662	2	0.34055	2	0.75456	2	6	2
Jinka	EV-I (Gumbel's)	σ=10.885 μ=51.805	0.12974	3	0.95133	3	4.7796	3	3	3
	Log Pearson-III	α=26.74 β=-0.04875 γ=5.3354	0.09467	1	0.33892	1	0.85682	1	**9**	**1**
	Lognormal	σ=0.24831 μ=4.0322	0.10523	2	0.45685	2	1.6102	2	6	2
Kumbi	EV-I (Gumbel's)	σ=12.972 μ=52.845	0.09889	3	0.45964	3	0.81587	3	3	3
	Log Pearson-III	α=610.33 β=0.01104 γ=-2.676	0.09095	1	0.32751	1	0.14475	1	**9**	**1**
	Lognormal	σ=0.26875 μ=4.0637	0.09662	2	0.34055	2	0.75456	2	6	2
Limu Genet	EV-I (Gumbel's)	σ=10.678 μ=55.604	0.09994	1	0.36198	1	1.3559	1	**9**	**1**
	Log Pearson-III	α=854.99 β=0.00749 γ=-2.301	0.11556	2	0.3793	2	1.3764	2	6	2
	Lognormal	σ=0.21565 μ=4.1001	0.1211	3	0.409	3	2.722	3	3	3
Shambu	EV-I (Gumbel's)	σ=12.972 μ=52.845	0.09889	3	0.45964	3	0.81587	3	3	3
	Log Pearson-III	α=610.33 β=0.01104 γ=-2.676	0.09095	1	0.32751	1	0.14475	1	**9**	**1**
	Lognormal	σ=0.26875 μ=4.0637	0.09662	2	0.34055	2	0.75456	2	6	2
Sokoru	EV-I (Gumbel's)	σ=12.972 μ=52.845	0.09889	3	0.45964	3	0.81587	3	3	3
	Log Pearson-III	α=610.33 β=0.01104 γ=-2.676	0.09095	1	0.32751	1	0.14475	1	**9**	**1**
	Lognormal	σ=0.26875 μ=4.0637	0.09662	2	0.34055	2	0.75456	2	6	2
Shebe	EV-I (Gumbel's)	σ=12.902 μ=46.103	0.15337	1	0.62593	2	0.91646	1	**8**	**1**
	Log Pearson-III	α=11.723 β=0.08244 γ=2.9736	0.15552	2	0.62166	1	2.1184	2	7	2

	Lognormal	σ=0.27808 μ=3.94	0.17305	3	0.69702	3	2.4519	3	3	1
Wolaita Sodo	EV-I (Gumbel's)	σ=12.972 μ=52.845	0.09889	3	0.45964	3	0.81587	3	3	3
	Log Pearson-III	α=610.33 β=0.01104 γ=-2.676	0.09095	1	0.32751	1	0.14475	1	**9**	**1**
	Lognormal	σ=0.26875 μ=4.0637	0.09662	2	0.34055	2	0.75456	2	6	2
Woliso /Giyon/	EV-I (Gumbel's)	σ=9.7349 μ=46.834	0.09643	1	0.42771	3	2.444	2	6	2
	Log Pearson-III	α=7975.3 β=-0.00266 γ=25.17	0.10739	2	0.34548	1	1.6509	1	**8**	**1**
	Lognormal	σ=0.23431 μ=3.9326	0.10812	3	0.35559	2	2.7499	3	4	3
Yayaotana	EV-I (Gumbel's)	σ=16.717 μ=48.759	0.1216	3	0.73087	2	2.0911	3	4	3
	Log Pearson-III	α=6.4561 β=0.12828 γ=3.1838	0.07778	1	0.31641	1	2.0047	2	**8**	**1**
	Lognormal	σ=0.32112 μ=4.012	0.10421	2	0.80132	3	1.8673	1	6	2

Accordingly, all GOF test criteria confirmed Log-Pearson Type III with a first rank for ten stations of the total. Whereas, for other stations, two criteria (K-S and A-D) and (A-D and Chi-square) with first rank confirmed the distribution for five stations. On the other hand, three criteria confirm Gumble's distribution with first rank for Limu Genet; whereas K-S and Chi-square confirmed it for Shebe station with first rank. The result also shown that, K-S scored first rank in all selected best fitted distributions. This conforms the recommendation by (Mehrannia and Pakgohar, 2014). Therefore, it can be concluded as K-S is the most important criteria which should be considered in selecting theoretical distribution for annual maximum rainfall data series.

Overall result indicated that, compatibility of sample data to Log Pearson Type III probability distribution occupying 83.3% of the total stations under consideration over the basin. This matches with the recent work which was analysis of IDF curve for selected meteorological stations in Northern Shewa, amhara region Ethiopia (Eyoel, 2014). Data of two stations fitted to Gumbel's distribution which is similar to the work carried on the city of London (Prodanovic and Simonovic, 2007). Besides, the method was applied on on Awash basin (Abrha, 2014).

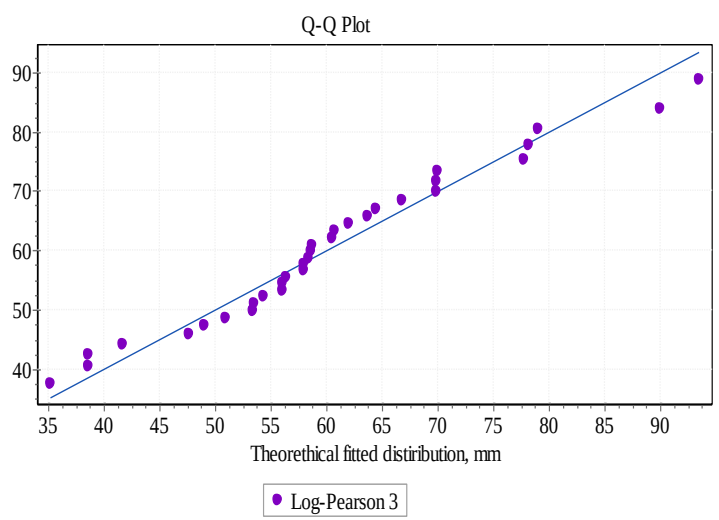

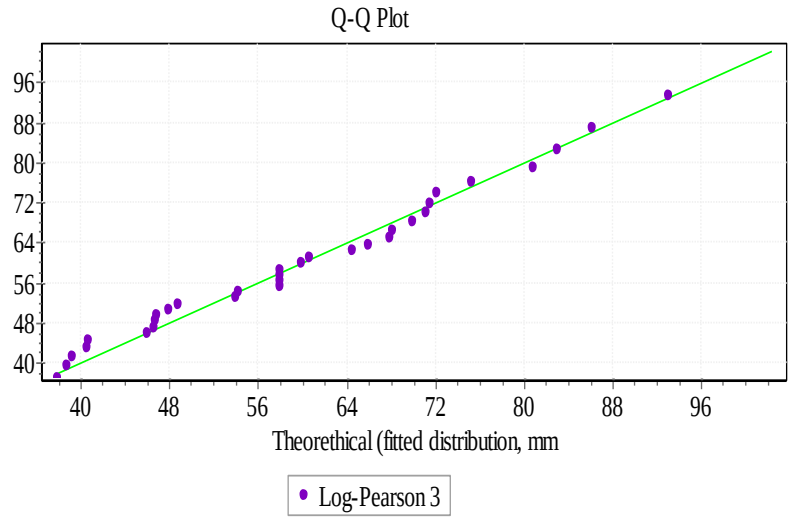

Figure: 4.10 Graphical representation of best fit probability distribution for Bulki (Minder) and Jimma stations respectively

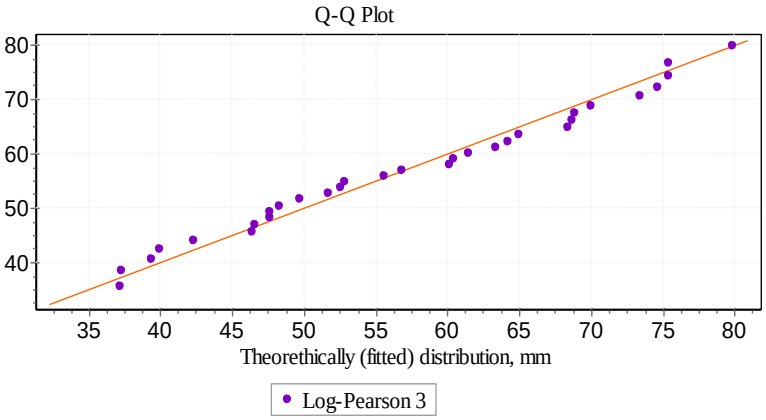

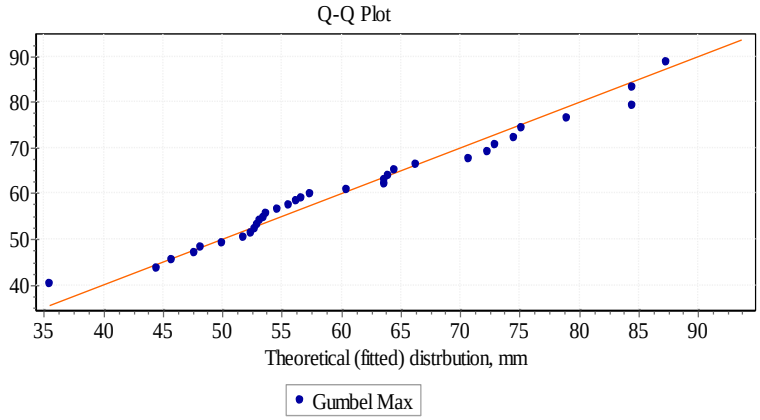

Figure: 4.11 Graphical representation of best fit probability distribution for Jinka and Limu Genet stations respectively

This graph shows the distribution of sample data and how well it follows the selected theoretical distribution. So far, selection of best fit theoretical distribution function was carried out based on GOF test. Therefore, the graph was not for comparison; rather for visual illustration of sample observed data of some stations over the basin with a selected best fitted theoretical distribution function. Figure 4.10 and 4.11 shows how well sample data of Jimma, Jinka and Bulki(minder) follow Log-Pearson Type III; whereas, Limu Genet data follows Gumble's distribution.

4.4 Bias Correction result

Even if RCM capture some small scale processes more realistically, uncertainties and considerable bias come from different sources still remain in the model. The target of post processes applied on the model output (bias correction) is to remove those uncertainties. For simple illustration, observed, raw model out puts and corrected rainfall amount of historical data series on a monthly basis for Jinka and Woliso Giyon station were presented in figure 4.12.

Through the process of bias correction, parameters (a & b) were computed for each month. Then, they had been further used for correction of future data series. Table 4.4 revels, output result obtained through bias correction steps for Jimma and Woliso Giyon station.

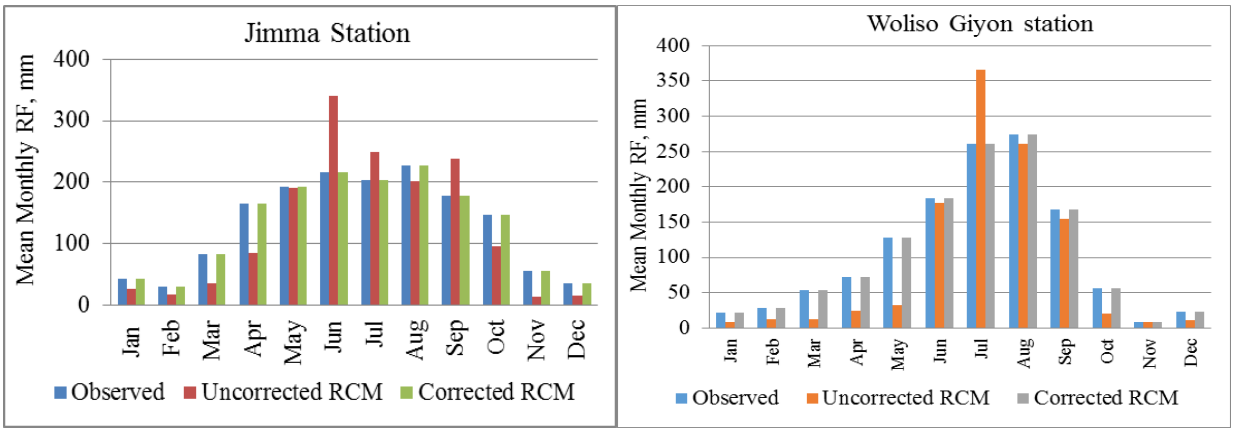

Figure: 4.12 Observed, both raw and corrected RCM output data of historical period on monthly basis.

As the figure depicts, raw RCM out puts attributed with significant biases when compared with respect to the observed data of the same period. As it was observed, positive bias (over estimation) is higher for May-July for majority of stations as high as up to (45-75) % and in September up to 51% in few of stations. On the other hand, negative bias (under estimation) of the model in representing ground data is higher in months (December- April) as low as up to (40-

65) % on some of stations. Therefore, those uncertainties and model bias were further removed under the application of bias correction.

Table 4.4 Parameters obtained during optimizing the mean and coefficient of variation of historical run of CORDEX data to observed data of Jinka station for a period (1980-2009)

Months	A	b	M	S	CV
Jan	8.85	0.33	2.15	6.18	2.88
Feb	10.45	0.15	1.40	4.12	2.95
Mar	16.01	0.16	3.40	7.23	2.13
Apr	0.83	1.04	5.34	8.19	1.53
May	0.01	2.48	4.89	9.35	1.91
Jun	0.10	0.94	3.66	6.19	2.35
Jul	0.26	1.58	3.22	6.83	2.12
Aug	0.42	1.25	2.34	5.80	2.48
Sep	0.63	1.20	2.78	6.17	2.22
Oct	3.97	0.75	6.16	9.98	1.62
Nov	16.55	0.25	3.57	8.83	2.48
Dec	2.41	0.78	2.42	7.14	2.95

As indicated from table, M and CV of scenario data and historically observed data become equal for corresponding value of a & b of each month respectively. In this case, mean relative error at monthly bases which measure how far the predicted value is from error relative to the observed value would become zero. The CV value after correction ranges between (2.95-1.53). The higher value in December indicates higher dispersion of data points around the mean which represents higher variability of rainfall. On the other hand, months with lower CV indicates where sufficient rainfall pattern was available relatively when compared to that of with lower value. As a result, historically observed data and historical run of scenario data would perfectly match at monthly basis over a period (1980-2009).

4.5 Comparison of historical climate with projected climate

As it was indicated, the trends of the average rainfall data over the basin from the past historical data over the last 34 years shows slight declining trend. Mid-21st century rainfalls from three scenarios were projected over the total basin. Accordingly, simple comparison was made between baseline period and projected period after analysis of 30 years' rainfall data series. The

comparison was made with regard to mean monthly and annual rainfall averaged over 30 years and the annual maximum rainfalls for both observed and simulated data were compared.

4.5.1 Mean Monthly rainfall

After the three scenario data were corrected, simple attempt was carried out to demonstrate the relationship of projected rainfall with respect to rainfall of baseline period for Woliso Giyon, Asendabo, Hosana and Jinka stations. For other stations it was compiled at Appendix 7.10.

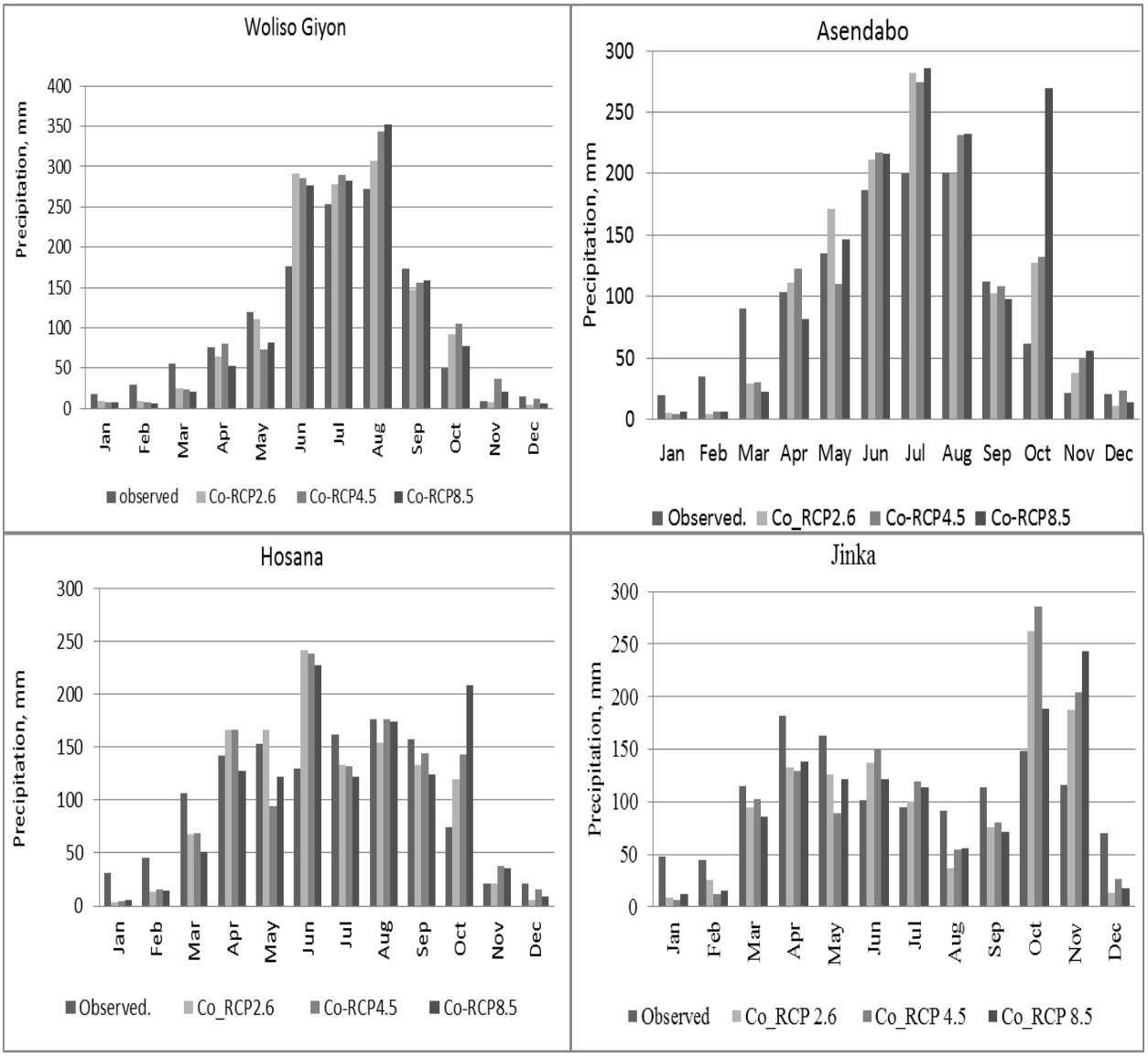

Figure: 4.13 Mean monthly precipitation for baseline period and projected period (mid-21st century) for some of station over the basin

Omo-Gibe basin can be considered as one Ethiopian river basin with high landscape and climatic zone difference within short distances. It was also observed that the total basin would not receive uniform seasonal rainfall pattern. Mean monthly rainfall experienced over the basin have high spatial as well as seasonal variation.

It was common practice among different researchers to look Ethiopian's rainfall occurrence pattern in different seasonal level. For instance, due to very mixed behavioral pattern of rainfall over the basin, (Mohammed, 2013) evaluate rainfall pattern in to four season; namely Summer which is main rainy season (Jun-August), Autumn (September-November), Winter (December-February) and Spring which is small rainy season (March-April). Accordingly, as shown above from a graph, the projected mean monthly amount of rainfall to be received in months of December-February from the three scenarios indicates declining trend. This shows that rainfall expected in winter season get decreasing. Moreover, the dry season might be extended up to March as indicated from the result. In spring, the projected mean monthly rainfall shows both increment and decrement for different stations over the basin. However, in summer, the projected rainfall shows somewhat slight increment would be expected over the basin. Particularly, it is expected that, there would not be significant change of rainfall over the basin.

Generally, it can be concluded that projected mean monthly rainfall pattern over the basin doesn't show such much difference from the observed data. However, comparative evaluation shows there is a probable expectation for a little bit decrements of rainfall in months of December-March over the majority of the basin. This might bring its own stress on water resources system of the basin.

4.5.2 Mean annual rainfall

Mean annual rainfall data averaged over a period (1980-2013) was computed for each station and the same analysis was made for the three scenarios of corrected data of a period (2040-2069). In order to investigate the potential changes in mean annual rainfall over the basin, mean areal precipitation was interpolated for the total basin. Then for figurative illustration, isoheytal map was drawn for observed and the three scenarios. The result is summarized as follows.

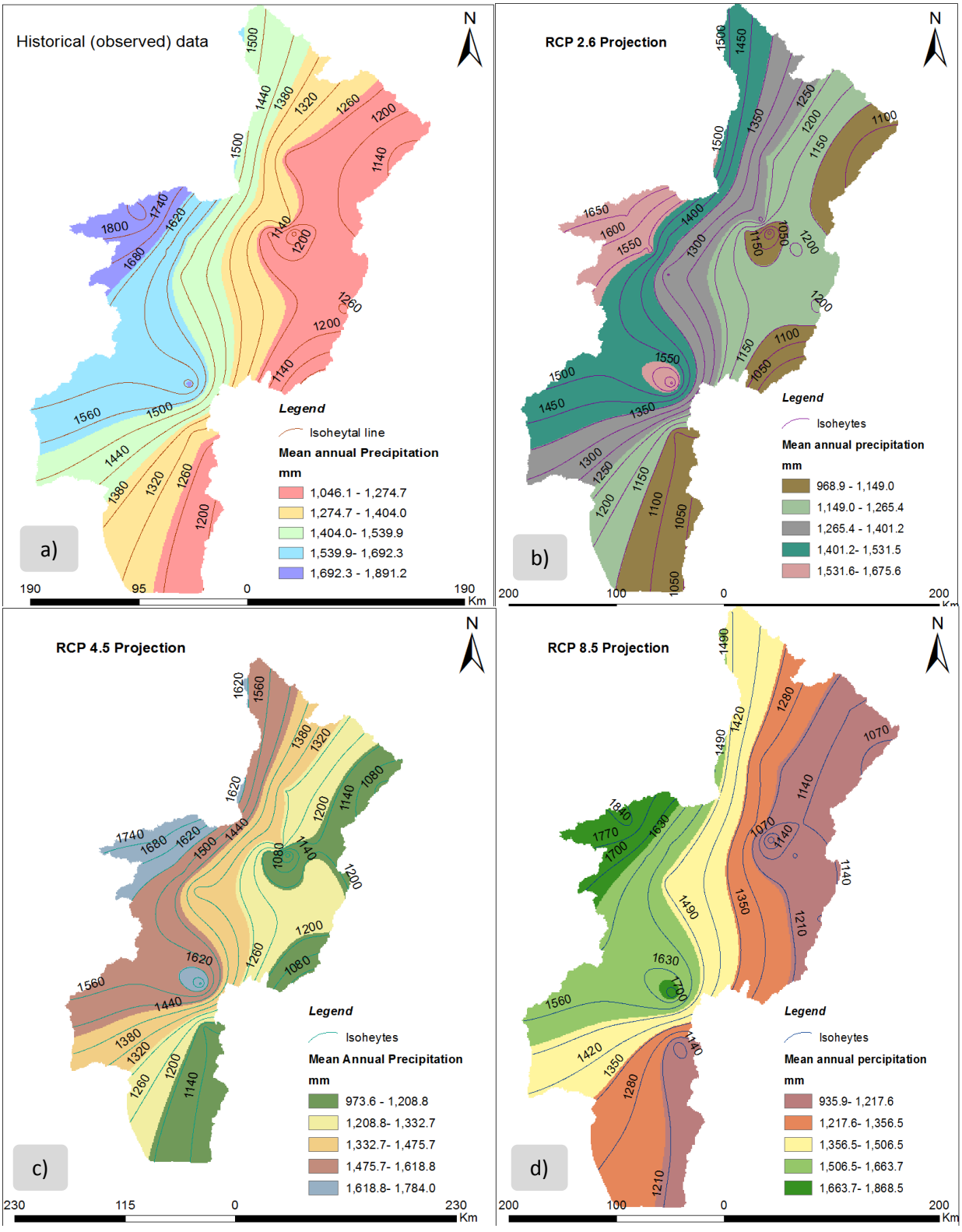

Figure: 4.14 spatial distribution of both observed and projected mean annual rainfall over the total basin

As shown in figure 4.14a), Omo-Gibe basin had received mean annual rainfall amount between a range (1046.1-1891.2) mm per year for the last decades. Western highland region of the basin received relatively high amount of rainfall per a year. From the RCP 2.6 scenario projection as shown in figure 4.14 b), the basin receives mean annual precipitation of (968.9-1675.6) mm per year which is less amount when compared to the historically observed data over the last three decades.

RCP 4.5 scenario projection as indicated on Figure 4.14c), mean annual rainfall to be received ranges between (973.6.6-1784) mm per year. This is also less in magnitude relative to historically observed data. But better estimate than RCP 2.6 projection when historically observed data is taken as a reference. In the same way, from RCP 8.5 in figure 4.14 d) projections, the mean annual rainfall which shall be received by Omo-Gibe basin ranges between (935.9-1868.5) mm per year. This shows relatively better result when compared to baseline period.

Generally, the three scenarios RCP 2.6, RCP 4.5, RCP 8.5 projected relatively less amount of mean annual rainfall is expected over Omo-Gibe basin when compared with the baseline period. This could be considered as the effect of expansion of dry season (decline of rainfall in December up to February). The result of the projection also amplifies trend analysis result carried over a period of (1980-2013). Besides, the finding of the projection more off matches with (Mohammed, 2013) as the potential change is not such much significant except in winter season. However the result matches with expectation of shorter spring rains in the mid-21st century over Eastern Africa including Ethiopia according to (IPCC's AR5 projection).

4.5.3 Extreme event (Annual maximum rainfall)

Figure 4.15 illustrates that there is a significant variation between rainfall intensities during baseline and projected period of different return period. It is observed that there is significant increment in severe storm in all stations except Wolaita Sodo station for which the projection under three scenarios show somewhat the same result with baseline period. For simple demonstration, three stations with their probable events expected to occur with a recurrence interval of 25, 50, 100 years for different durations were presented. For the rest of stations, it was compiled in appendix 7.3.

a) Arbaminch station b) Jimma station c) Jinka Station

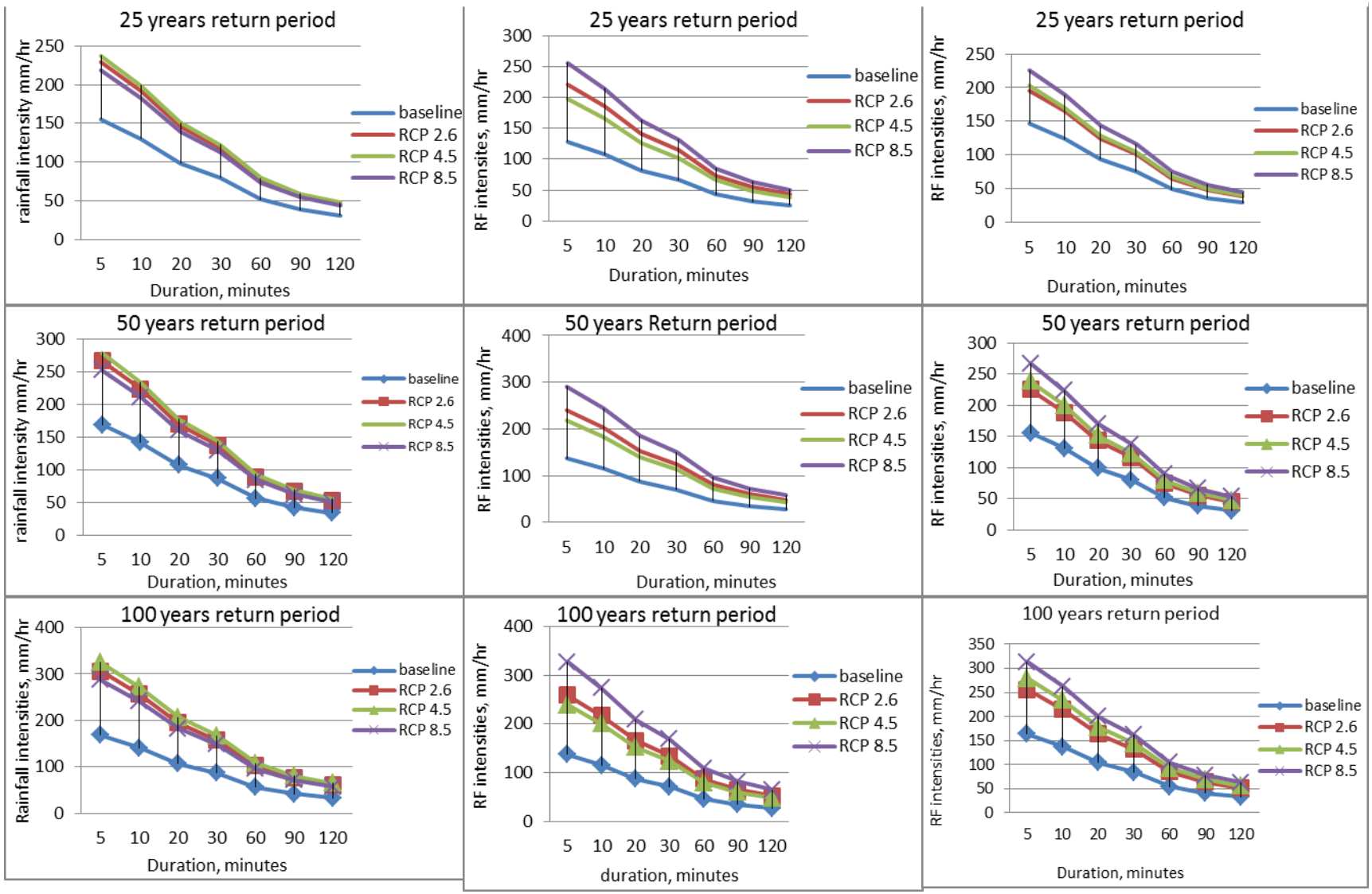

Figure: 4.15 Comparison between intensities (mm/hr) of observed historical data and mid-21st century of some of stations for various return periods.

The summary of figure 4.15 provides a possible potential change of rainfall intensities for some of arbitrarily selected stations over the basin due to climate change. As the figure depicts, the projected increase in future extreme rainfall intensities is greater at shorter durations and longer return periods for the all scenarios. The significant variations in the quintiles for shorter duration emphasize the importance of disaggregation of daily based data series into fine temporal resolution (5, 10, 20, 30, 30, 60, 90 and 120) minutes. According to (ERA) recommendation, the design of gutters and inlets to be based on shorter rainfall durations as fine as up to 15 minutes for serious conservatism. Since storm sewer inlet design needs special consideration, the projected increment of rainfall intensities for shorter duration may have significant impact on those designed under conventional standards.

So far, the result indicated that there is significant increment in the probability of occurrence severe storm over the basin for different recurrence interval. It is also indicated from historical data that; the basin is characterized by highly variable rainfall pattern. In this work, rainfall analysis was carried out for 18 representative stations for both observed and projected data. For figurative illustration of spatial distribution of rainfall over the basin as well as the expected change for projected time due to impact of climate change over the basin isoheytal map was established for the study area. Comparisons was made for rainfall events (mm/hr) having 25, 50 and 100 years' recurrence interval computed from observed as well as projected data from three scenarios expected to occur for a duration of 20 minutes. The spatial variation over the basin was shown with the established different isoheytal map. For simple illustration intensities with 25 years' recurrence interval was discussed here.

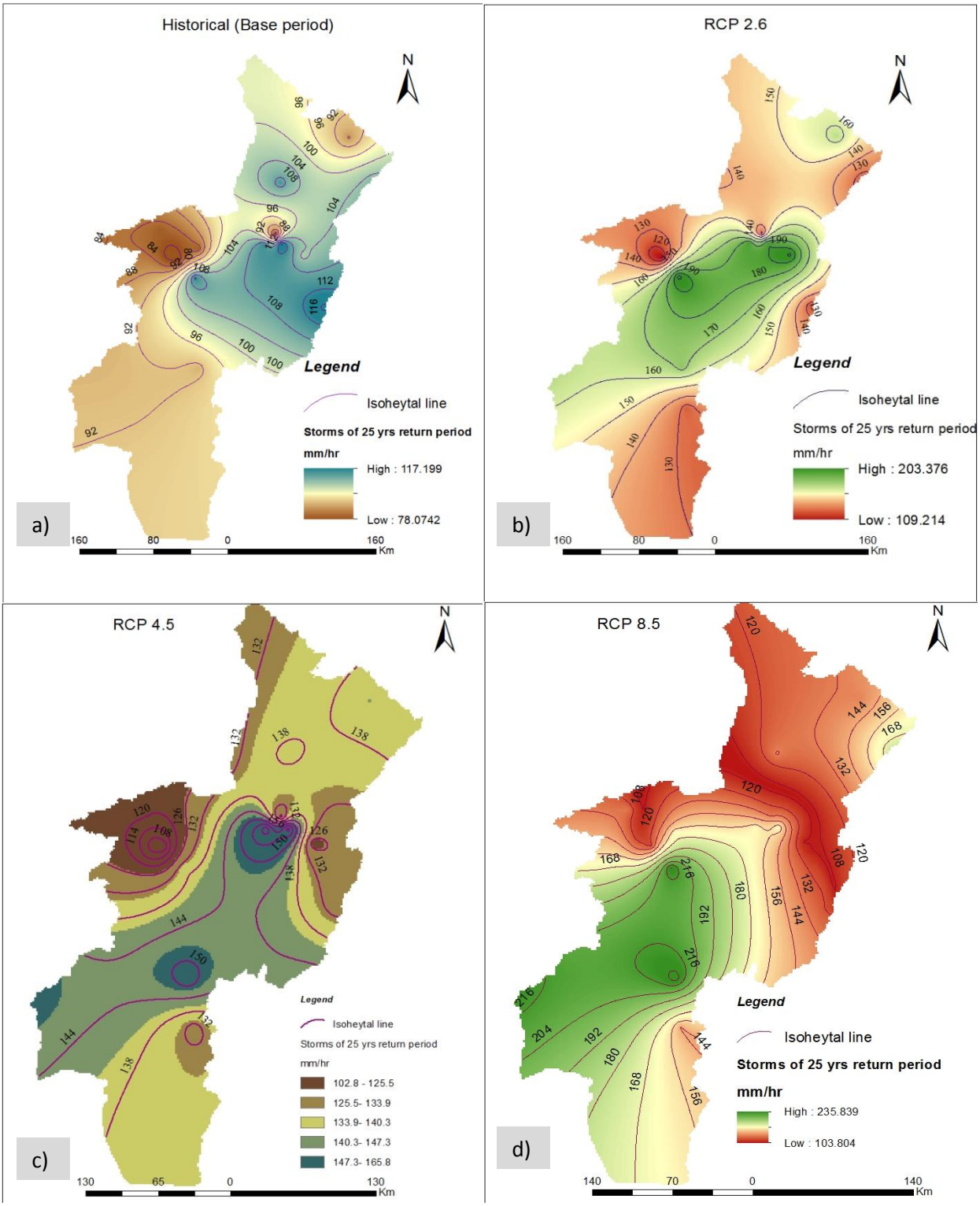

Figure: 4.16 Isoheytal map established for events having a probability of occurrence within 25 years for a duration of 20 minutes projected from both observed and scenario data

As shown in figure 4.16a), rainfall intensity with duration of 20 minutes which have a probability of occurrence within 25 years estimated from annual maximum of observed data ranges between (78-117.2) mm/hr. The spatial variation is as shown with isoheytal line on the map. Figure 4.16b) shows RCP 2.6 scenario and the magnitudes ranges between (109.2-203.4) mm/hr. which have relatively larger magnitude when compared to historical observation in fig. 4.16a). However, RCP 4.5 and RCP 8.5 scenario projected that the magnitude of extrapolated event having similar probability of occurrence over the basin ranges (102.8-165.8) and (103.8-235.8) mm/hr respectively for a period mid-21st century. The overall result from climate change simulations based on climate representatives of 21st century showed that, there is a considerable spatial variation of extreme rainfall. Besides, it found that the effect of climate change impact on extreme event shows significant increment over the total basin. From comparative evaluation, RCP 2.6 and RCP 4.5 projected the incremental values with in (40-73) & (31-41) % respectively. On the other hand, RCP 8.5 projected the probable event for the return period might raise up to its double value. Therefore, it can be conclude the result with high certainty that, there will be high probability for future increment of severe storm over the total basin so that it needs special attention to mitigate these adverse impacts.

4.6 Construction of IDF curve for representative stations

The IDF curves were plotted on a normal paper. Duration is on abscissa and the intensity i is on ordinate. For simple demonstration, basin wide IDF curve established from areal precipitation for both baseline and projected period for Omo-Gibe basin were presented below. Further, for each station, the established IDF curve for both baseline period and projected periods were attached in appendix 7.2. It is observed from all result that rainfall intensity gets increasing when rainfall duration goes decreasing.

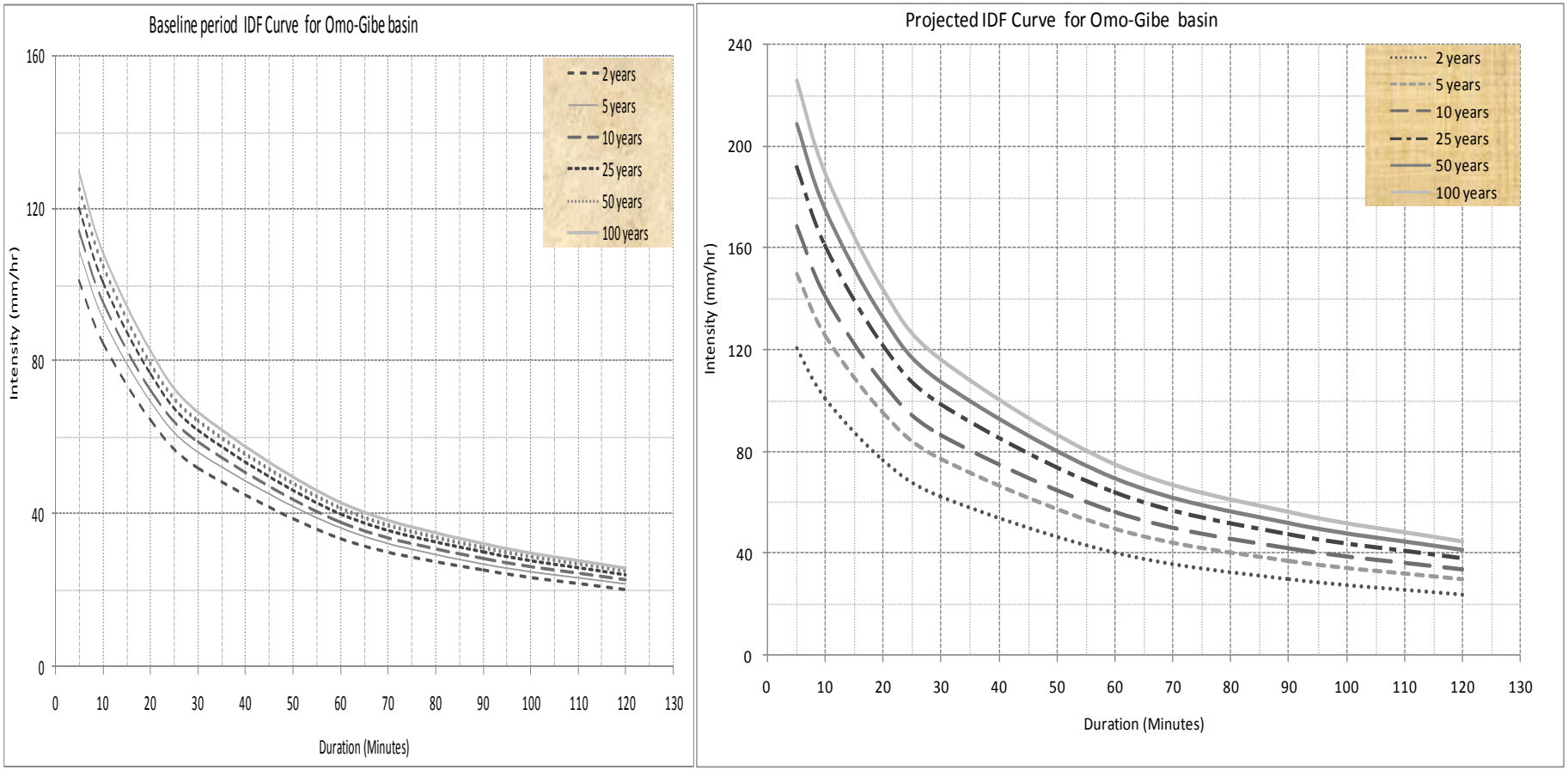

Figure: 4.17 IDF curve established for baseline period and under the of impact of climate change projected for mid-21st century for Omo-Gibe basin

The analysis performed in this study detects a significant change between the baseline and the projected period. Almost in all stations, the occurrence of severe storm expected for the future period under a changing climate condition has shown increment in magnitude when compared with a baseline period. More interesting result from this study is considerable differences of severe storm's magnitude between the periods varies with spatial variation over the basin. Accordingly, the average incremental value for RCP 2.6 scenario is (10-39) %. Whereas, for RCP 4.5 and RCP 8.5 scenario (8.3-37) and (11.3-52) % respectively. This deviation brought incredible value differences between the two periods on the extrapolated rainfall intensities computed from the projected data series. RCP 2.6 scenario projection shows the difference falls in (40-73) %; for RCP 4.5 scenario projection, (31-41) % except Bonga and Wolaita Sodo stations where the changes is non-significant. Furthermore, RCP 8.5 projection scenario has shown a substantial change fall in (19.5-57) % except a tremendous change as high as up to its double value particularly in south western part of the basin Therefore, the two scenarios show a moderate change which match with (De Paola *et al.*, 2014).

5 Conclusions and Recommendations

5.1 Conclusions

Rainfall occurrence over Omo-Gibe basin varies spatially and temporally. Trend analysis of both annual rainfall and annual maximum rainfall from historically observed data indicates, declining trend when averaged over a total basin. However, the occurrence of severe storm for stations in the western and some southern part of the basin had shown increasing trend; whereas, stations in the northern and central part of north east region of Omo-Gibe basin, had shown declining trends.

Three distribution functions namely, Log normal, Log Person Type III and Gumbel EV-I were used for analysis; and GOF tests were used to identify the best probability distribution function. Accordingly, Log Person Type III probability distribution was found to be the best fitting function to data of selected stations.

Omo-Gibe basin had received mean annual rainfall amount between a range (1046.1-1891.2) mm per year for the last decades. Western highland region of the basin received relatively high amount of rainfall per a year. From the RCP 2.6 scenario projection, the basin receives mean annual precipitation of (968.9-1675.6) mm. RCP 4.5 scenario projection as indicated mean annual rainfall to be received ranges between (973.6.6-1784) mm per year. In the same way, RCP 8.5 projected mean annual of (935.9-1868.5) mm. This shows relatively better result when compared to baseline period. Generally, the three scenarios RCP 2.6, RCP 4.5, RCP 8.5 projected relatively less amount of mean annual rainfall is expected over Omo-Gibe basin when compared with the baseline period.

Almost in all stations, the occurrence of severe storm expected for the future period under a changing climate condition has shown increment in magnitude when compared with a baseline period. Accordingly, the average incremental value for RCP 2.6 scenario is (10-39) %. Whereas, for RCP 4.5 and RCP 8.5 scenario (8.3-37) and (11.3-52) % respectively. This deviation brought incredible value differences between the two periods on the extrapolated rainfall intensities computed from the projected data series. RCP 2.6 scenario projection shows the difference falls in (40-73) %; for RCP 4.5 scenario projection, (31-41) % except Bonga and Wolaita Sodo stations where the changes is non-significant. Furthermore, RCP 8.5 projection scenario has

shown a substantial change fall in (19.5-57) % except a tremendous change as high as up to its double value particularly in south western part of the basin.

5.2 Recommendations

Rainfall variability trend from the past observed data indicates somewhat complex spatial variability over the total basin. Since each region of the basin has their own physiographic and land use land cover characteristics, the current study should be extended at sub basin level and be compiled finally for the total basin.

Design flood and other hydrological risk analysis require rainfall records of shorter duration. Thus, Improvement in the collection of fine-resolution (short duration) precipitation data at various gauges should be made for good quality of data. NMA can easily achieve this by mounting automatic recording on some stations so this could help for performing quality checking of data.

In addition to a type of climate model being used, the reliability of output of climate models depends up on the quality of input data. For relatively reliable future projection, high quality and reliable input data is very important. Most of existing stations over the total basin are with a bulk of missed data. NMA should give due attention and manage this defect; so that, stakeholders and researchers be provided with reliable data for planning and designing adaptation mechanism to impact of climate change

The analysis of this study, considered three different scenarios used to evaluate changes in rainfall characteristics. For all scenarios, the result indicated rainfall magnitude (as well as intensity) will be different in the future. ERA should revise and update its IDF curve in its Drainage Design Manual by considering the potential deviation expected due to impact of climate change. Further, water resource professionals, designers and concerned institutions in the study area can use IDF curve of this research output of a station appropriate to a specific site.

Expectation for future expansion of dry season was one of this research finding. The occurrence of this natural phenomenon would expect to have a tangible adverse effect on socio economy of societies as most of population depends up on rain fed agriculture. Therefore, Ministry of Agriculture, NMA and other stake holder should extend further analysis for proposing appropriate adaptation mechanism.

References

ABDELLA K.M. (2013) The Effect of Climate Change on Water Resources Potential of Omo Gibe Basin, Ethiopia:. *PhD Dissertation, München, Germany*.

ABRHA, B. G. (2014) SPATIAL AND TEMPORAL RAINFALL INTENSITY-DURATIONFREQUENCY PARAMETERS VARIABILITY FOR AWASH RIVER BASIN, ETHIOPIA. Haraomaya, Ethiopia, Haromaya University.

ARPITA, M. & MUJUMDAR, P. P. (2015) *Regional hydrological impacts of climate change: implications for water management in India*. *IAHS Publ.*, 366.

BEN-ZVI, A. (2009) Rainfall Intensity-Duration-Frequency Relationships Derived from Large Partial Duration Series. *Journal of Hydrology: Regional Studies*, 367**,** 104-114.

BERHANU, B., SELESHI, Y. & MELESSE, A. M. (2014) Surface Water and Groundwater Resources of Ethiopia: Potentials and Challenges of Water Resources Development *Research Gat: Ethiopian Institute of Water Resources (EIWR) Addis Ababa University, Addis Ababa, Ethiopia* uploaded and get open access on 05 February 2016.

BERNARD, M. M. (1932) Formulas for rainfall intensities of long durations . *Trans. ASCE*, 96**,** 592-624.

BINIYAM, Y. & KEMAL, A. (2017) The Impacts of Climate Change on Rainfall and Flood Frequency: The Case of Hare Watershed, Southern Rift Valley of Ethiopia. *J Earth Sci Clim Change*, 8.

BOKE A. S. (2017) Comparative Evaluation of Spatial Interpolation Methods for Estimation of Missing Meteorological Variables over Ethiopia. *Journal of Water Resource and Protection*, 9**,** 945-959: https://doi.org/10.4236/jwarp.2017.98063.

BOKKE, A. S., TAYE, M. T., WILLEMS, P. & SIYOUM, S. A. (2017) Validation of General Climate Models (GCMs) over Upper Blue Nile River Basin, Ethiopia. *Atmospheric and Climate Sciences*, 7**,** 65-75: http://dx.doi.org/10.4236/acs.2017.71006.

BROWN, C., GREENE, A. M., BLOCK, P. & GIANNINI (2008) A. Review of downscaling methodologies for Africa climate applications. *IRI Technical Report 08-05: IRI Downscaling Report*, International Research Institute for Climate and Society, Columbia University.

CAMBERLIN P. (1997) Rainfall anomalies in the source region of the Nile and their connection with the Indian summer monsoon. *Journal of Climate*, 10**,** 1380-1392.

CHOW, V. T. (1953) *Frequency analysis of hydrologic data with special application to rainfall intensities, bulletin no. 414 Cross Reff*, University of Illinois Eng. Expt. Station [CrossRef].

CHOW, V. T., MAIDMENT, D. R. & MAYS, L. W. (1987) *Applied Hydrology*, New york, St. Louis San Francisco Auckland Bogota, Mc Graw-Hill International Edition: Civil Engineering Series.

CHRISTENSEN, J., F, B., OB, C. & P, L.-P. (2008) On the need for bias correction of regional climate change projections of temperature and precipitation. *Geophys Res Lett* 35.

CONWAY D. (2000) The climate and hydrology of the Upper Blue Nile River. *Geogr J*, 166**,** 49-62.

DE PAOLA, F., GIUGNI, M., TOPA, M. E. & BUCCHIGNANI, E. (2014) Intensity-Duration-Frequency (IDF) rainfall curves, for data series and climate projection in African cities *SpringerPlus: http://www.springerplus.com/content/3/1/133*. , 3.

DOSIO, A., PANITZ, H. J., SCHUBERT-FRISIUS, M. & LÜTHI, D. (2014) Dynamical downscaling of CMIP5 global circulation models over CORDEX-Africa with COSMO-CLM: evaluation over the present climate and analysis of the added value. *Clim Dyn*, 44**,** 2637-2661.

EHRET, U., ZEHE, E., WULFMEYER, V., WARRACH-SAGI, K. & LIEBERT, J. (2012) ‘‘Should we apply bias correction to global and regional climate model data? *Discuss: HESS opinions* 9**,** 5355-5387.

ENDRIS, H. S., OMONDI, P., JAIN, S., LENNARD, C., HEWITSON, B., CHANG’A, L., AWANGE, J. L., DOSIO, A., KETIEM, P., NIKULIN, G., PANITZ, H.-J., BUCHNER, M., STORDAL, F. & TAZALIKA, L. (2013) Assessment of the Performance of CORDEX Regional Climate Models in Simulating East African Rainfall. *JOURNAL OF CLIMATE*, 26**,** 8453-8775.

EPCC (2015) Ethiopian panel on Climate Change , *First Assessment Report, - Working Group II* CLIMATE CHANGE IMPACT, VULNERABILITY, ADAPTATION AND MITIGATION *Water and Energy*. *Published by the Ethiopian Academy of Sciences*, IV.

ERA (2013) Ethiopian Road Authority: Drainage Design Manual federal democratic republic of Ethiopia. Addis Ababa, Ethiopia.

EYOEL, Y. (2014) Intensity Duration Frequency (IDF) Curve Analysis for Selected Meteorological Stations In North Shewa, Amhara Region, Ethiopia. *School of Graduate Studies; M.Sc. Thesis.* Haramaya, Ethiopia, Haramaya University.

FANG, G., YANG, J., CHEN, Y. N. & ZAMMIT, C. (2015) Comparing bias correction methods in downscaling meteorological variables for a hydrologic impact study in an arid area in China. *Published in Hydrol. Earth Syst. Sci***,** 2547-2559 [Cross ref].

GIORGI, F., JONES, C. & ASRAR, G. (2009) Addressing climate information needs at the regional level: the CORDEX framework. *World Meteorol Organ (WMO) Bull*, 58(July)**,** 175-183.

HAILE, A. T. & RIENTJES, T. (2015) Evaluation of regional climate model simulations of rainfall over theUpper Blue Nile basin. *Atmospheric Research***,** 57-64: http://dx.doi.org/10.1016/j.atmosres.2015.03.013.

HASSANZADEH, E., NAZEMI, A. & ELSHORBAGY, A. J. (2014) Quantile-Based Downscaling of Precipitation using Genetic Programming: Application to IDF Curves in the City of Saskatoon. *Hydrol. Eng.***,** 943-955.

IPCC (2007) Intergovernmental Panel on Climate Change; synthesis report, contribution of working groups I, II and III to the fourth assessment report of the Intergovernmental Panel on Climate Change, Geneva, Switzerland.

IPCC (2012) Managing the Risks of Extreme Events and Disasters to Advance Climate Change Adaptation. A Special Report of Working Groups I and II of the Intergovernmental Panel on Climate Change [Field, C.B., V. Barros, T.F. Stocker, D. Qin, D.J. Dokken, K.L. Ebi, M.D. Mastrandrea, K.J. Mach, G.-K. Plattner, S.K. Allen, M. Tignor, and P.M. Midgley (eds.)] Cambridge University Press, Cambridge, UK, and New York, NY, USA, pp 582.

IPCC (2013) Intergovernmental Panal on Climate Change; Summary for Policymakers, in: Climate Change : The Physical Science Basis, Contribution of Working Group I to the Fifth Assessment Report of the Intergovernmental Panel on Climate Change, edited by: Stocker, T. F., Qin, D., Plattner, G.-K., Tignor, M., Allen, S. K., Boschung, J., Nauels, A., Xia, Y., Bex, V., and Midgley, P. M Cambridge University Press, Cambridge, UK and New York, NY, USA, .

IPCC (2014) The IPCC's fifth assessement report /What's in it for affrica? (CDKN) Climate and Development Knowledge Network, licensed under a Creative Commons Attribution.

JAHNVI, P., BHATT, H. M., GANDHI, K. B. & GOHIL (2014) Generation of Intensity Duration Frequency Curve Using Daily Rainfall Data for Different Return Period. *Journal of International Academic Research for Multidisciplinary Dept. of Civil Engineering, Shantilal Shah Engineering College, Bhavnagar, Gujarat, India*, 2(2).

KEWTAE KIM (2007) Application of Intensity-Duration-Frequency Curve for Korean Rainfall Data using Cumulative Distribution Function. *Graduate School* Korea, Yonsei University.

KIPARSKY, M., MILMAN, A. & VICUN, S. (2012) Climate and Water Knowledge of Impacts to Acti on on Adaptation. *Annual Reviews Environmental Resources. 10.1146/annurev-environ-050311-093931. environ. annualreviews.org.*

KITE, G. W. (1977) *Frequency and Risk Analysis in Hydrology*. *Water Resources Publications, Fort Collins, Colo. [CrossRef]*.

KOUTSOYIANNIS, D., KOZONIS, D. & MANETAS, A. (1998) A mathematical framework for studying rainfall intensity-duration-frequency relationships. *J. Hydrol. , 206***,** 118-135.

LENDERINK, G., A. BUISHAND & DEURSEN, W. V. (2007) Estimates of future discharges of the river Rhine using two scenario methodologies: direct versus delta approach. . *Hydrology and Earth System Sciences Discussions, European Geosciences Union,,* 11**,** 1145-1159, [Cross ref].

LENDERINK, G. & MEIJGAARD, E. V. (2008) Increase in hourly precipitation extremes beyond expectations from temperature changes. *Nat. Geosci.,* 1**,** 511-514.

LI, J. & HEAP, A. D. (2008) *A Review of Spatial Interpolation Methods for Environmental Scientists*. *Geosciences Australia,* Record 2008/23**,** 137 [Cross ref].

MARAUN, D. (2013) Bias correction, quantile mapping and downscaling: revisiting the inflation issue. *J Clim* 26**,** 2137−2143.

MCSWEENEY, CMN & G, L. (2012) UNDP Climate Change Country Profiles Ethiopia. *http://country-profiles.geog.ox.ac.uk. Accessed 4 Aug 2013*.

MEHDI, B., MRENA, C. & DOUGLAS, A. (2006) Adapting to climate change: An introduction for Canadian Municipalities. *Canadian Climate Impacts and Adaptation Research Network (C-CIARN): http://www.c-ciarn.ca/.*

MEHRANNIA, H. & PAKGOHAR, A. (2014) Using Easy Fit Software for Goodness-Of-Fit Test and Data Generation

International Journal of Mathematical Archive (IJMA), 5(1)**,** 118-124.

MILLY, P. & C.D. (2008) Stationarity is dead: whither water management *Science,,* 319**,** 573-574. [CrossRef].

MIRHOSSEINI, G., SRIVASTAVA, P. & STEFANOVA, L. (2012) The impact of climate change on rainfall Intensity-Duration-Frequency (IDF) curves in Alabama: ; USA. . *Reg Environ Change***,** 1-9.

MIRHOSSEINI, G., SRIVASTAVA, P. & STEFANOVA, L. (2013) The impact of climate change on rainfall Intensity-Duration-Frequency (IDF) curves in Alabama. *Reg Environ Change,* 13**,** 25-33.

MOFED (2010) Ministry of Finance and Economic Development (Growth and Transformati on Plan (GTP): Policy matrix. Addis Ababa: Federal Democrati c Republic of Ethiopia. [CrossRef].

MOHAMMED, A. K. (2013) The Effect of Climate Change on Water Resources Potential of Omo Gibe Basin, Ethiopia:. *PhD Dissertation, München, Germany*.

MOSS, R. H., EDMONDS, J. A., HIBBARD, K. A., MANNING, M. R., ROSE, S. K., VAN VUUREN, D. P. & WILBANKS, T. J. (2010) The next generation of scenarios for climate change research and assessment *Nature,* 463**,** 47-56.

MOWR (2011) (Ministry of Water Resources, now called Ministry of Water, Irrigation and Energy). Ethiopia. Strategic Framework for Managed Groundwater Development. htt p://metameta.nl/wp-content/up loads/2012/10/2011_03 08_eth_frwrk_FINALSF.pdf [CrossRef].

NAPA (2007) Climate Change National Adaptation Program of Action (NAPA) of Ethiopia; The federal democratic republic of Ethiopia, Minstry of Water Resources; National Meteorological Agency (NMA). Addis Ababa, Ethiopia.

NGUYEN, V. T. V., NGUYEN, T. D. & CUNG, A. (2007) A statistical approach to downscaling of sub-daily extreme rainfall processes for climate-related impact studies in urban areas. *Water Sci. Technol. Water Supply 7***,** 183-192. [CrossRef].

NMA (1996) Climatic and agroclimatic resources of Ethiopia. National meteorological services agency of Ethiopia. *Meteorol Res.,* Rep Ser: 1**,** 1-137 [CrossRef].

NMA (2006) National Meteorology Agency: Agro-meteorology bulletin. Addis Ababa, Ethiopia [CrossRef].

OVEREEM, A., BUISHAND, A. & HOLLEMAN, I. (2008) Rainfall depth-duration-frequency curves and their uncertainties. *Journal of Hydrology: Regional Studies,* 348**,** 124-134.

PAPPAS, C., PAPALEXIOU, S. M. & KOUTSOYIANNIS, D. (2014) A quick gap filling of missing hydrometeorological data. *Journal of Geophysical Research: Atmospheres,* 119**,** 9290–9300: doi:10.1002/2014JD021633.

.

PIANI, C., HAERTER, J. O. & COPPOLA, E. (2010) Statistical bias correction for daily precipitation in regional climate models over Europe. *Theor. Appl. Climatol*, 99**,** 187-192, [Cross ref].

PRODANOVIC, P. & SIMONOVIC, S. P. (2007) Development of rainfall intensity duration frequency curves for the City of London under the changing climate. Department of Civil and

Environmental Engineering, . *Report 058* London, Ontario, Canada,, The University of Western Ontario.

RATY, O., RAISANEN, J. & YLHAISI, J. (2014) Evaluation of delta change and bias correction methods for future daily precipitation: intermodel cross-validation using ENSEMBLES simulations. *ClimDyn,* 42**,** 2287−2303.

REDA, D. T., ENGIDA, A. N., ASFAW, D. H. & HAMDI, R. (2014) Analysis of precip- itati on based on ensembles of regional climate model simulati ons and observati onal databases over Ethiopia for the period 1989- 2008. *Internati onal Journal of Climatology. DOI: 10.1002/joc.4029.*

RIAHI, K., RAO, S., KREY, V., CHO, C., CHIRKOV, V., FISCHER, G., KINDERMANN, G., NAKICENOVIC, N. & RAFAJ, P. (2011) RCP 8.5—A scenario of comparatively high greenhousegas emissions. *Springer: International Institute for Applied Systems Analysis (IIASA), 2361 Laxenburg, Austria*

RICHARD WOODROOFE & ASSOCIATES (1996) Omo-Gibe River basin Integrated Development Master Plan Study Final Report Vol. VI Water resources Surveys and Inventories. Addia Ababa, ministry of Water Resources.

SARR, M., SEIDOU, O., TRAMBLAY, Y. & EL ADLOUNI, S. (2015) Comparison of downscaling methods for mean and extreme precipitation in Senegal. *Journal of Hydrology: Regional Studies,* 4**,** 369-385.

SEABY, L. P., REFSGAARD, J. C., SONNENBORG, T. O., STISEN, S., CHRISTENSEN, J. H. & JENSEN, K. H. (2013) Assessment of robustness and significance of climate change signals for an ensemble of distribution-based scaled climate projections. *Journal of Hydrology: Regional Studies,* 486**,** 479-493 [Cross ref].

SEAGER, R. & VECCHI, G. (2010) Greenhouse warming and the 21st century hydroclimate of southwestern North America, U. S. A. *Proc. Natl. Acad. Sci.,* 107(50)**,** 21, 277-21,282.

SELESHI Y & ZANKE U (2004) Recent changes in rainfall and rainy days in Ethiopia. *Int J Climatol,* 24**,** 973-983.

SHANKO D. & CAMBERLIN P. (1998) The effects of the southwest Indian Ocean tropical cyclones on Ethiopian drought. *Int J Climatol,* 18**,** 1373-1388.

SHRESTHA, A., BABEL, M. S., WEESAKUL, S. & VOJINOVIC, Z. (2017) Developing Intensity-Duration-Frequency (IDF) Curves under Climate Change Uncertainty: The Case of Bangkok, Thailand:. *water, MDPI,* 9**,** 1-22

STEPANEK, P., ZAHRADNÍEK, P., FARDA1, A., SKALAK, P., TRNKA, M., MEITNER, J. & RAJDL, K. (2016) Projection of drought-inducing climateconditions in the Czech Republic according toEuro-CORDEX models. *Clim Res* 70**,** 179-193.

TABARI, H., TAYE, M. T. & WILLEMS, P. (2015) Water availability change in central Belgium for the late 21st century. *Global Planet Change* 131**,** 115-123.

TAYLOR, K., STOUFFER, R. & MEEHL, G. (2012) An overview of CMIP5 and the experiment design. *Bull Am Meteorol Soc,* 93(4)**,** 485-498.

TEUTSCHBEIN, C. & SEIBERT, J. (2012) Bias correction of regional climate model simulations for hydrological climate-change impact studies: Review and evaluation of different methods. *Journal of Hydrology,* 456–457 12-29.

THOMSON, A. M., CALVIN, K. V., SMITH, S. J., KYLE, G. P., VOLKE, A., PATEL, P., DELGADO-ARIAS, S., BOND-LAMBERTY, B., WISE, M. A., CLARKE, L. E. & EDMONDS, J. A. (2011) RCP4.5: A Pathway for Stabilization of Radiative Forcing by 2100. *Climatic Change*.

USAID (2014) A REVIEW OF DOWNSCALING METHODS FOR CLIMATE CHANGEPROJECTIONS. IN TRZASKA, S. & SCHNARR, E. (Eds.) *AFRICAN AND LATIN AMERICAN RESILIENCE TO CLIMATE CHANGE (ARCC).* USA Government

VAN HAREN, R., VAN OLDENBORGH, G. J., LENDERINK, G. & HAZELEGER, W. (2013) Evaluation of modeled changes in extreme precipitation in Europe and the Rhine basin *Environ. Res. Lett.,* 8 [CrossRef].

VAN PELT, S. C., BEERSMA, J. J., BUISHAND, T. A., VAN DEN HURK, B. J., M., J. & KABAT, P. (2012) Future changes in extreme precipitation in the Rhine basin based on global and regional climate model simulations. *Hydrol. Earth Syst. Sci.,*, 16**,** 4517-4530 [CrossRef].

VAN VUUREN, D., E, S., MGJ, D. E., S, D., A, H., M, I., K, K. G., T, K., MENDOZA BELTRAN A & R, O. (2011a) RCP2.6: Exploring the possibility to keep global mean temperature change below 2°C. . *Climatic Change*.

VAN VUUREN, D. P., EDMONDS, J., KAINUMA, M., RIAHI, K., THOMSON, A., HIBBARD, K., HURTT, G. C., KRAM, T., KREY, V., LAMARQUE, J.-F., MASUI, T., MEINSHAUSEN, M., NAKICENOVIC, N., SMITH, S. J. & ROSE, S. K. (2011b) The representative concentration pathways: an overview. *Clamatic change*, 109**,** 5−31: DOI 10.1007/s10584-011-0148-z

WAGESHO, N., GOEL, N. K. & JAIN, M. K. (2013) Temporal and spatial variability of annual and seasonal rainfall over Ethiopia. *Hydrological Sciences Journa*, 58**,** 354-373; http://dx.doi.org/10.1080/02626667.2012.754543.

WATER RESOURCES COUNCIL (1981) now called Interagency Advisory Committee on Water Data), Guidelines for determining flood flow frequency, . *bulletin 17B, available from Office of Water Data Coordination,*, U.S. Geological Survey, Reston, VA 22092.

WETTERHALL, F. (2012) Conditioning model output statistics of regional climate model precipitation on circulation patterns. *Nonlin. Processes Geophys.*, 19**,** 623-633.

YANG, W., ANDREASSON, J., GRAHAM, L. P., OLSSON, J., ROSBERG, J. & WETTERHALL, F. (2010) Distribution-based scaling to improve usability of regional climate model projections for hydrological climate change impacts studies. *Hydrol. Res.*, 41(3-4)**,** 211-229.

YEKAMBESSOUN NTCHA MPO, A. E. L., GANIYU TITILOPE OYERINDE, BENJAMIN KOUASSI YAO, ABEL AKAMBI AFOUDA (2017) Comparison of Daily Precipitation Bias Correction Methods Based on Four Regional Climate Model Outputs in Ouémé Basin, Benin. *Hydrology.*, 4**,** 58-71.

ZORITA, E. & VON STORCH, H. (1999) The analog method as a simple statistical downscaling technique: comparison with more complicated methods. *Journal of Climate 2*(8)**,** 2474-2489 [Cross ref].

Appendices

Appendix 7.1 Double Mass Curve analysis result for some of selected representative stations

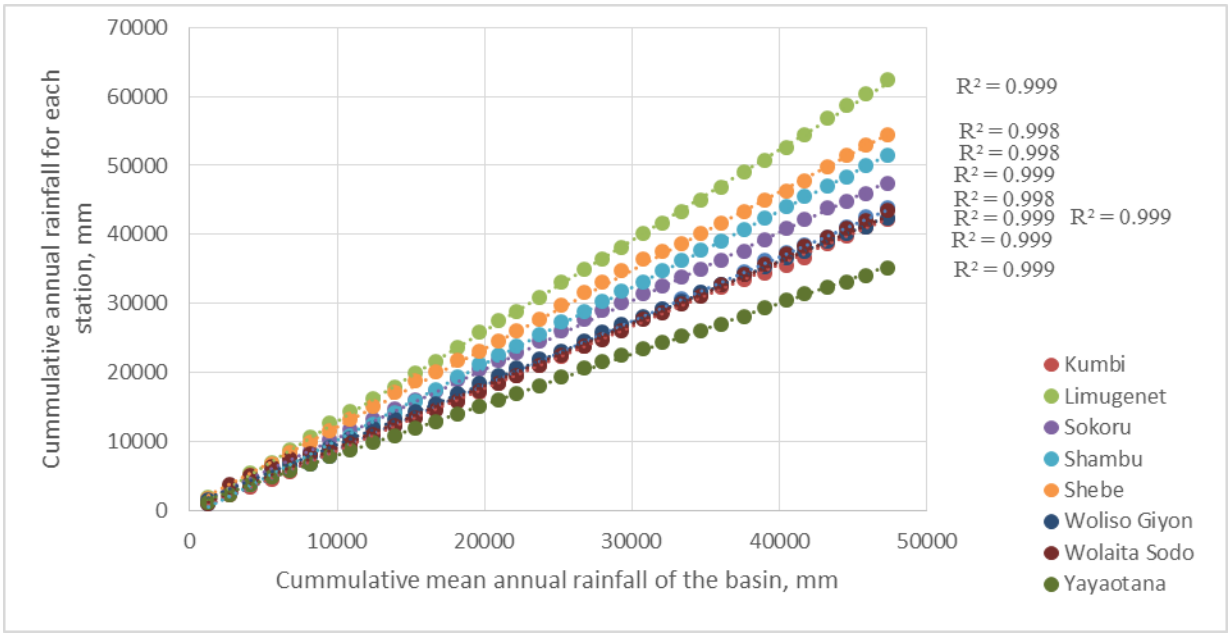

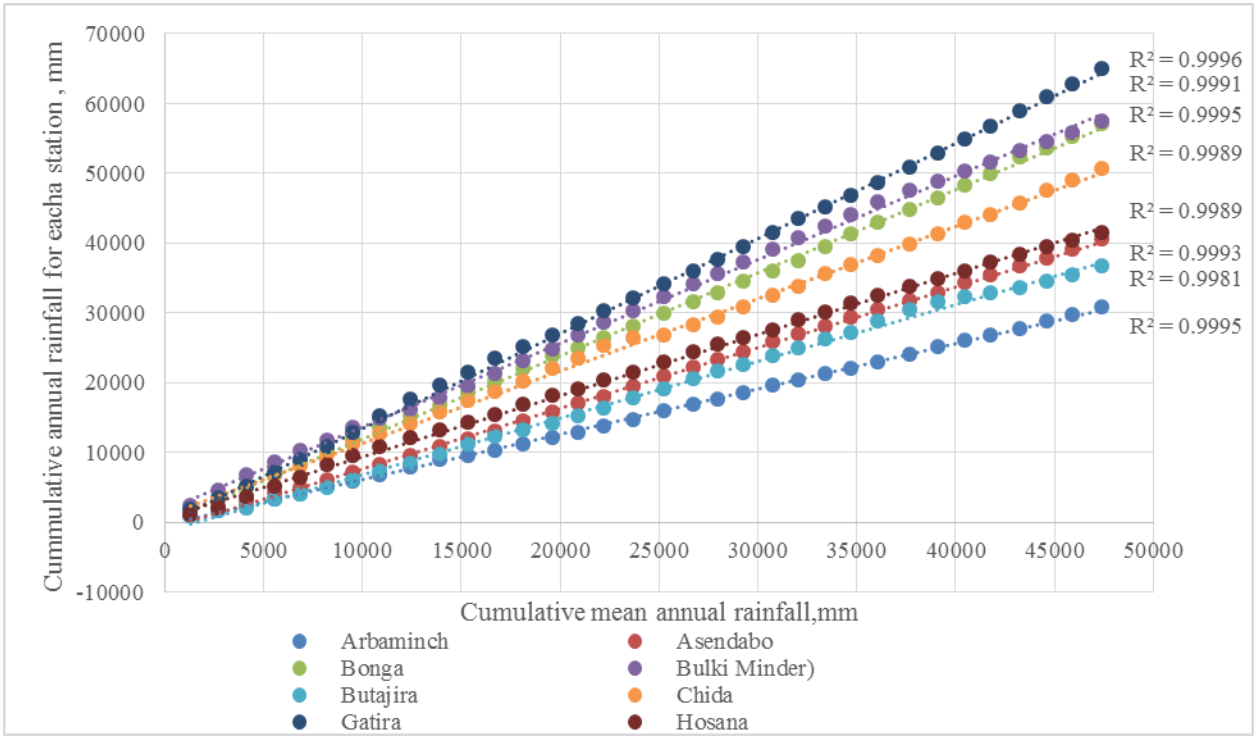

Appendix 7.2 Base period and Projected IDF Curve established for each stations

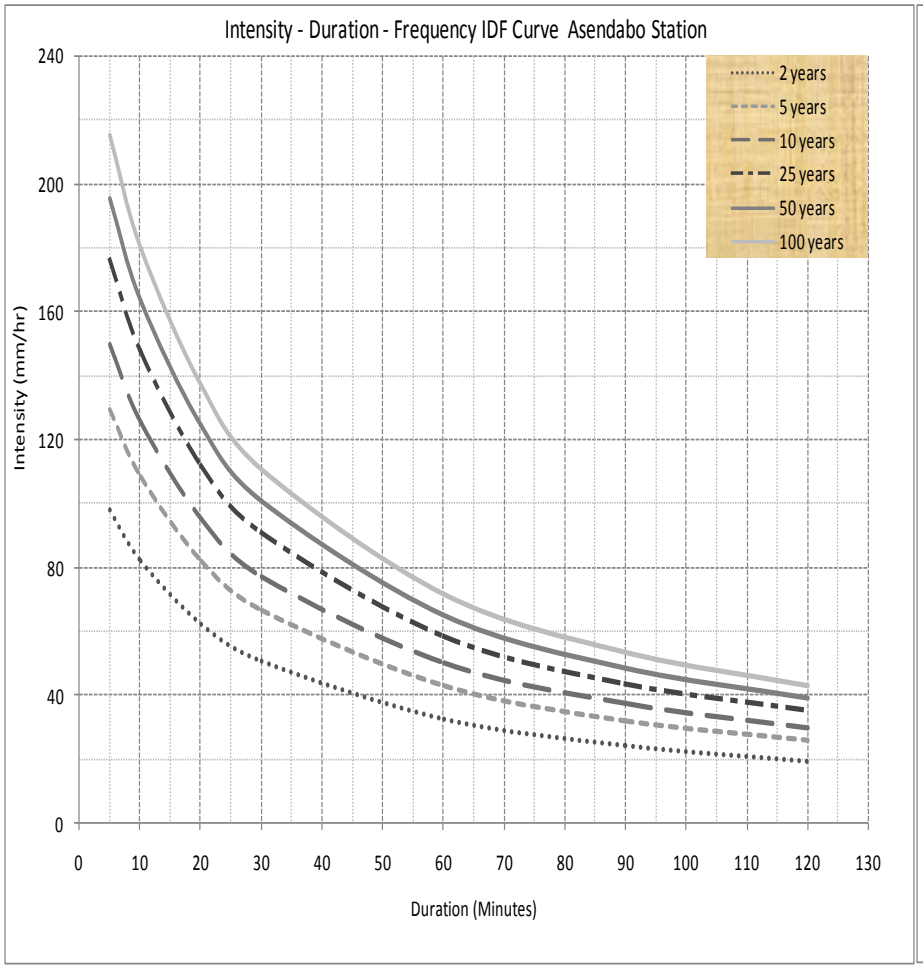

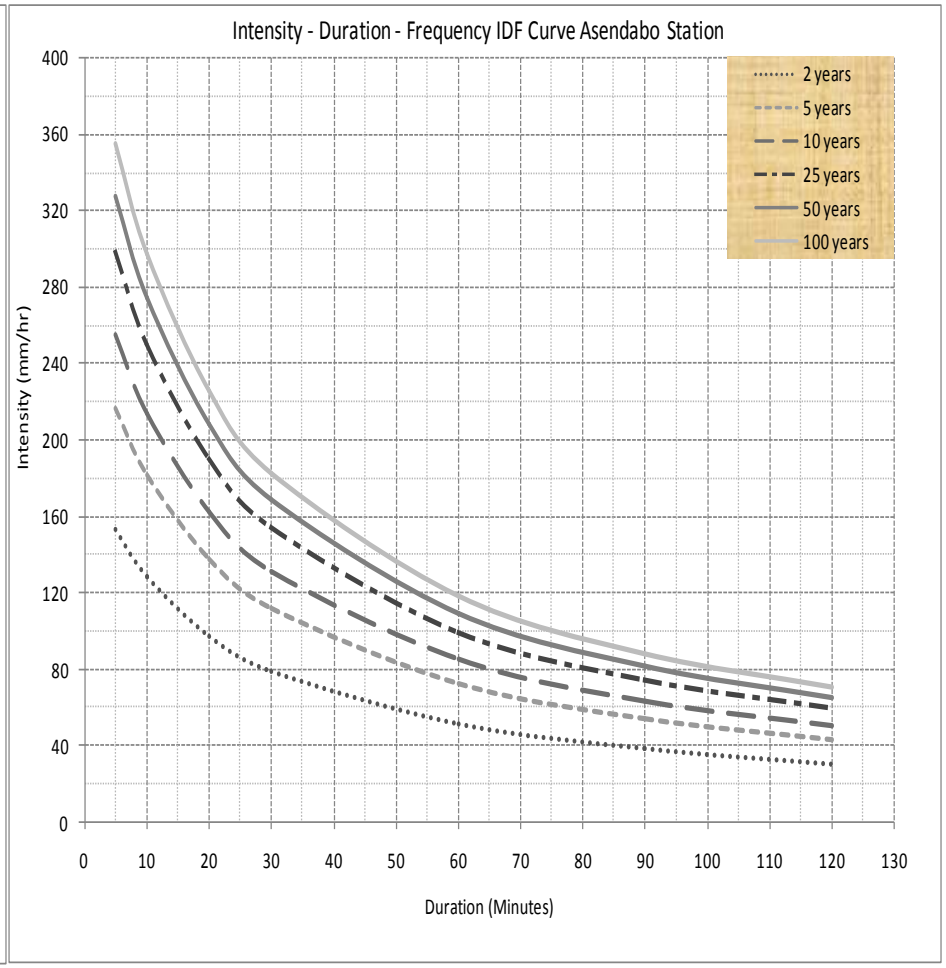

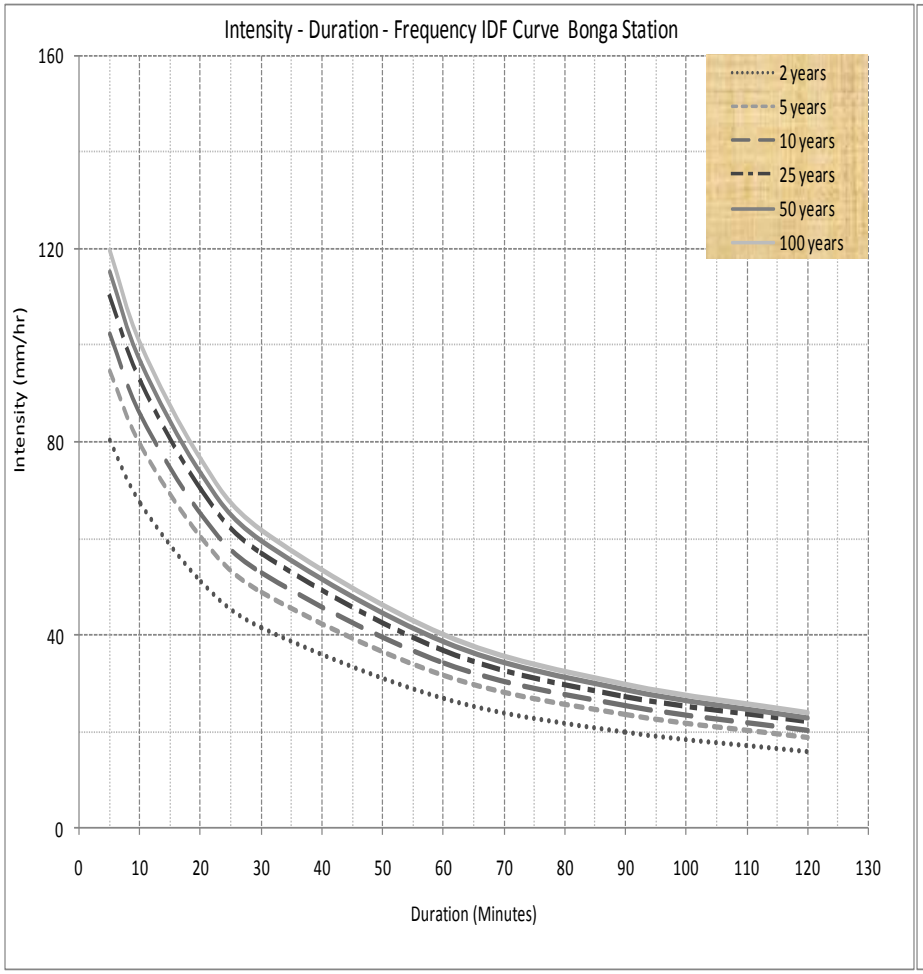
Intensity - Duration - Frequency IDF Curve Bonga Station
Intensity (mm/hr)
Duration (Minutes)
2 years
5 years
10 years
25 years
50 years
100 years
0
40
80
120
160
0
10
20
30
40
50
60
70
80
90
100
110
120
130

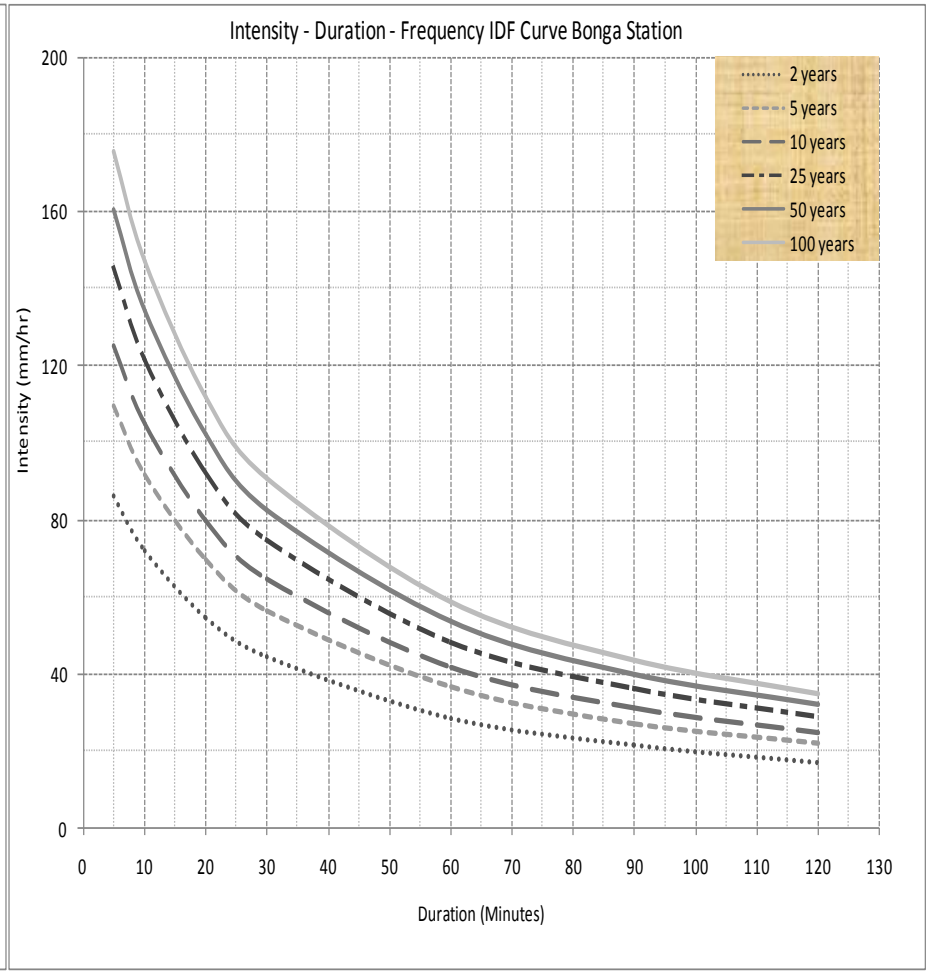
Intensity - Duration - Frequency IDF Curve Bonga Station
Intensity (mm/hr)
Duration (Minutes)
2 years
5 years
10 years
25 years
50 years
100 years
0
40
80
120
160
200
0
10
20
30
40
50
60
70
80
90
100
110
120
130

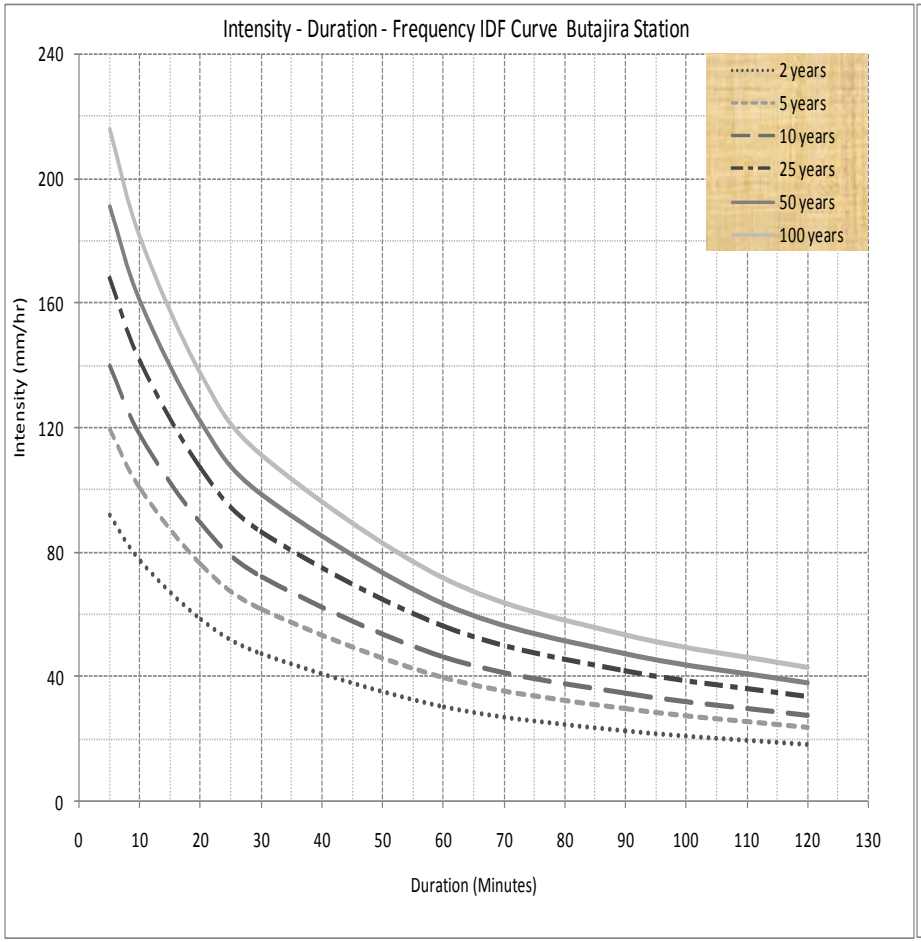
Intensity - Duration - Frequency IDF Curve Butajira Station
2 years
5 years
10 years
25 years
50 years
100 years
Intensity (mm/hr)
Duration (Minutes)
0
40
80
120
160
200
240
0
10
20
30
40
50
60
70
80
90
100
110
120
130

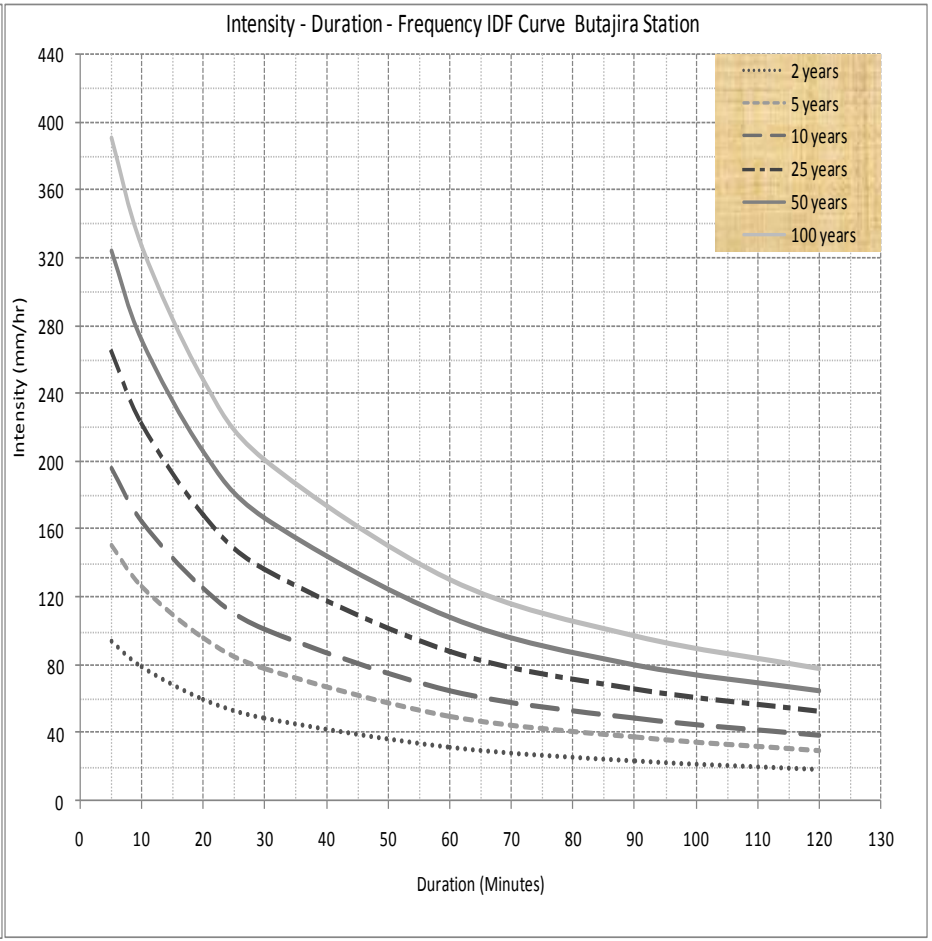
Intensity - Duration - Frequency IDF Curve Butajira Station
2 years
5 years
10 years
25 years
50 years
100 years
Intensity (mm/hr)
Duration (Minutes)
0
40
80
120
160
200
240
280
320
360
400
440
0
10
20
30
40
50
60
70
80
90
100
110
120
130

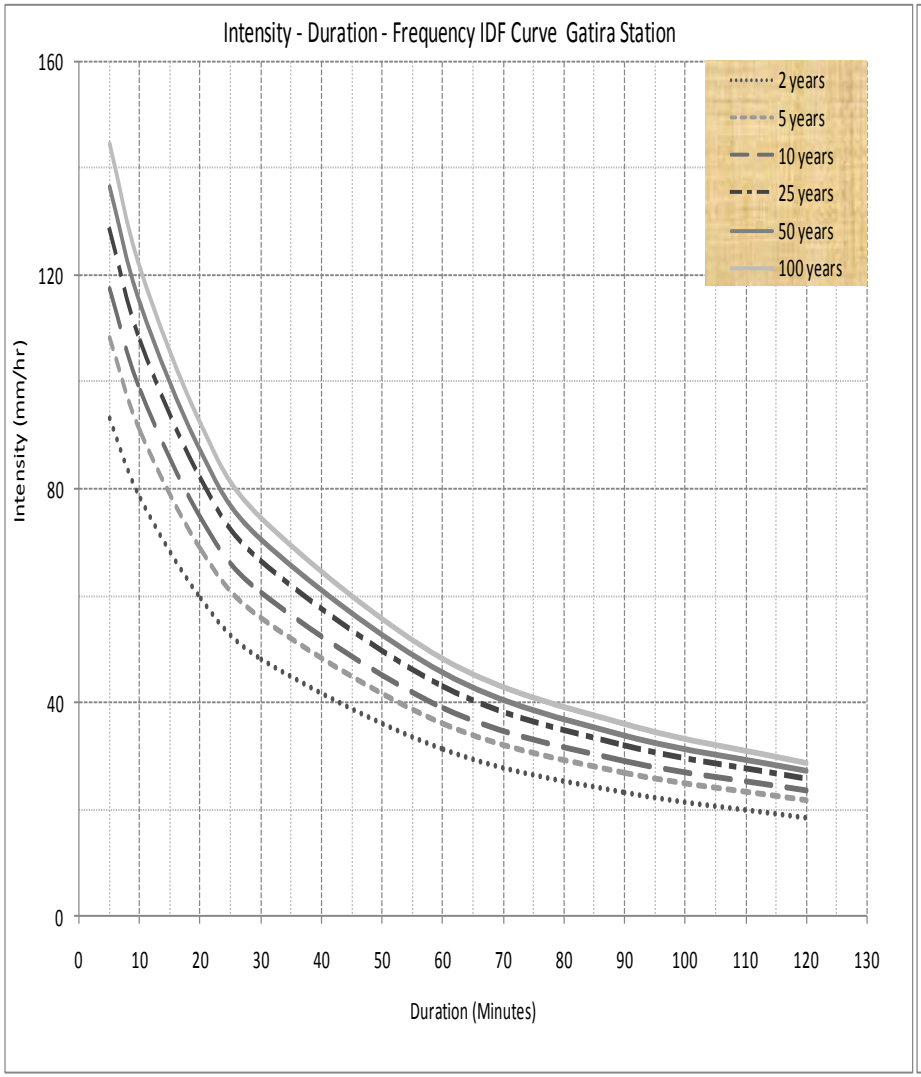
Intensity - Duration - Frequency IDF Curve Gatira Station
Intensity (mm/hr)
Duration (Minutes)
2 years
5 years
10 years
25 years
50 years
100 years
0
40
80
120
160
0
10
20
30
40
50
60
70
80
90
100
110
120
130

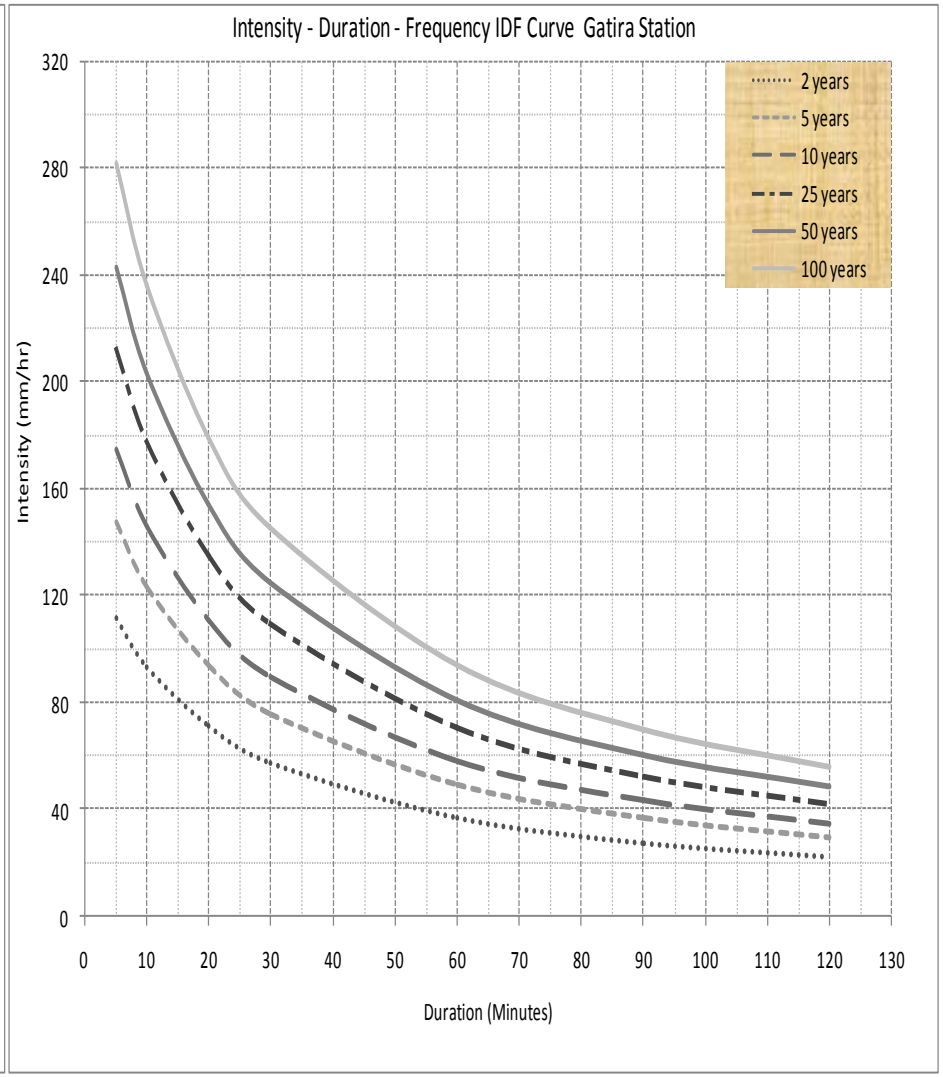
Intensity - Duration - Frequency IDF Curve Gatira Station
Intensity (mm/hr)
Duration (Minutes)
2 years
5 years
10 years
25 years
50 years
100 years
0
40
80
120
160
200
240
280
320
0
10
20
30
40
50
60
70
80
90
100
110
120
130

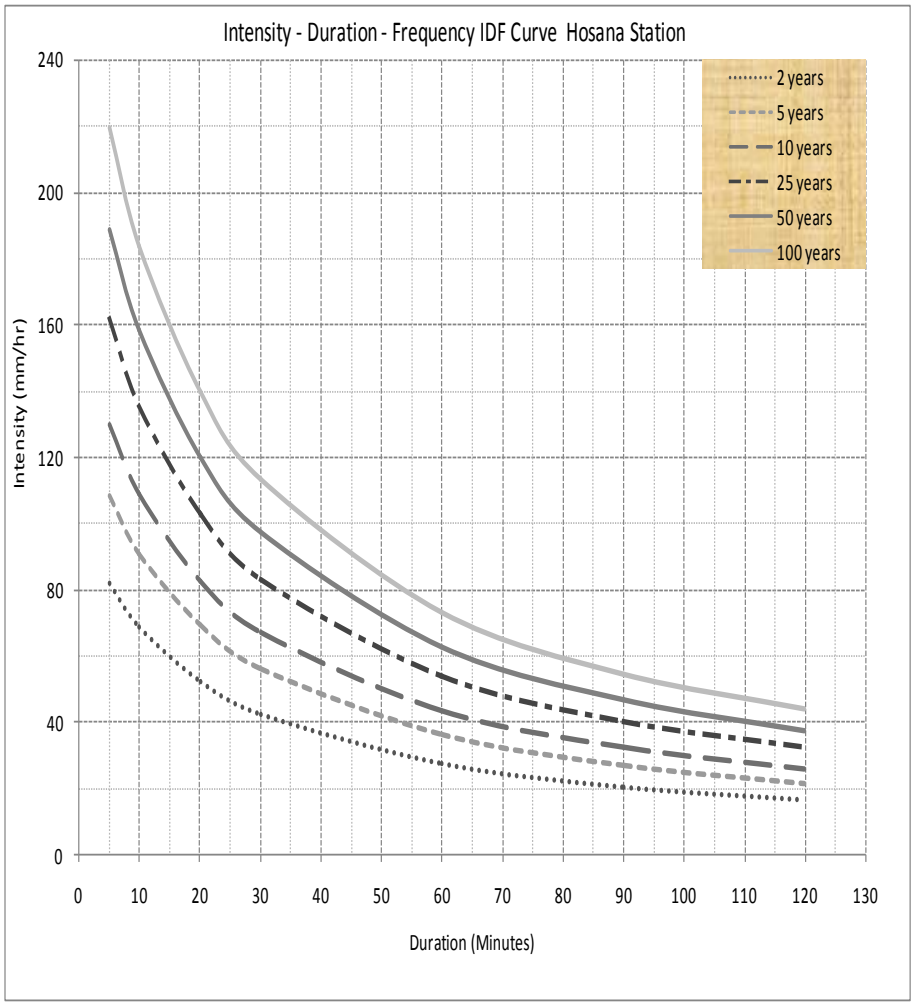
Intensity - Duration - Frequency IDF Curve Hosana Station
Intensity (mm/hr)
Duration (Minutes)
2 years
5 years
10 years
25 years
50 years
100 years
0
40
80
120
160
200
240
0
10
20
30
40
50
60
70
80
90
100
110
120
130

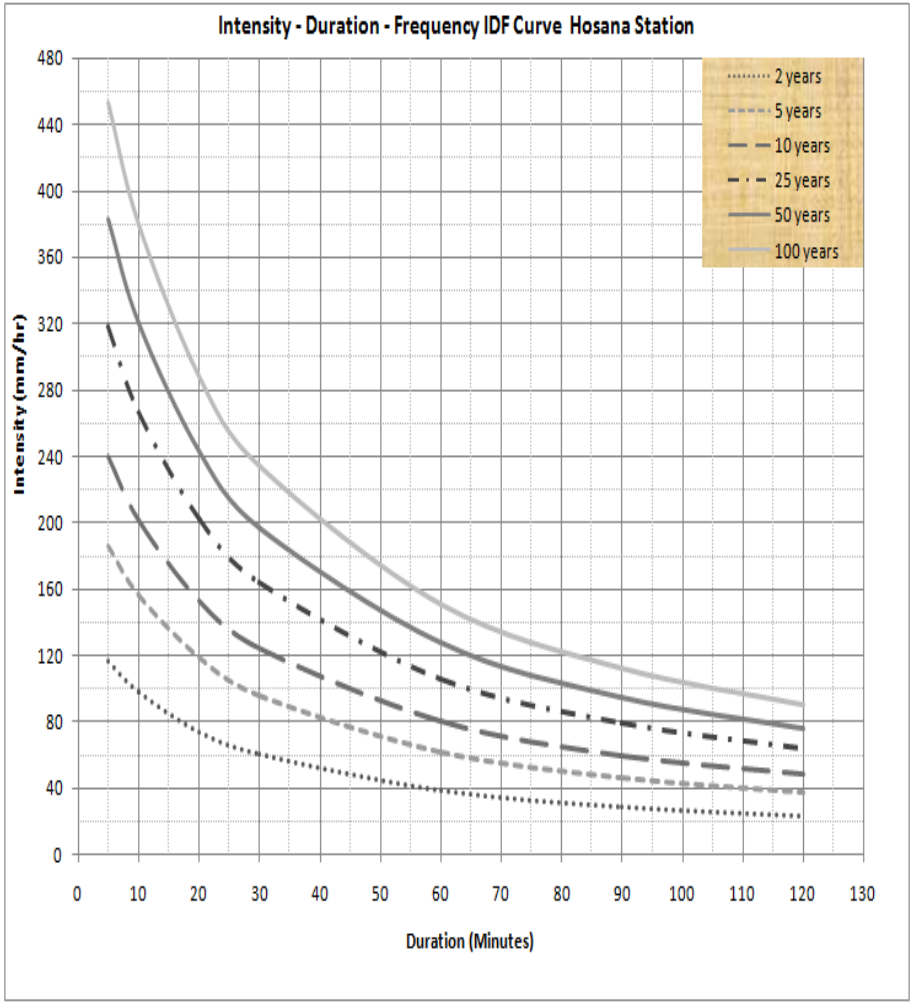
Intensity - Duration - Frequency IDF Curve Hosana Station
Intensity (mm/hr)
Duration (Minutes)
2 years
5 years
10 years
25 years
50 years
100 years
0
40
80
120
160
200
240
280
320
360
400
440
480
0
10
20
30
40
50
60
70
80
90
100
110
120
130

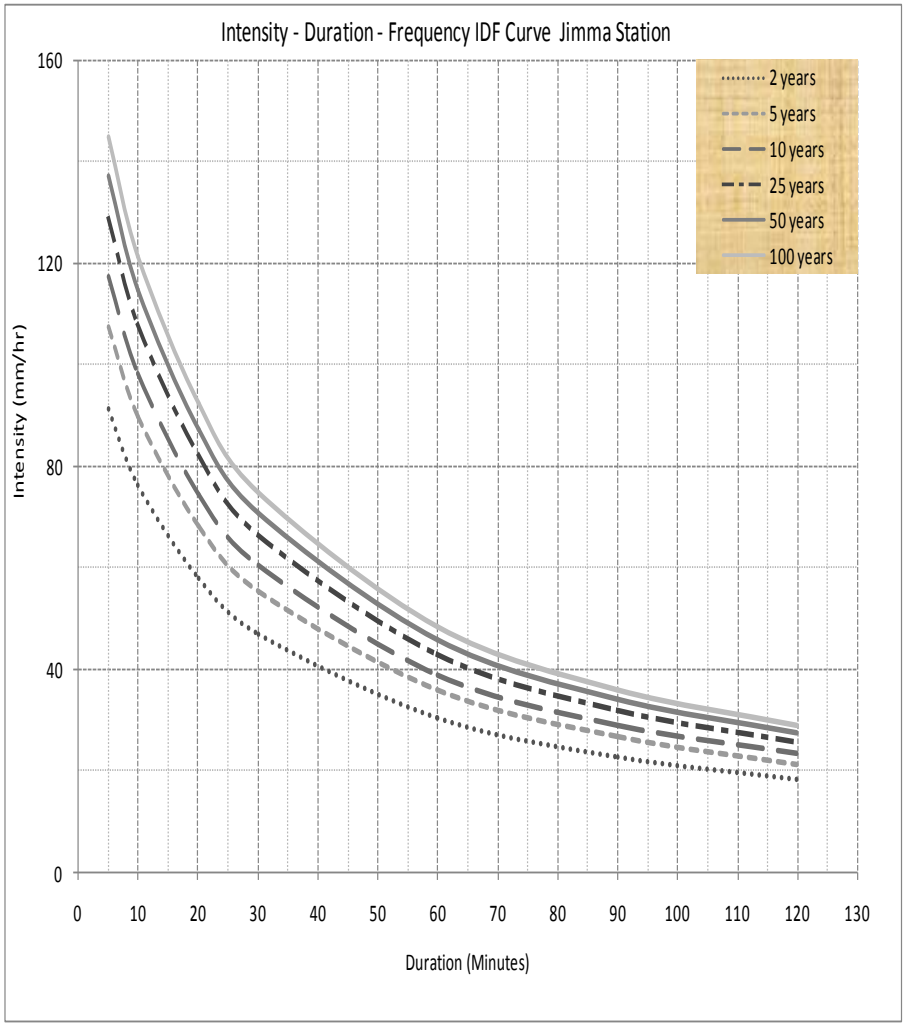
Intensity - Duration - Frequency IDF Curve Jimma Station
Intensity (mm/hr)
Duration (Minutes)
2 years
5 years
10 years
25 years
50 years
100 years
0
40
80
120
160
0
10
20
30
40
50
60
70
80
90
100
110
120
130

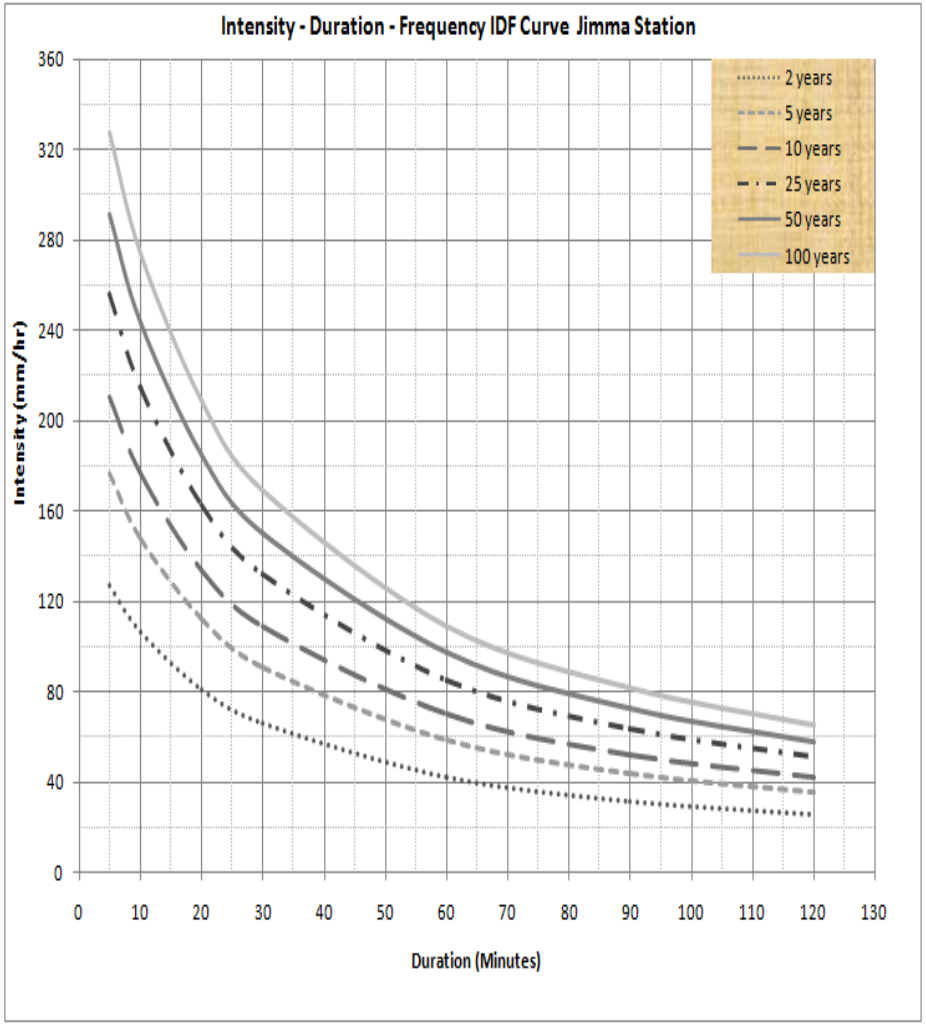
Intensity - Duration - Frequency IDF Curve Jimma Station
Intensity (mm/hr)
Duration (Minutes)
2 years
5 years
10 years
25 years
50 years
100 years
0
40
80
120
160
200
240
280
320
360
0
10
20
30
40
50
60
70
80
90
100
110
120
130

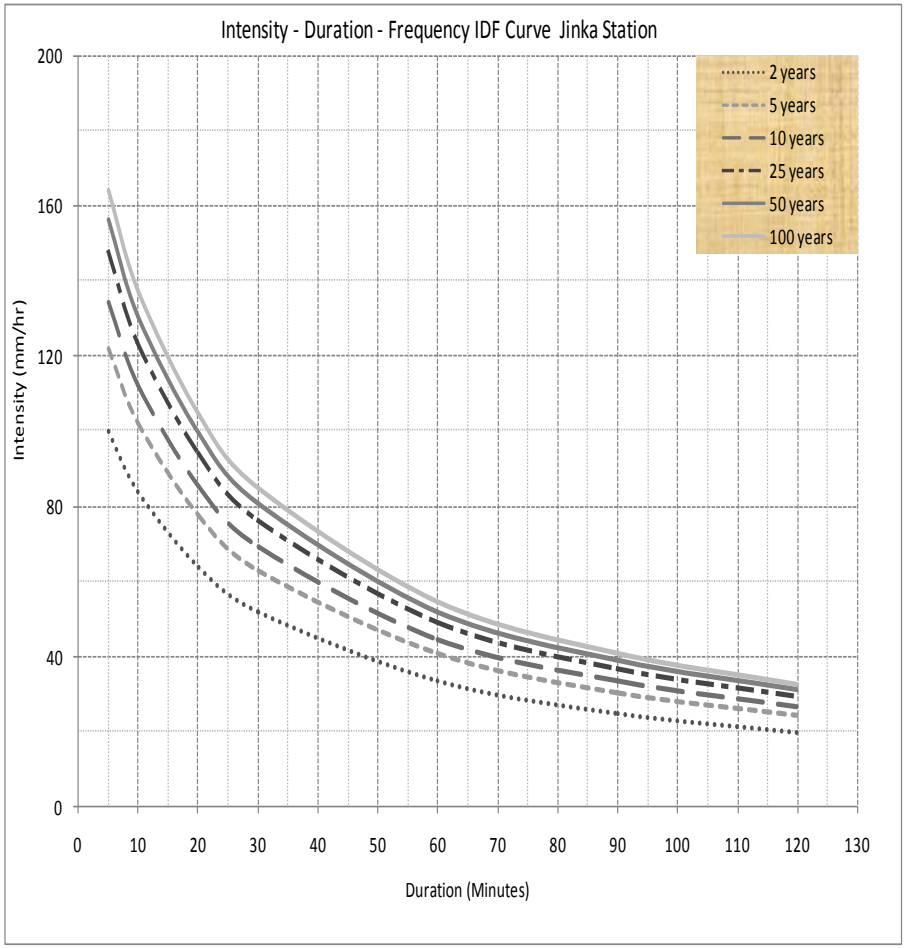
Intensity - Duration - Frequency IDF Curve Jinka Station
2 years
5 years
10 years
25 years
50 years
100 years
Intensity (mm/hr)
Duration (Minutes)
0
40
80
120
160
200
0
10
20
30
40
50
60
70
80
90
100
110
120
130

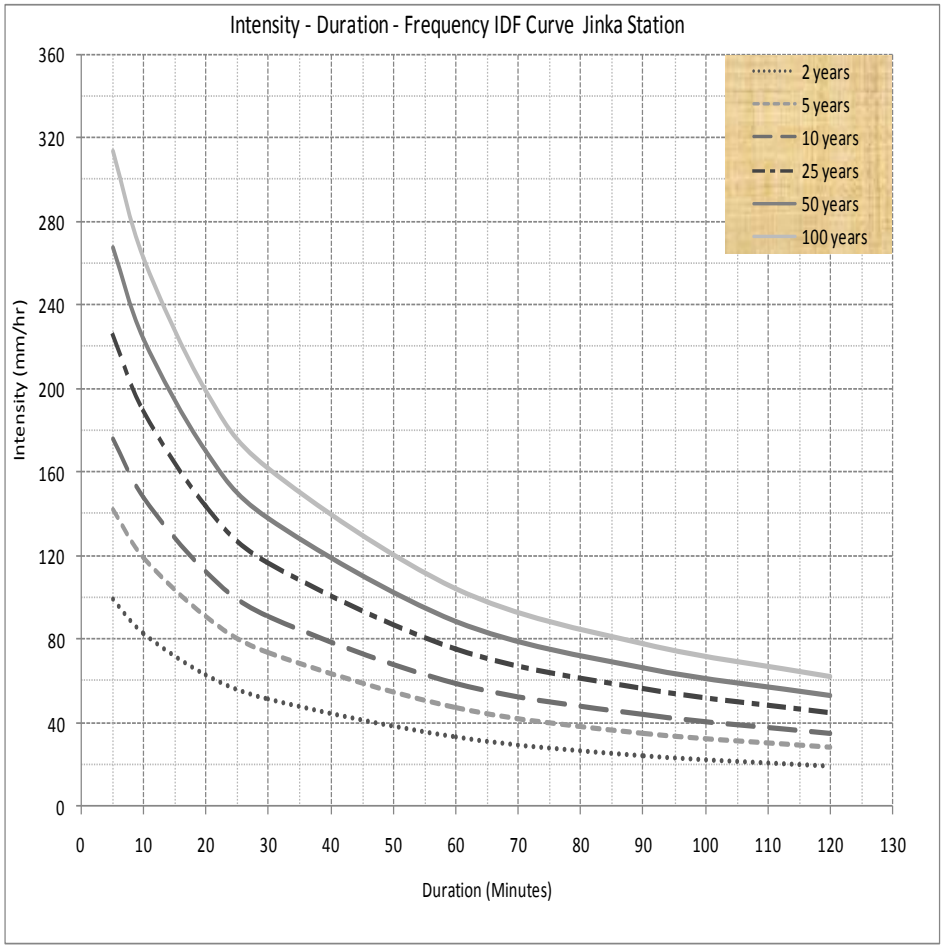
Intensity - Duration - Frequency IDF Curve Jinka Station
2 years
5 years
10 years
25 years
50 years
100 years
Intensity (mm/hr)
Duration (Minutes)
0
40
80
120
160
200
240
280
320
360
0
10
20
30
40
50
60
70
80
90
100
110
120
130

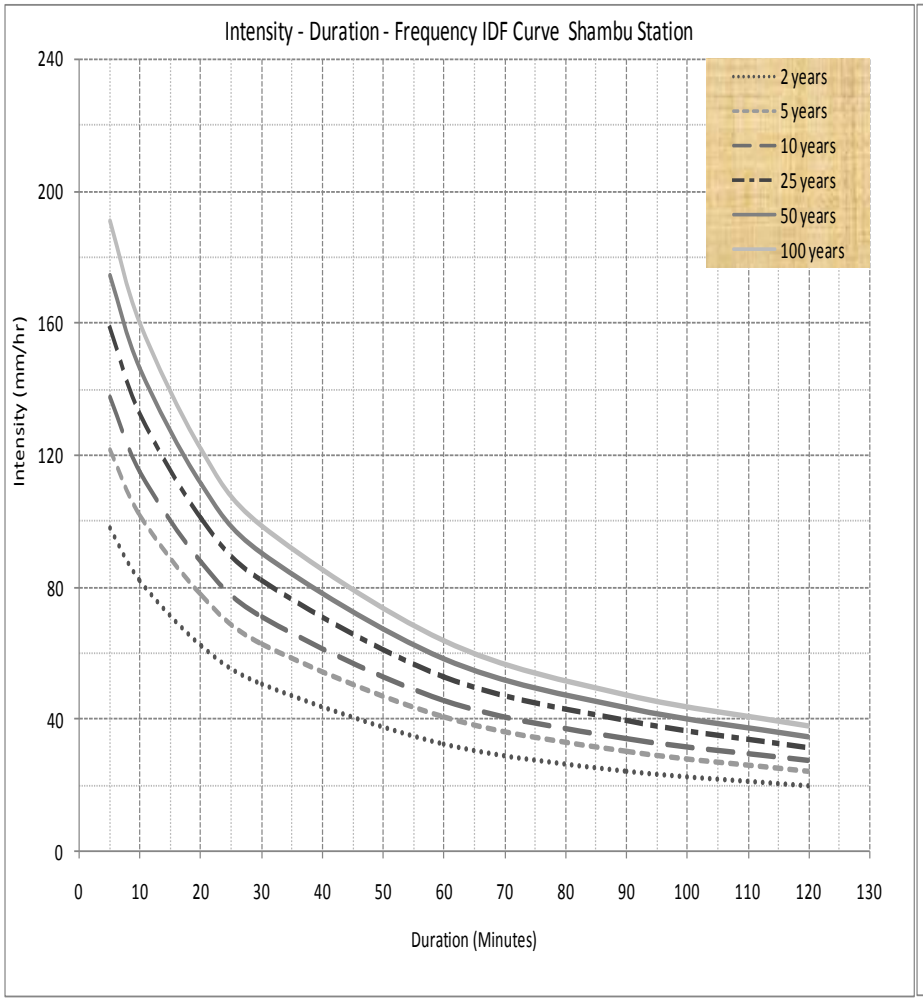
Intensity - Duration - Frequency IDF Curve Shambu Station
Intensity (mm/hr)
Duration (Minutes)
2 years
5 years
10 years
25 years
50 years
100 years
0
40
80
120
160
200
240
0
10
20
30
40
50
60
70
80
90
100
110
120
130

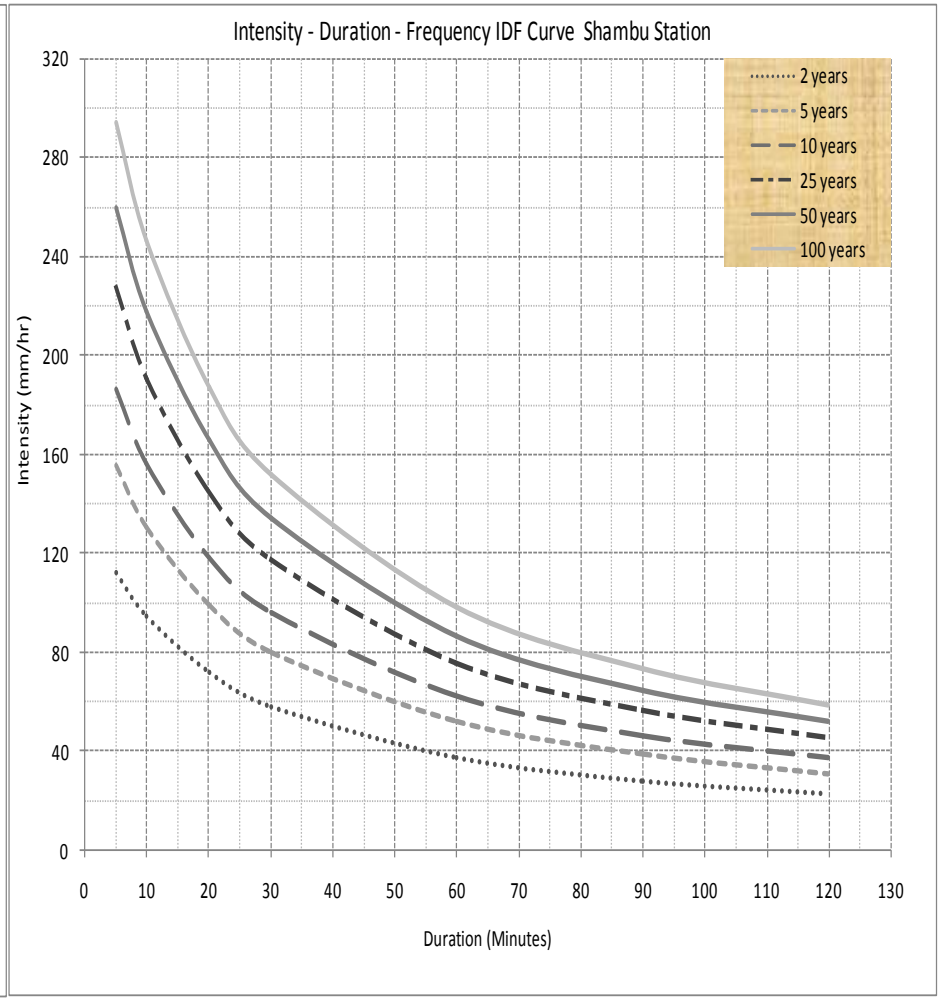
Intensity - Duration - Frequency IDF Curve Shambu Station
Intensity (mm/hr)
Duration (Minutes)
2 years
5 years
10 years
25 years
50 years
100 years
0
40
80
120
160
200
240
280
320
0
10
20
30
40
50
60
70
80
90
100
110
120
130

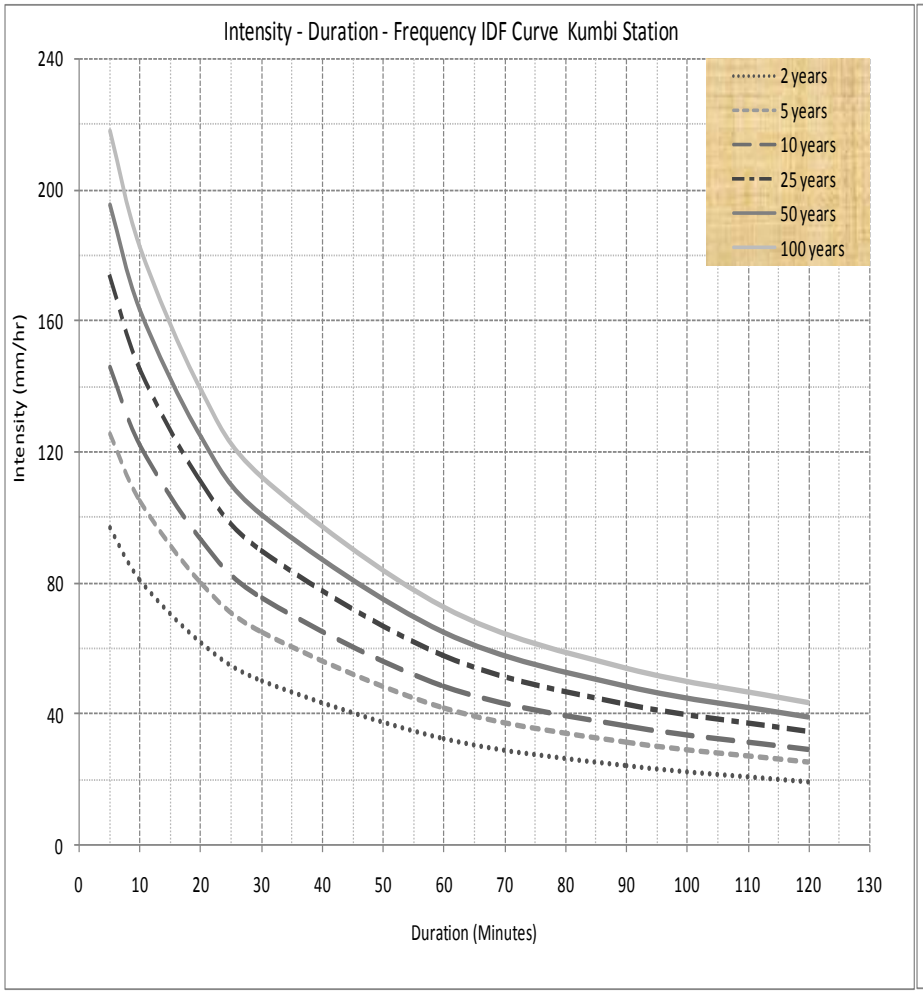
Intensity - Duration - Frequency IDF Curve Kumbi Station
Intensity (mm/hr)
Duration (Minutes)
2 years
5 years
10 years
25 years
50 years
100 years
0
40
80
120
160
200
240
0
10
20
30
40
50
60
70
80
90
100
110
120
130

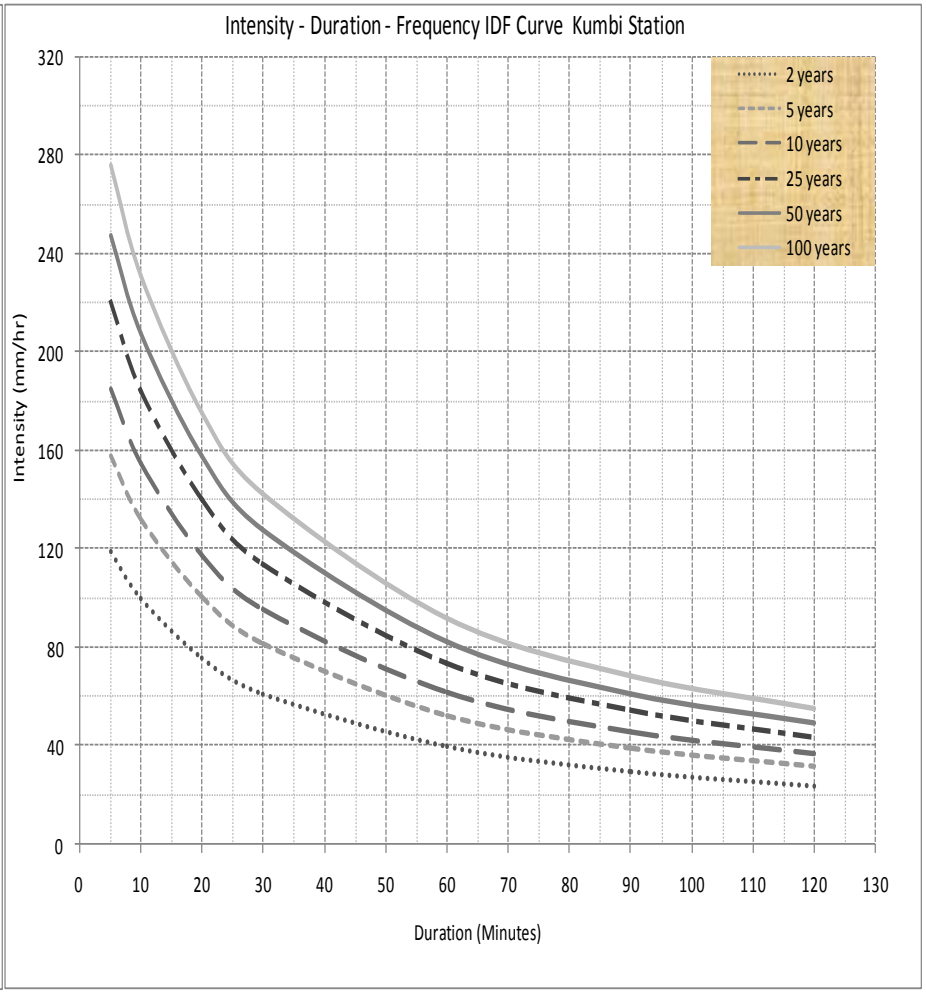
Intensity - Duration - Frequency IDF Curve Kumbi Station
Intensity (mm/hr)
Duration (Minutes)
2 years
5 years
10 years
25 years
50 years
100 years
0
40
80
120
160
200
240
280
320
0
10
20
30
40
50
60
70
80
90
100
110
120
130

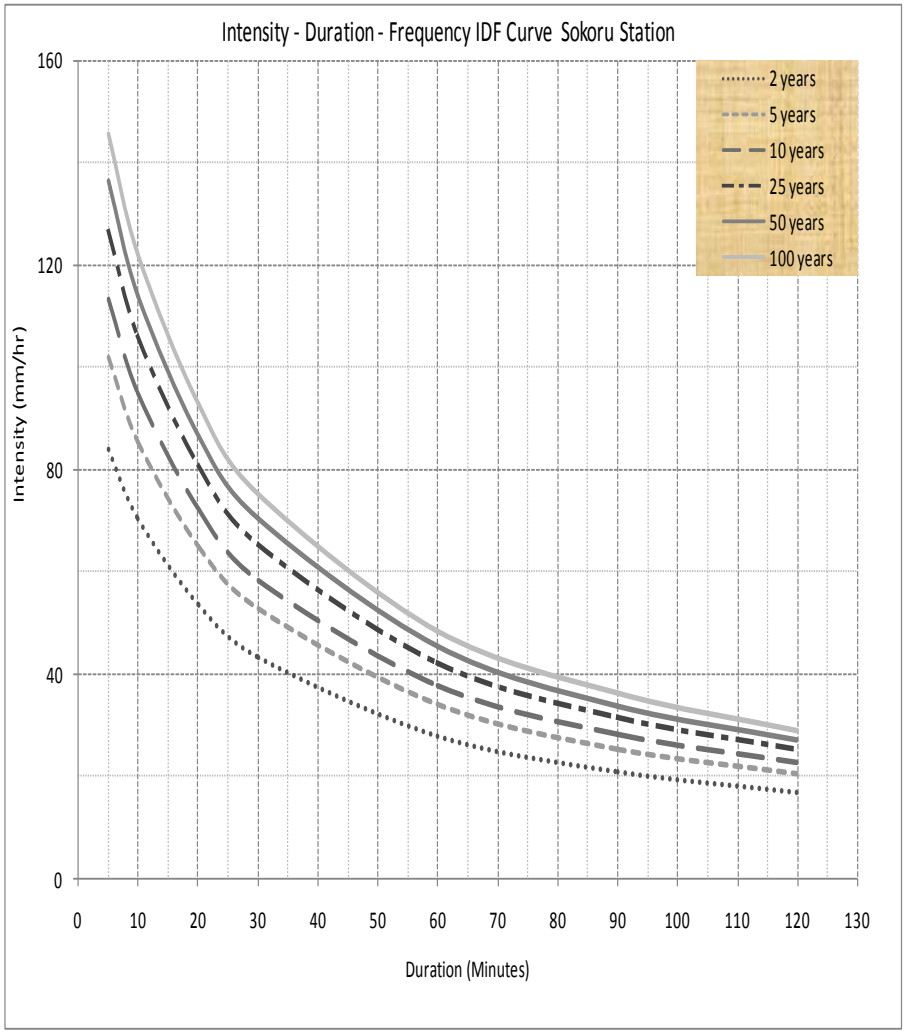
Intensity - Duration - Frequency IDF Curve Sokoru Station
2 years
5 years
10 years
25 years
50 years
100 years
Intensity (mm/hr)
Duration (Minutes)
0
40
80
120
160
0
10
20
30
40
50
60
70
80
90
100
110
120
130

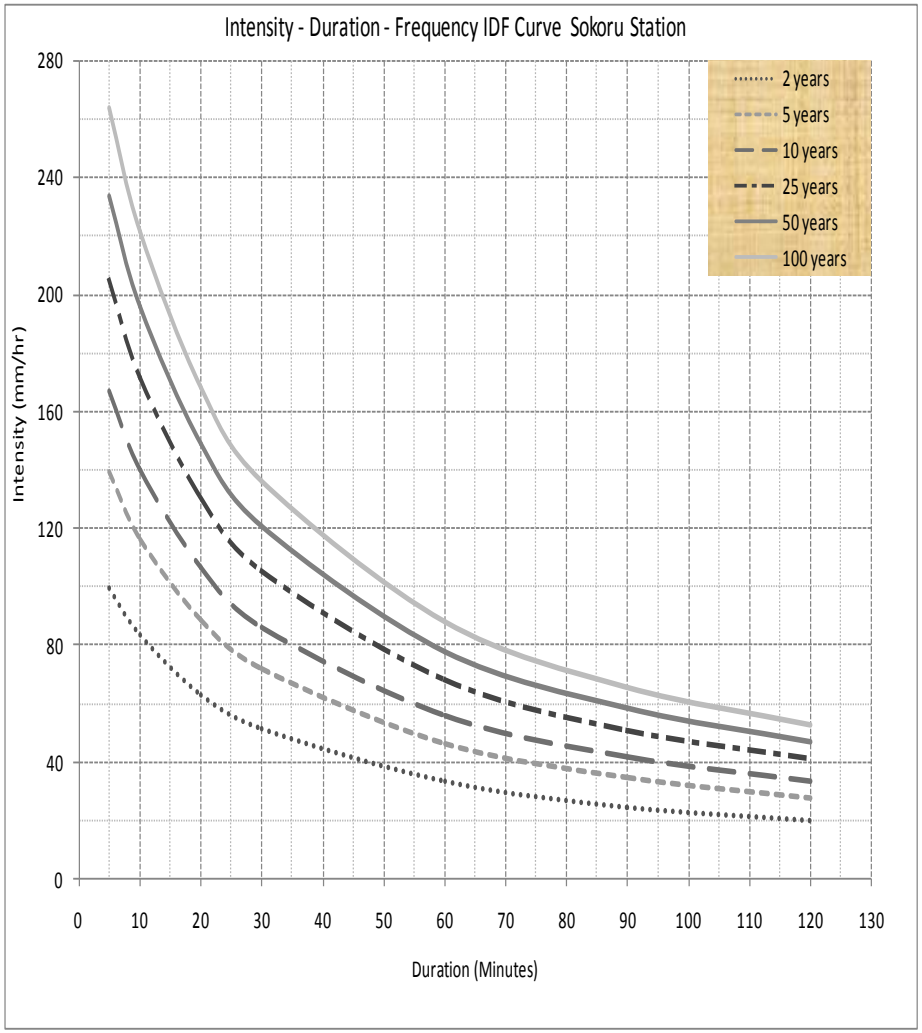
Intensity - Duration - Frequency IDF Curve Sokoru Station
2 years
5 years
10 years
25 years
50 years
100 years
Intensity (mm/hr)
Duration (Minutes)
0
40
80
120
160
200
240
280
0
10
20
30
40
50
60
70
80
90
100
110
120
130

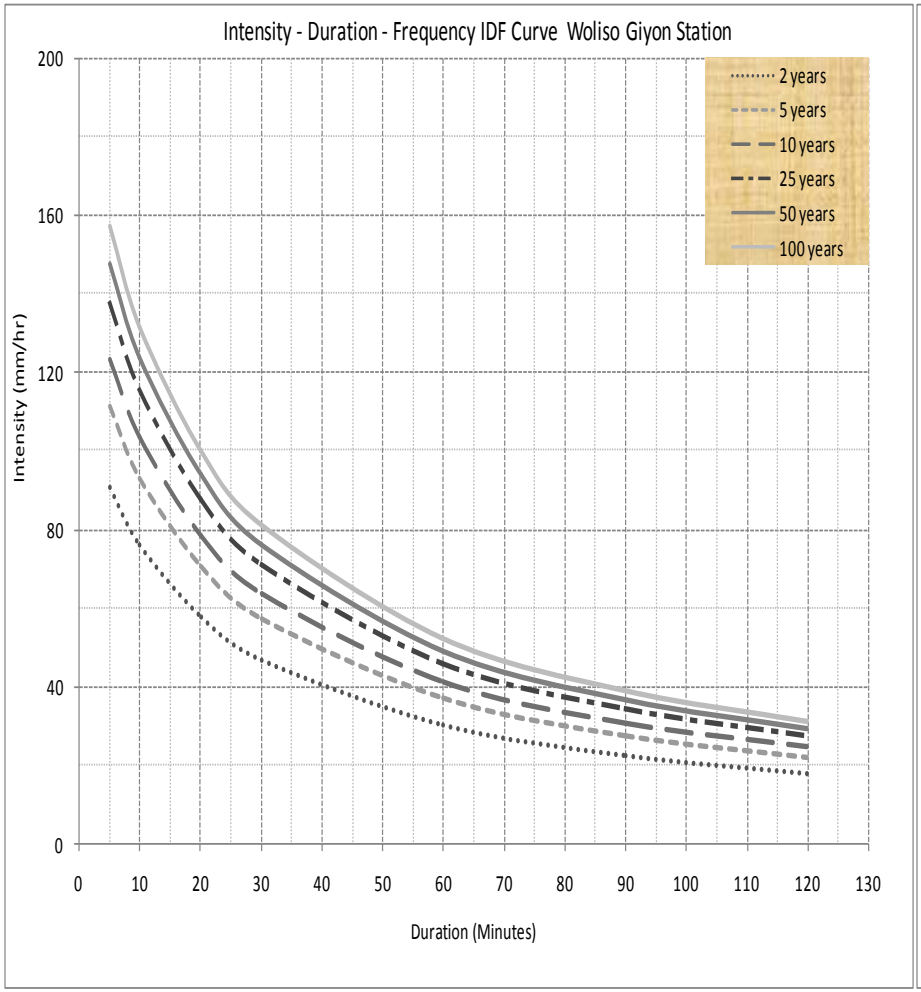
Intensity - Duration - Frequency IDF Curve Woliso Giyon Station
2 years
5 years
10 years
25 years
50 years
100 years
Intensity (mm/hr)
Duration (Minutes)
0
40
80
120
160
200
0
10
20
30
40
50
60
70
80
90
100
110
120
130

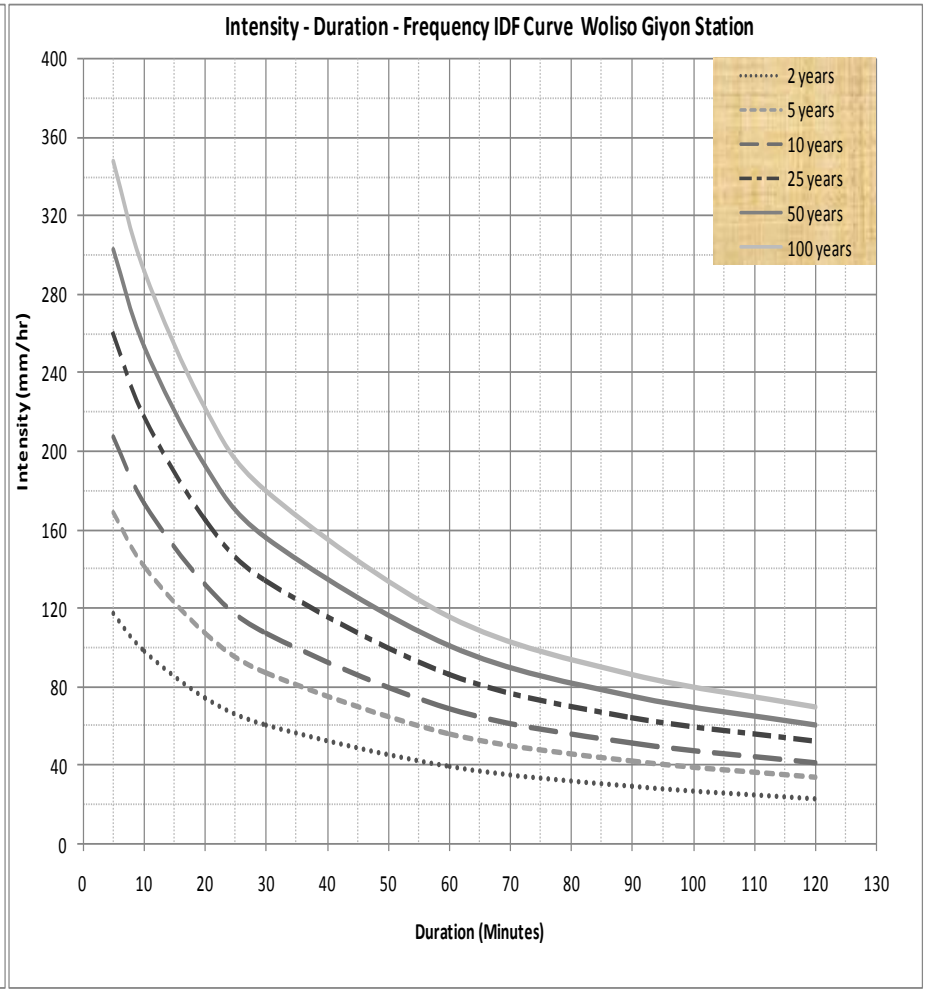
Intensity - Duration - Frequency IDF Curve Woliso Giyon Station
2 years
5 years
10 years
25 years
50 years
100 years
Intensity (mm/hr)
Duration (Minutes)
0
40
80
120
160
200
240
280
320
360
400
0
10
20
30
40
50
60
70
80
90
100
110
120
130

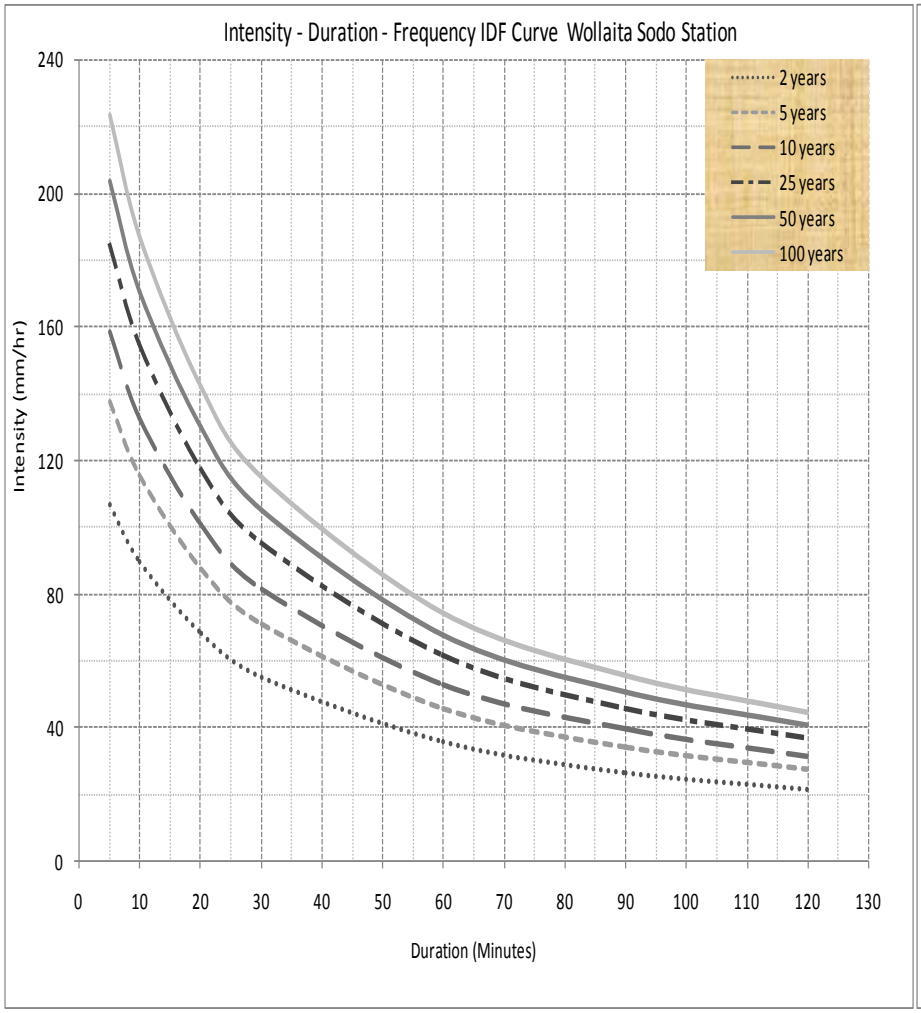
Intensity - Duration - Frequency IDF Curve Wollaita Sodo Station
Intensity (mm/hr)
Duration (Minutes)
2 years
5 years
10 years
25 years
50 years
100 years
0
40
80
120
160
200
240
0
10
20
30
40
50
60
70
80
90
100
110
120
130

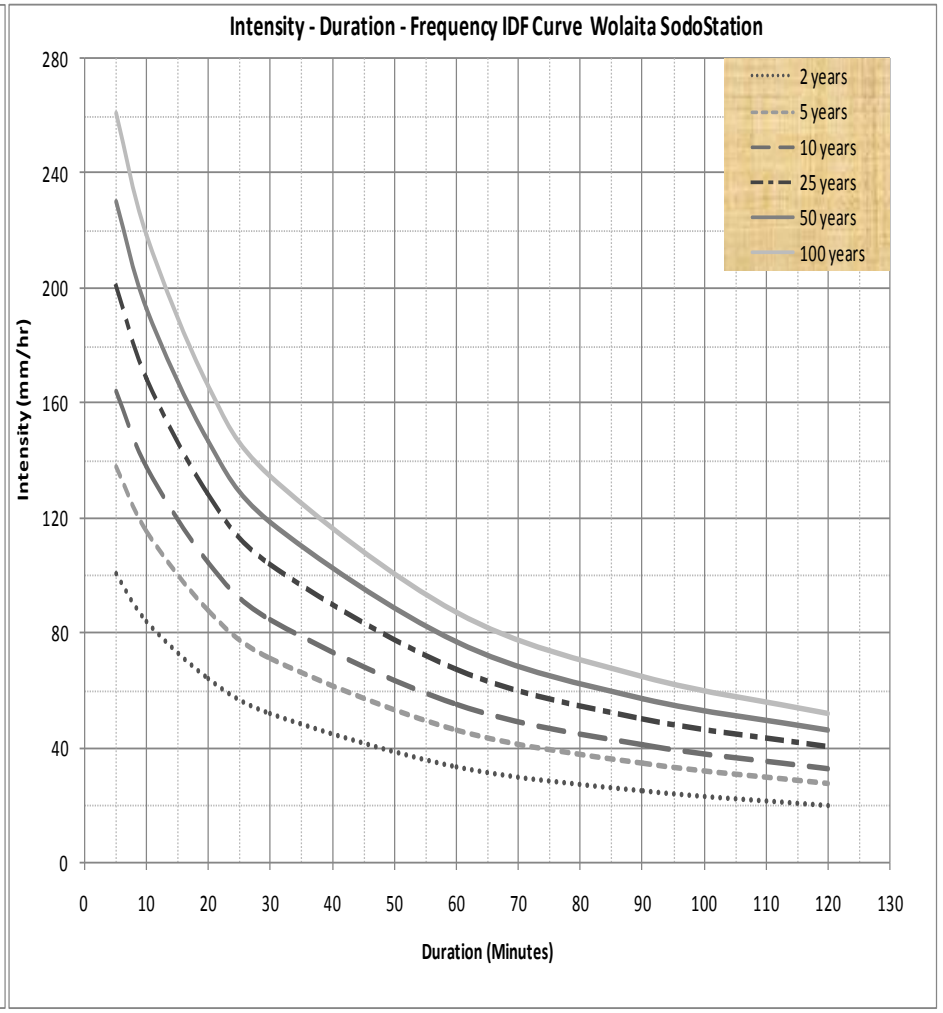
Intensity - Duration - Frequency IDF Curve Wolaita SodoStation
Intensity (mm/hr)
Duration (Minutes)
2 years
5 years
10 years
25 years
50 years
100 years
0
40
80
120
160
200
240
280
0
10
20
30
40
50
60
70
80
90
100
110
120
130

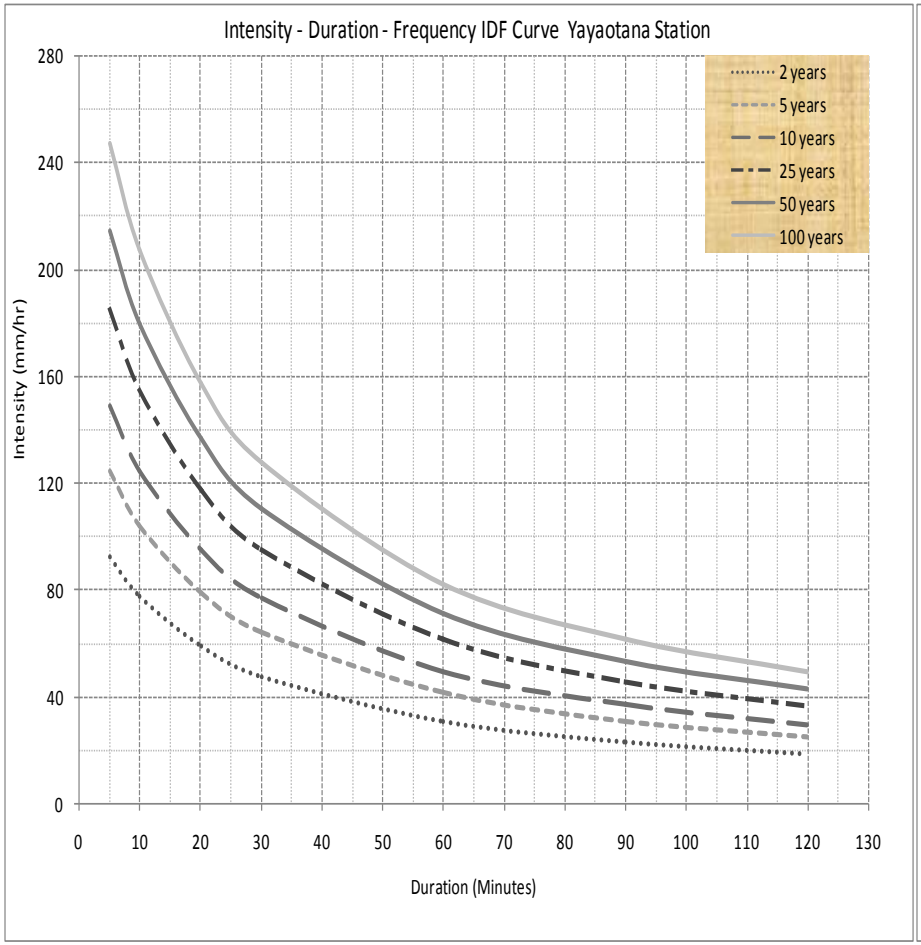
Intensity - Duration - Frequency IDF Curve Yayaotana Station
Intensity (mm/hr)
Duration (Minutes)
2 years
5 years
10 years
25 years
50 years
100 years
0
40
80
120
160
200
240
280
0
10
20
30
40
50
60
70
80
90
100
110
120
130

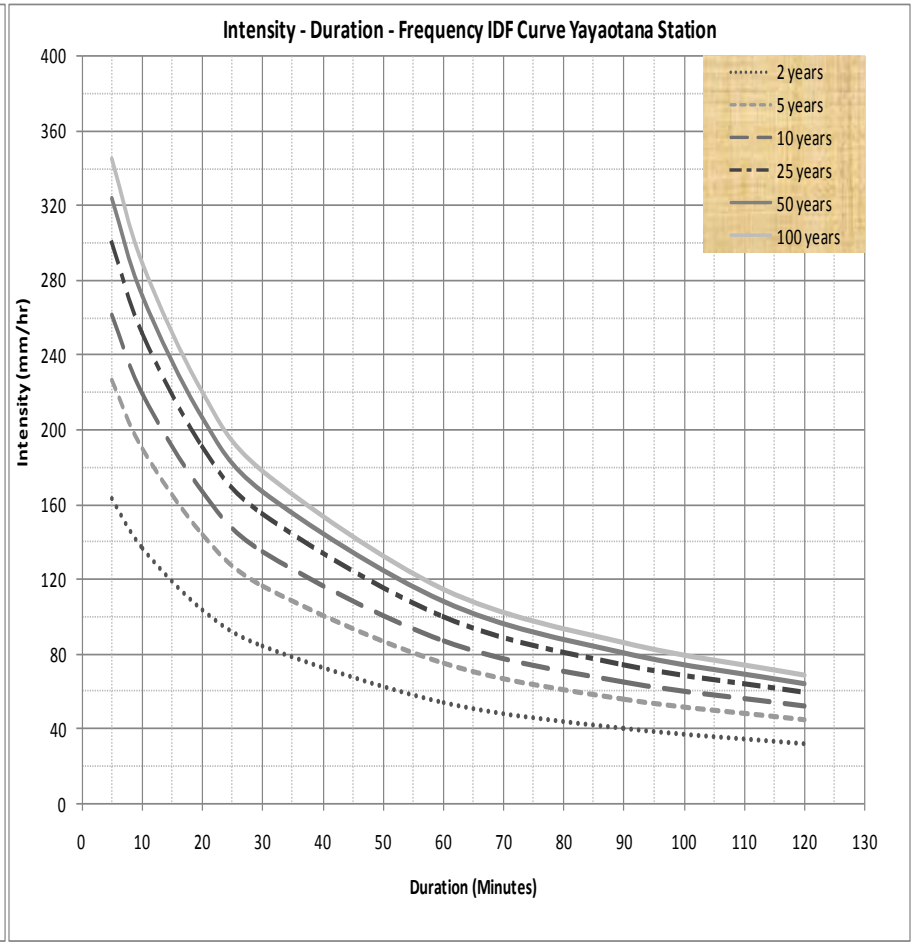
Intensity - Duration - Frequency IDF Curve Yayaotana Station
Intensity (mm/hr)
Duration (Minutes)
2 years
5 years
10 years
25 years
50 years
100 years
0
40
80
120
160
200
240
280
320
360
400
0
10
20
30
40
50
60
70
80
90
100
110
120
130

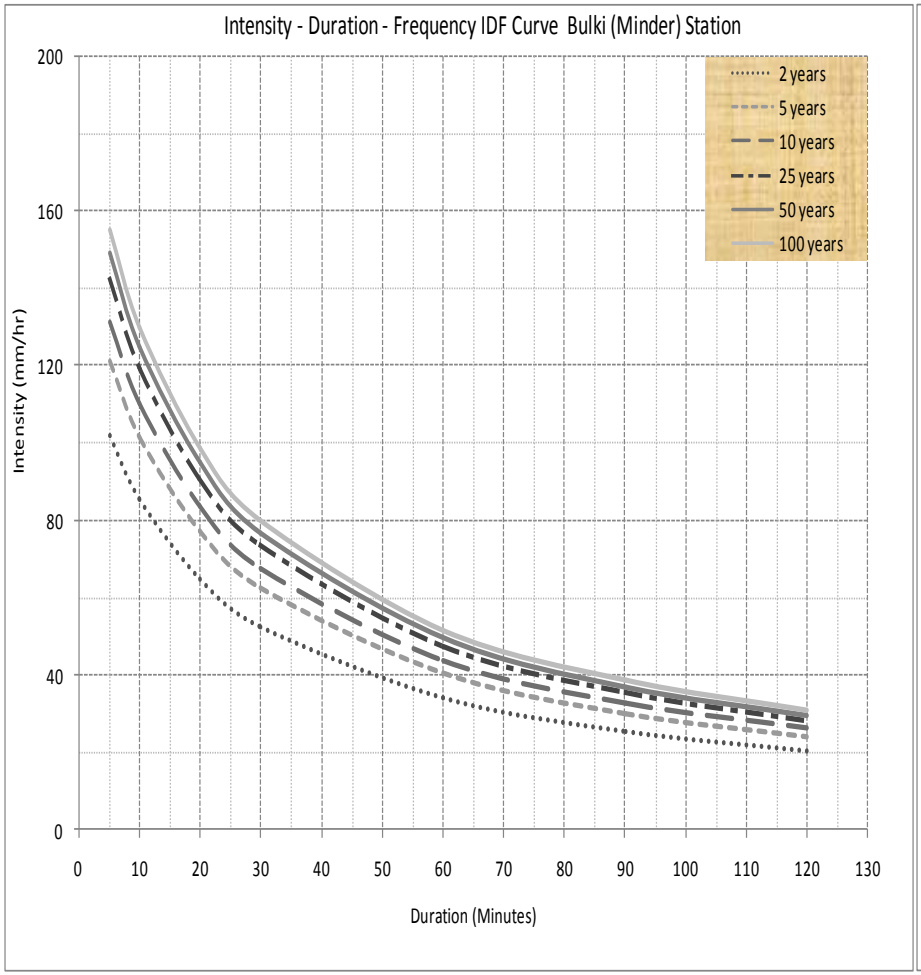
Intensity - Duration - Frequency IDF Curve Bulki (Minder) Station
Intensity (mm/hr)
Duration (Minutes)
2 years
5 years
10 years
25 years
50 years
100 years
0
40
80
120
160
200
0
10
20
30
40
50
60
70
80
90
100
110
120
130

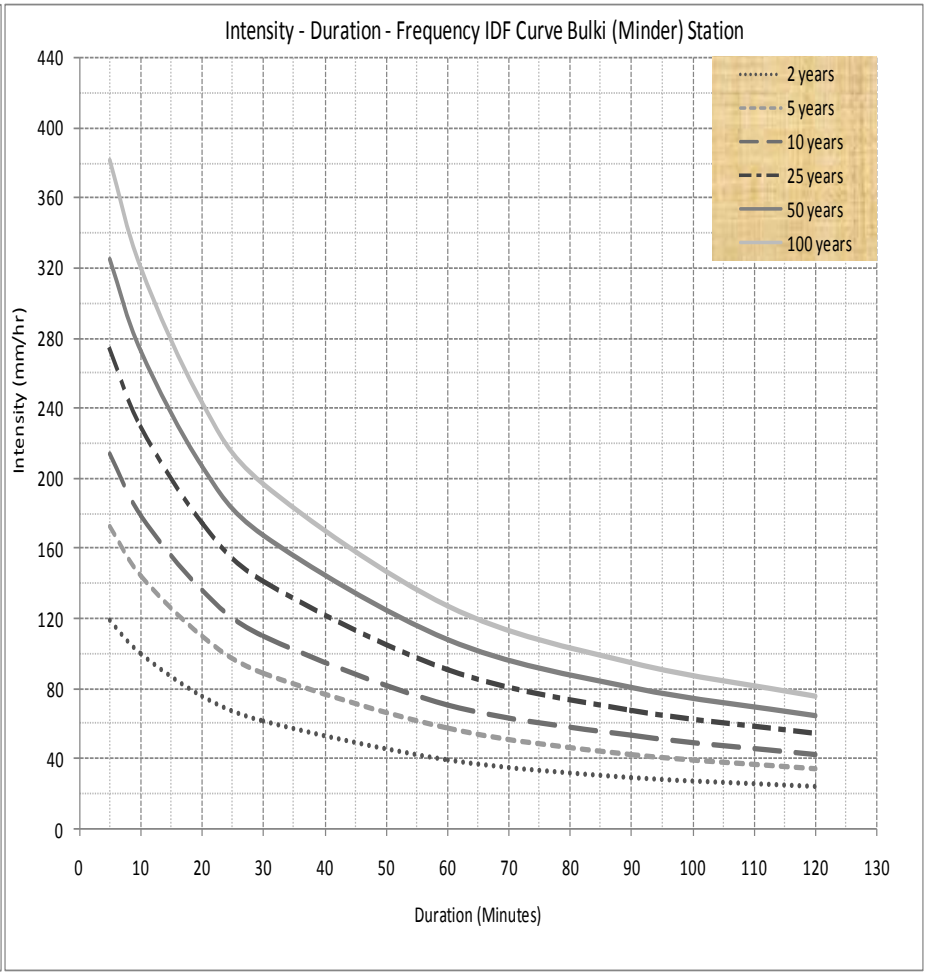
Intensity - Duration - Frequency IDF Curve Bulki (Minder) Station
Intensity (mm/hr)
Duration (Minutes)
2 years
5 years
10 years
25 years
50 years
100 years
0
40
80
120
160
200
240
280
320
360
400
440
0
10
20
30
40
50
60
70
80
90
100
110
120
130

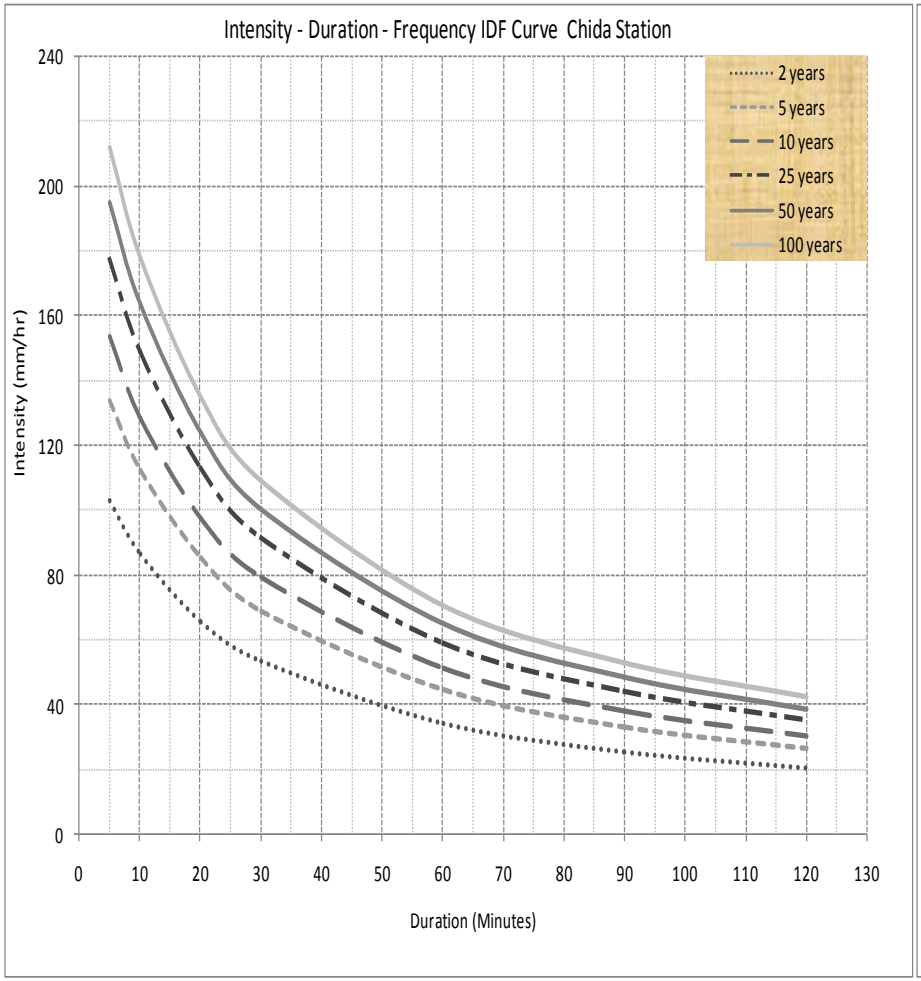
Intensity - Duration - Frequency IDF Curve Chida Station
Intensity (mm/hr)
Duration (Minutes)
2 years
5 years
10 years
25 years
50 years
100 years
0
40
80
120
160
200
240
0
10
20
30
40
50
60
70
80
90
100
110
120
130

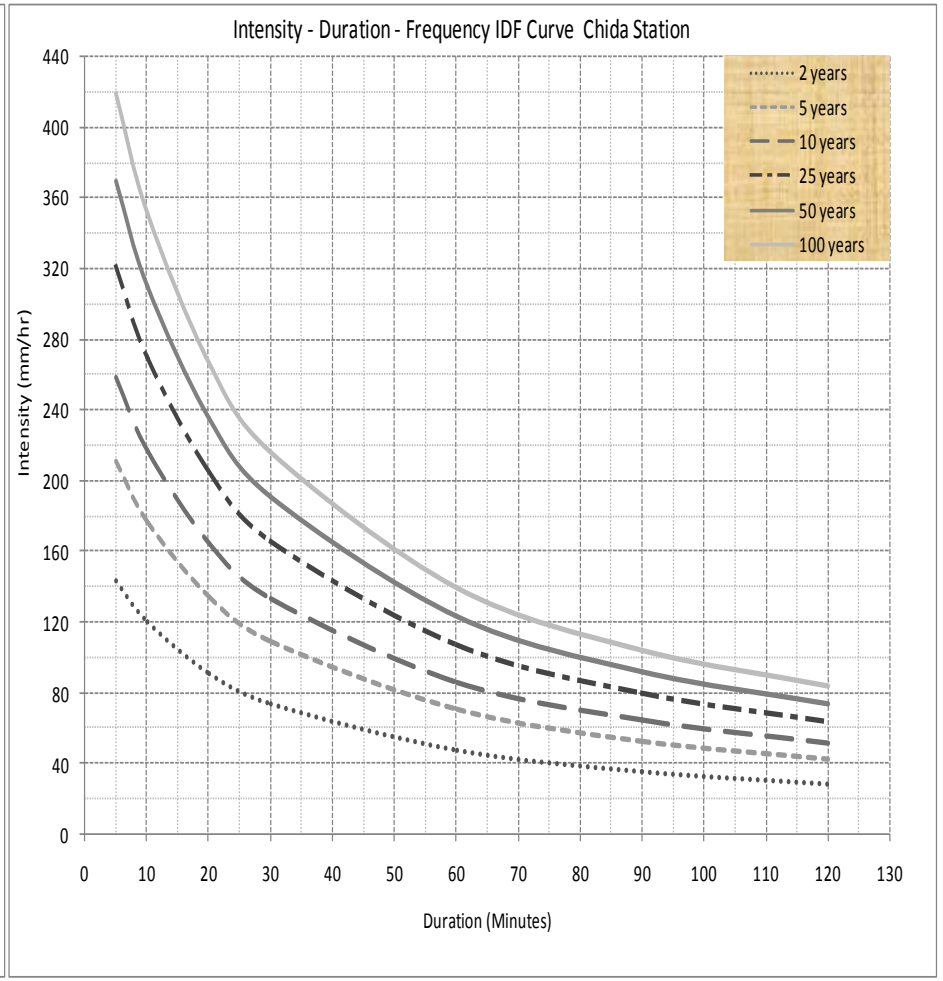
Intensity - Duration - Frequency IDF Curve Chida Station
Intensity (mm/hr)
Duration (Minutes)
2 years
5 years
10 years
25 years
50 years
100 years
0
40
80
120
160
200
240
280
320
360
400
440
0
10
20
30
40
50
60
70
80
90
100
110
120
130

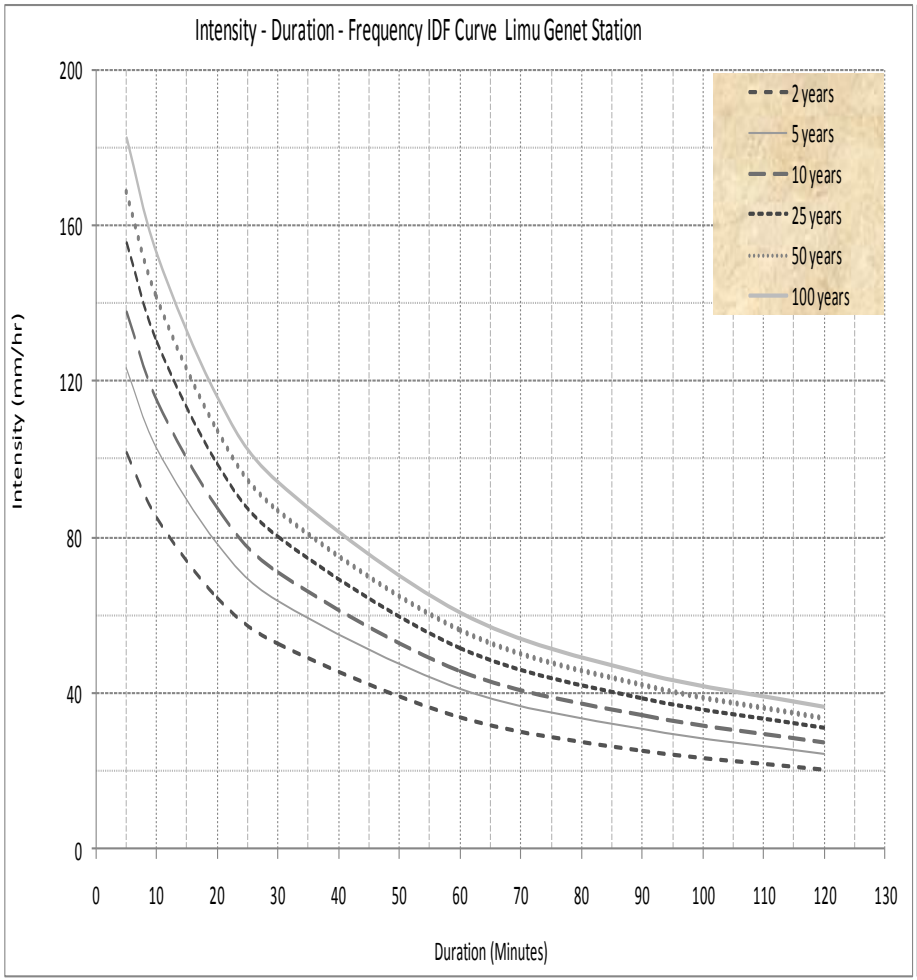
Intensity - Duration - Frequency IDF Curve Limu Genet Station
Intensity (mm/hr)
Duration (Minutes)
2 years
5 years
10 years
25 years
50 years
100 years
0
40
80
120
160
200
0
10
20
30
40
50
60
70
80
90
100
110
120
130

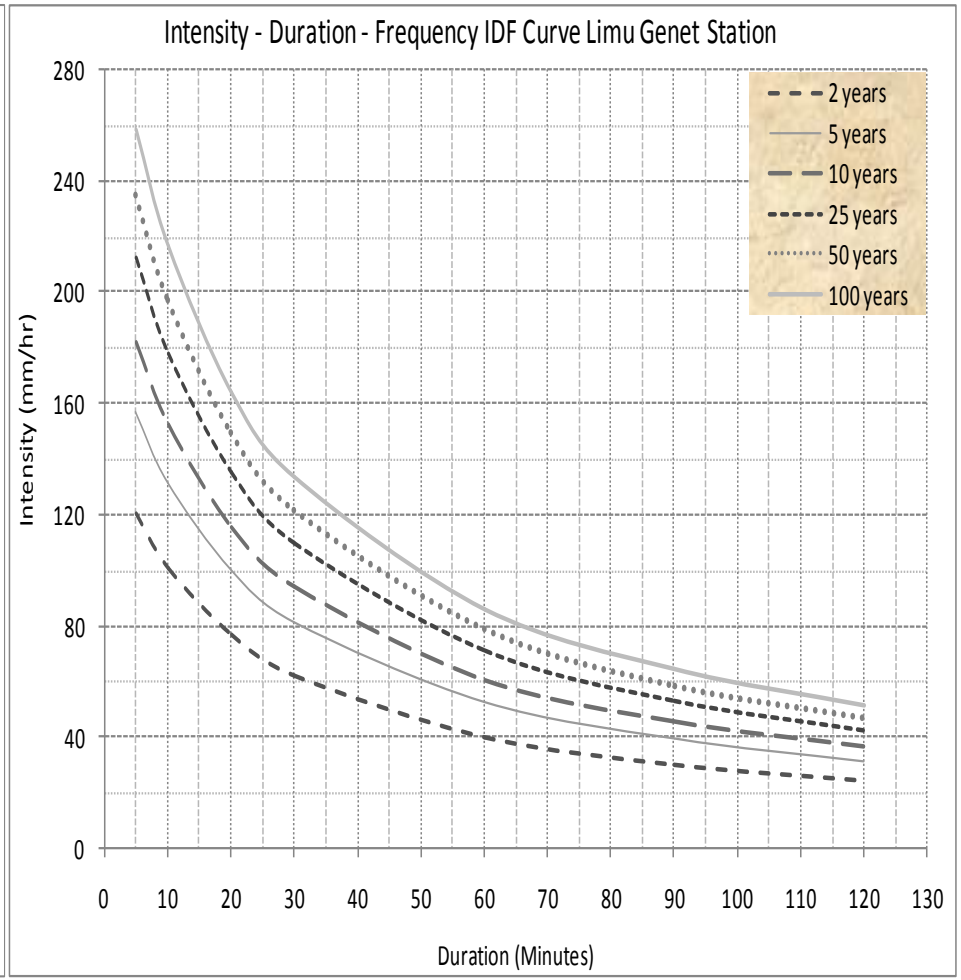
Intensity - Duration - Frequency IDF Curve Limu Genet Station
Intensity (mm/hr)
Duration (Minutes)
2 years
5 years
10 years
25 years
50 years
100 years
0
40
80
120
160
200
240
280
0
10
20
30
40
50
60
70
80
90
100
110
120
130

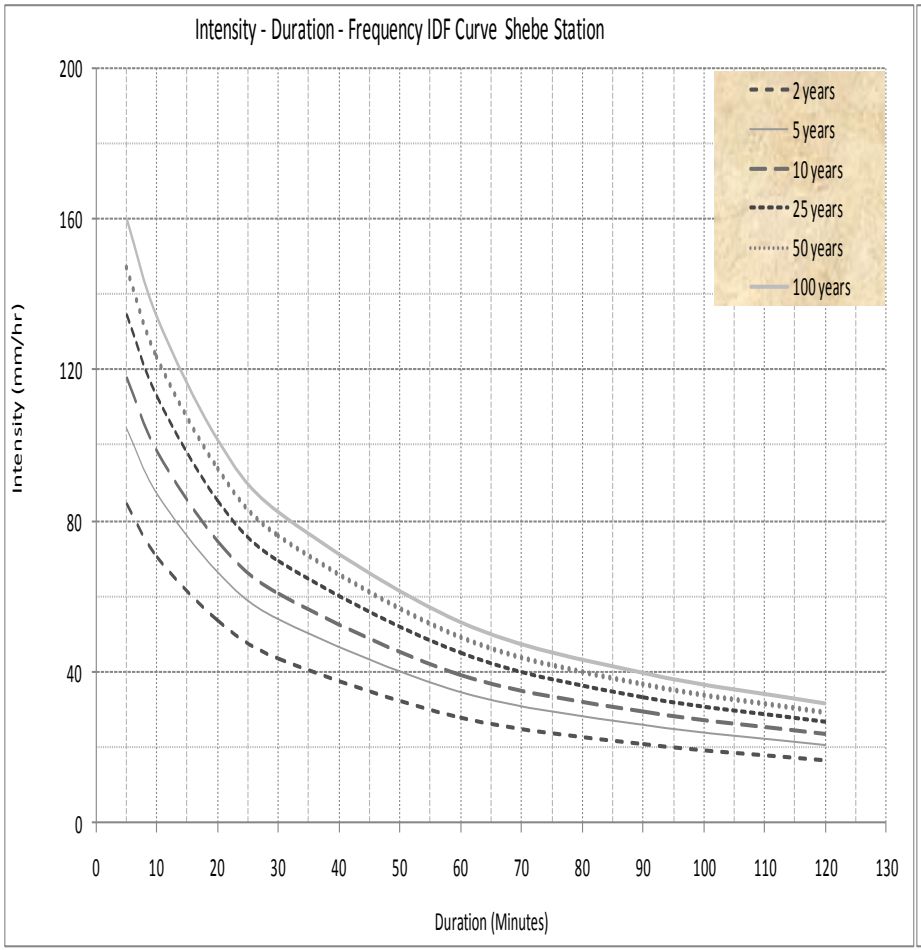
Intensity - Duration - Frequency IDF Curve Shebe Station
Intensity (mm/hr)
Duration (Minutes)
2 years
5 years
10 years
25 years
50 years
100 years
0
40
80
120
160
200
0
10
20
30
40
50
60
70
80
90
100
110
120
130

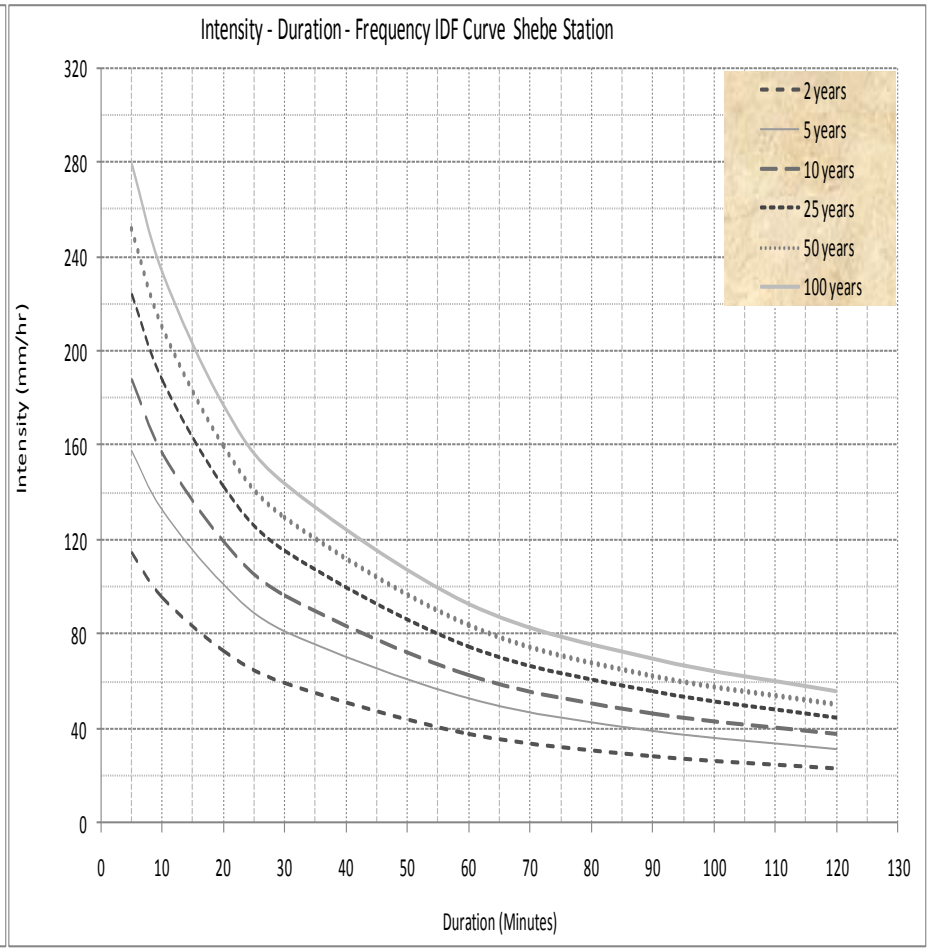
Intensity - Duration - Frequency IDF Curve Shebe Station
Intensity (mm/hr)
Duration (Minutes)
2 years
5 years
10 years
25 years
50 years
100 years
0
40
80
120
160
200
240
280
320
0
10
20
30
40
50
60
70
80
90
100
110
120
130

Appendix 7.3 Comparison between intensities (mm/hr) of observed historical; data and mid 21st century of some of stations for various return periods

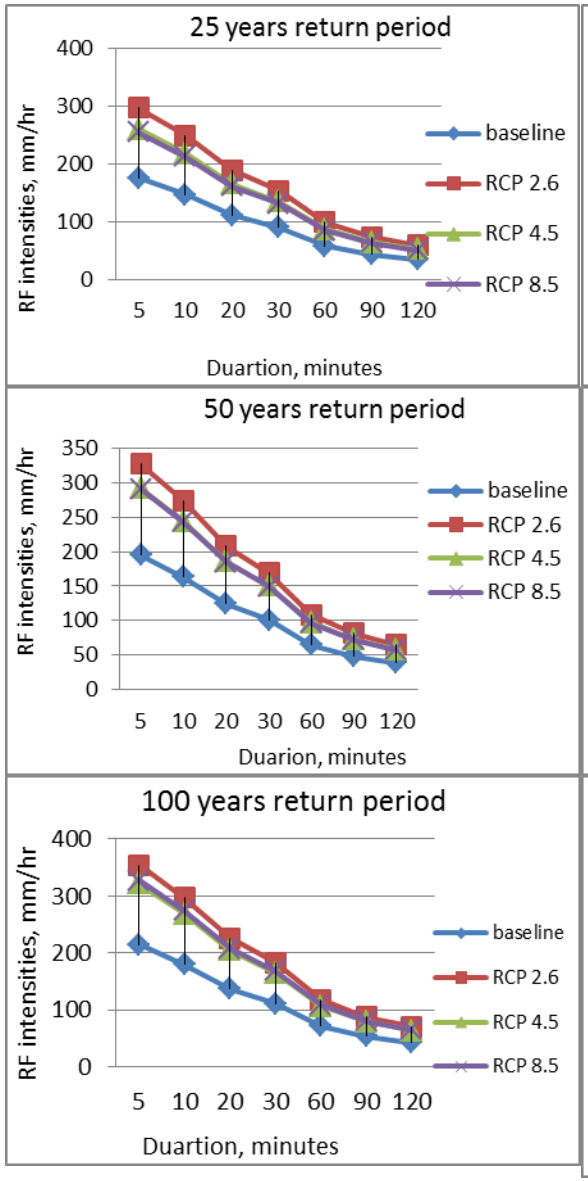

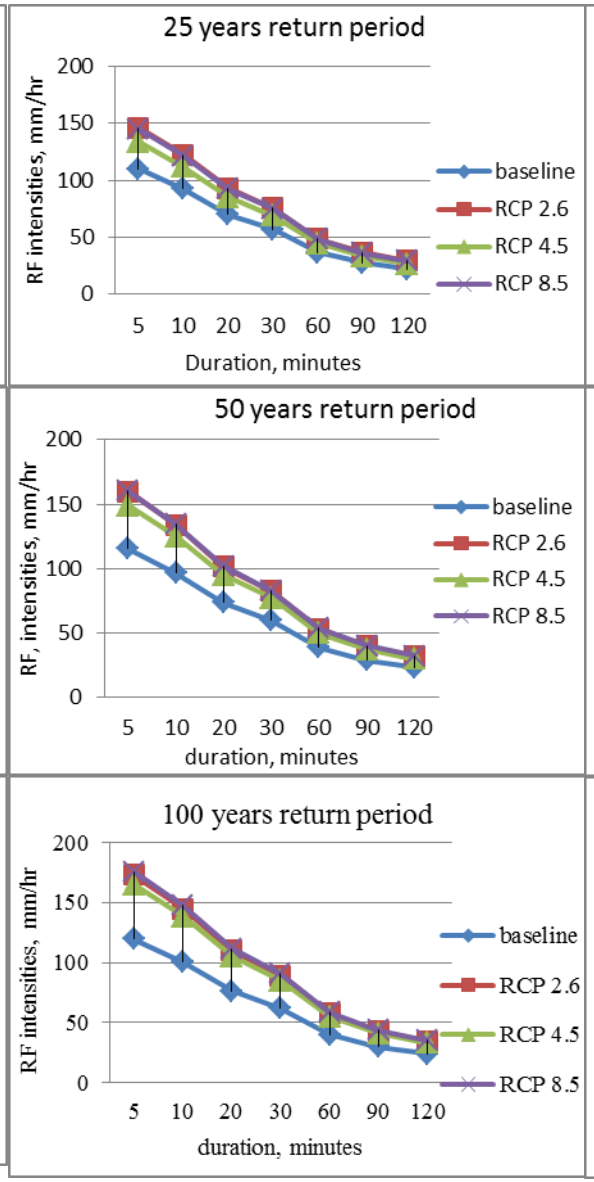

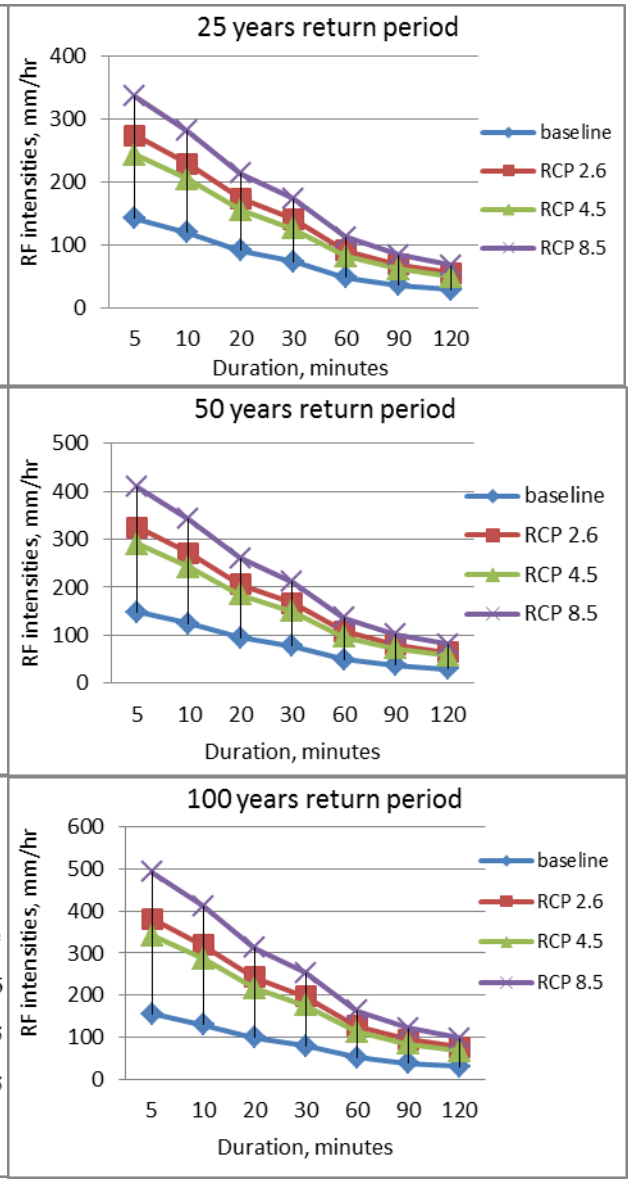

a) Asendabo b) Bonga c) Bulki (Minder)

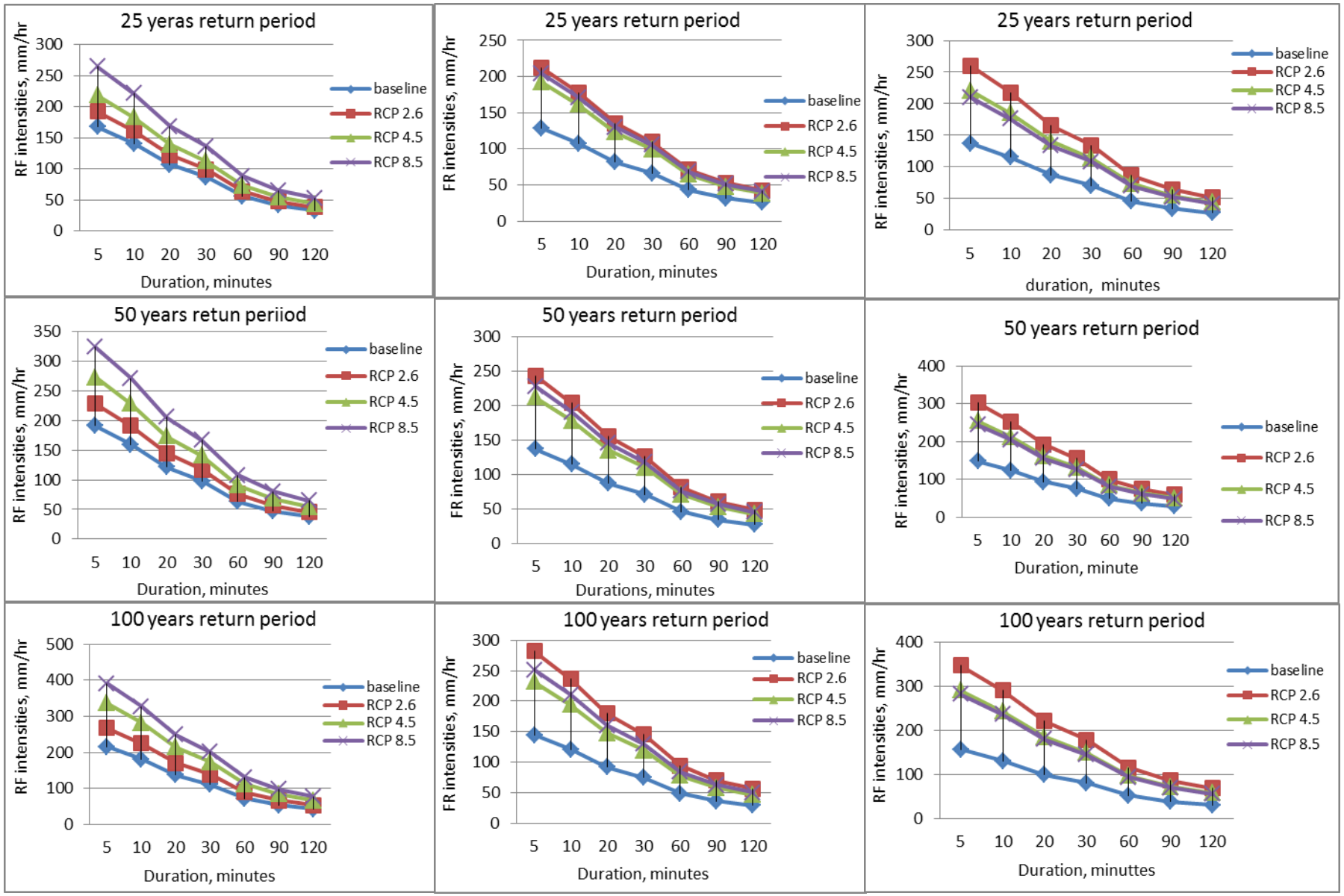

d) Butajira e) Gatira f) Woliso/Giyon/

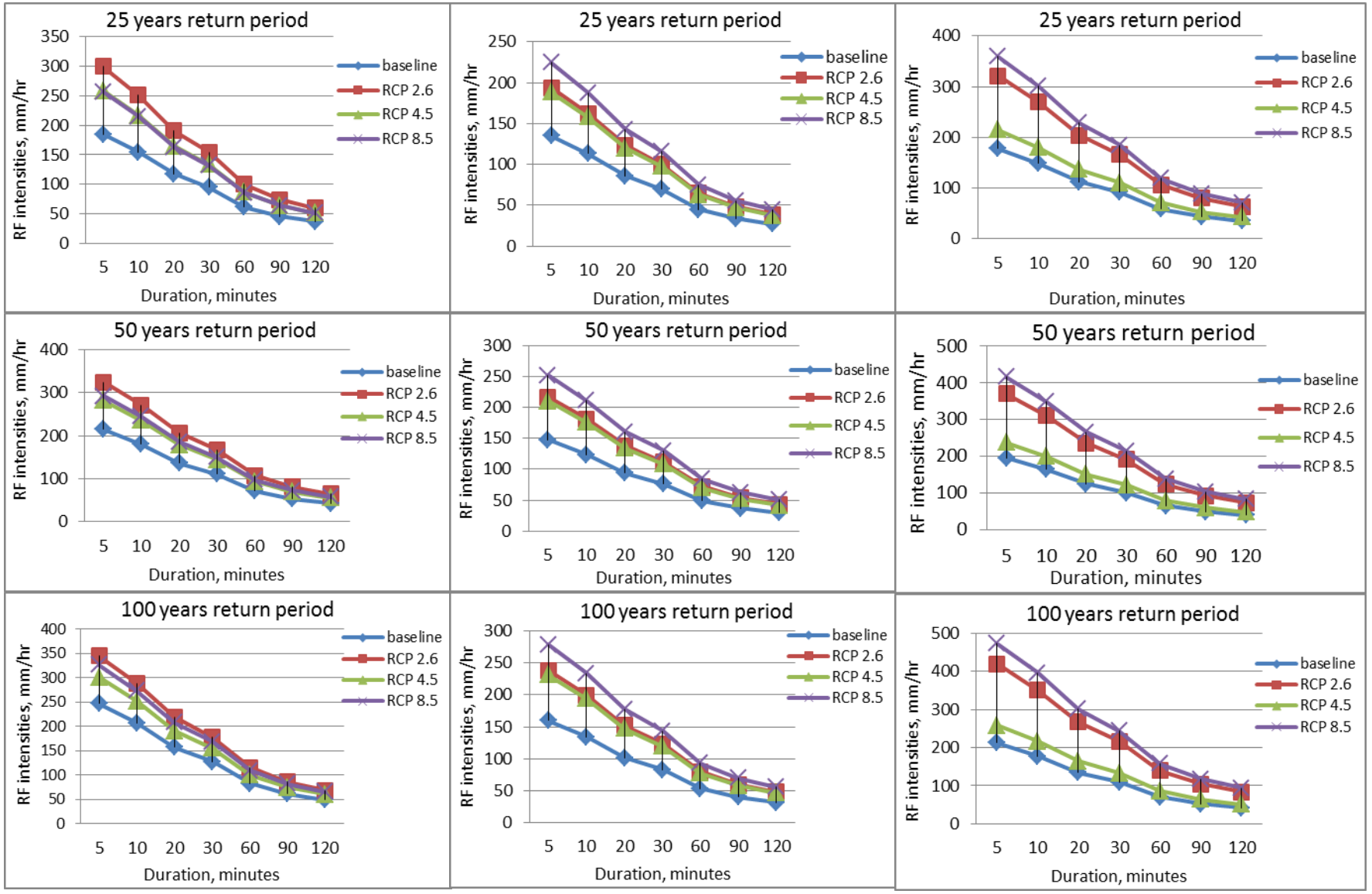

g) Yayaotan h) Shebe i) Chida

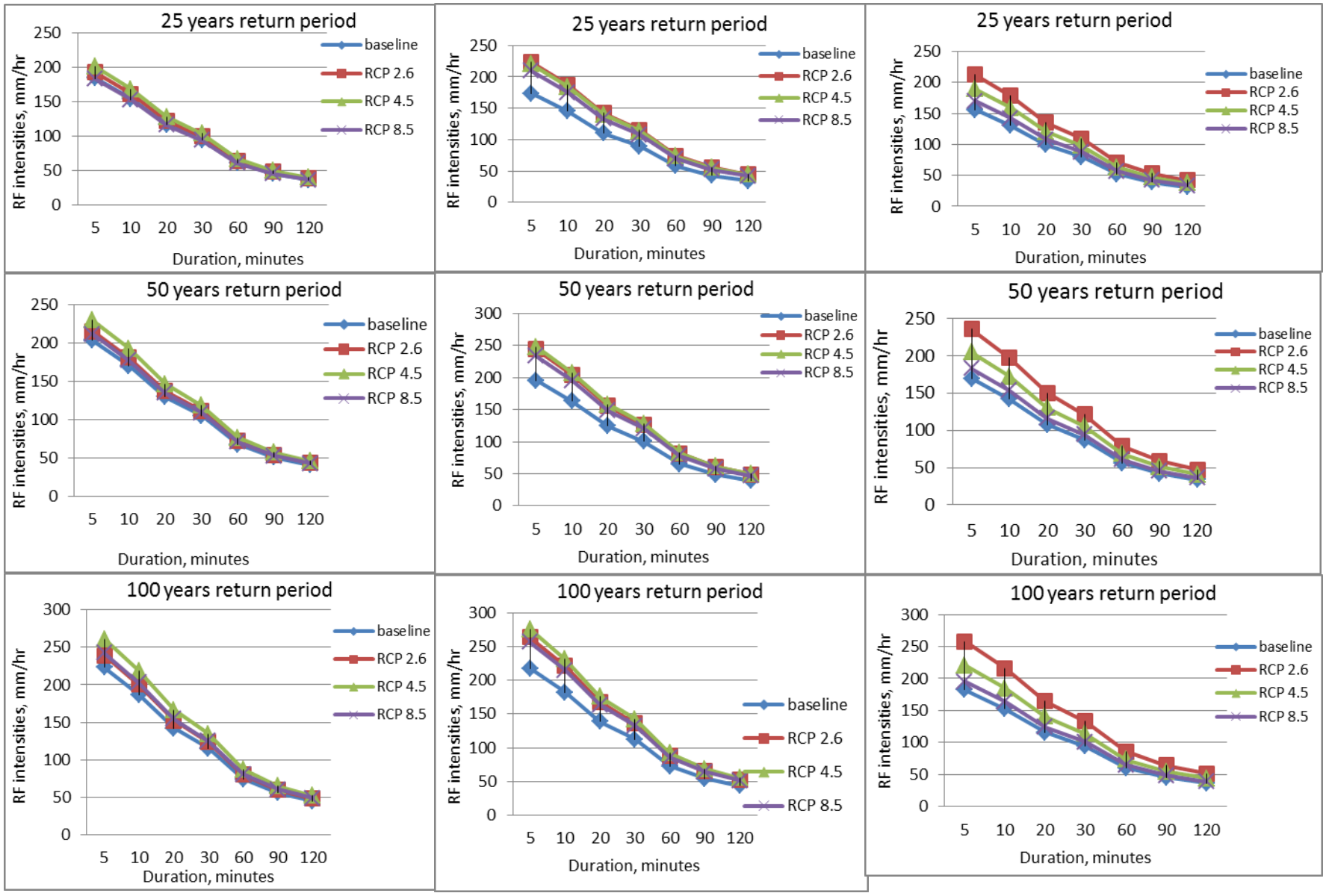

i) Wolaita Sodo k) Kumbi l) Limu Genet

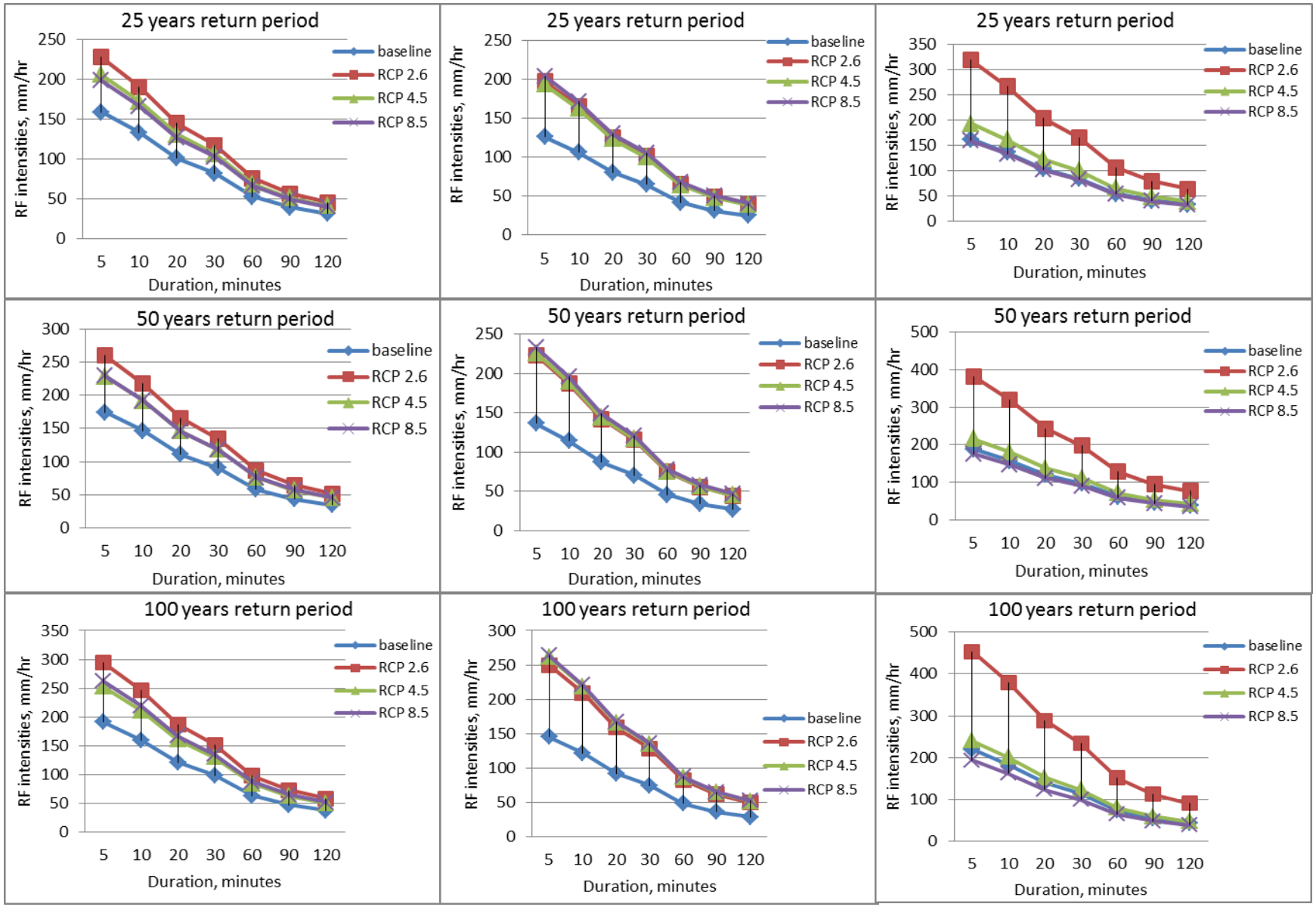

i) Shambu k) Sokoru l) Hosana

Appendix 7.4**:** Mean monthly precipitation for baseline period and projected period (mid 21st century) for some of station over the basin

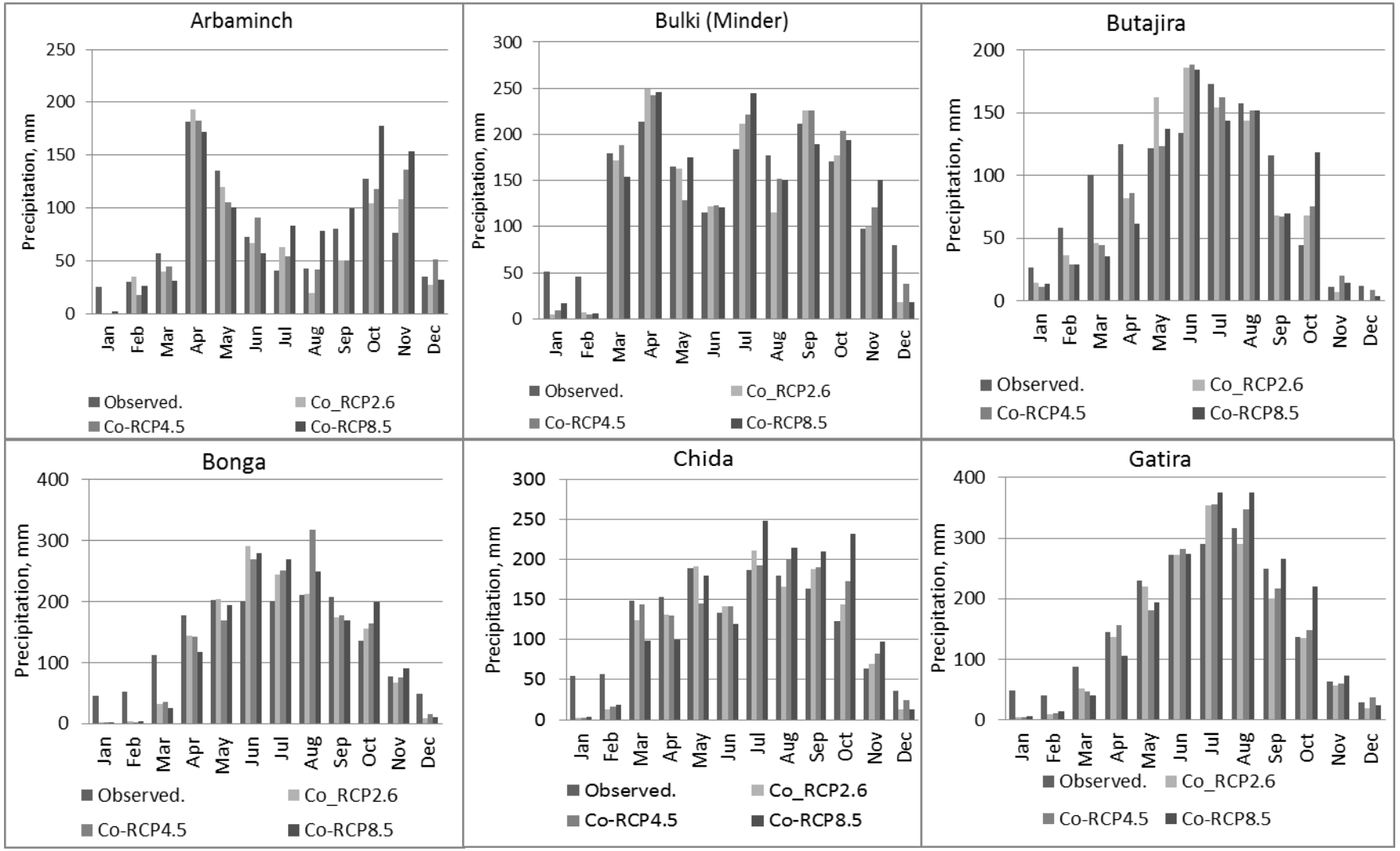

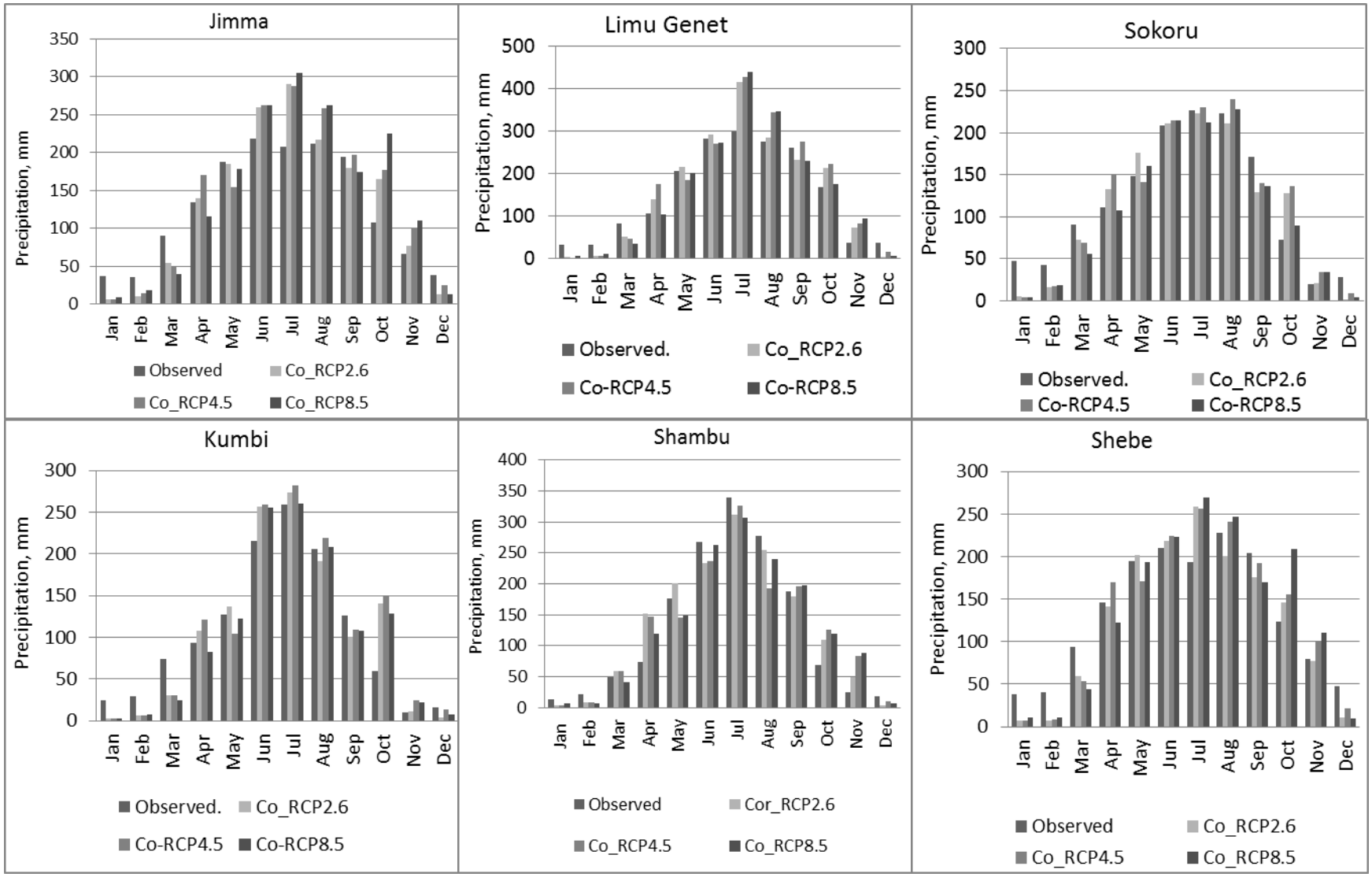
Jimma
Precipitation, mm
350
300
250
200
150
100
50
0
Jan Feb Mar Apr May Jun Jul Aug Sep Oct Nov Dec
Observed
Co_RCP2.6
Co_RCP4.5
Co_RCP8.5
Limu Genet
Precipitation, mm
500
400
300
200
100
0
Jan Feb Mar Apr May Jun Jul Aug Sep Oct Nov Dec
Observed.
Co_RCP2.6
Co-RCP4.5
Co-RCP8.5
Sokoru
Precipitation, mm
300
250
200
150
100
50
0
Jan Feb Mar Apr May Jun Jul Aug Sep Oct Nov Dec
Observed.
Co_RCP2.6
Co-RCP4.5
Co-RCP8.5
Kumbi
Precipitation, mm
300
250
200
150
100
50
0
Jan Feb Mar Apr May Jun Jul Aug Sep Oct Nov Dec
Observed.
Co_RCP2.6
Co-RCP4.5
Co-RCP8.5
Shambu
Precipitation, mm
400
350
300
250
200
150
100
50
0
Jan Feb Mar Apr May Jun Jul Aug Sep Oct Nov Dec
Observed
Cor_RCP2.6
Co_RCP4.5
Co_RCP8.5
Shebe
Precipitation, mm
300
250
200
150
100
50
0
Jan Feb Mar Apr May Jun Jul Aug Sep Oct Nov Dec
Observed
Co_RCP2.6
Co_RCP4.5
Co_RCP8.5

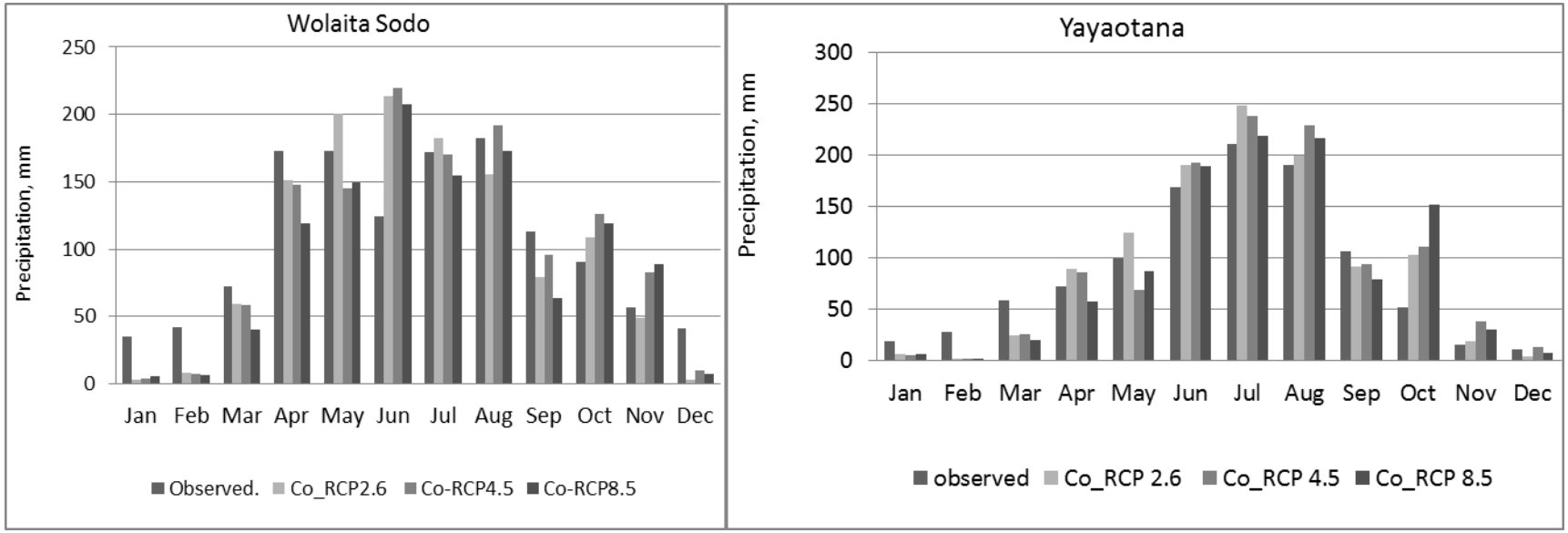
Wolaita Sodo
Precipitation, mm
250
200
150
100
50
0
Jan Feb Mar Apr May Jun Jul Aug Sep Oct Nov Dec
Observed. Co_RCP2.6 Co-RCP4.5 Co-RCP8.5
Yayaotana
Precipitation, mm
300
250
200
150
100
50
0
Jan Feb Mar Apr May Jun Jul Aug Sep Oct Nov Dec
observed Co_RCP 2.6 Co_RCP 4.5 Co_RCP 8.5

Appendix 7.5**:** Summary of descriptions of Realization Methods

Scenarios	Scenario Characteristics
RCP 2.6	Low emissions and was developed by the IMAGE modeling team of the PBL Netherlands Environmental Assessment Agency. Here radiative forcing reaches 3.1 W/m2 before it returns to 2.6 W/m2 by 2100. In order to reach such forcing levels, ambitious greenhouse gas emissions reductions would be required over time. There is no comparable SRES scenario. This future would require: – Declining use of oil – Low energy intensity – A world population of 9 billion by year 2100 – Use of croplands increase due to bio-energy production – More intensive animal husbandry – Methane emissions reduced by 40 per cent – CO_2 emissions stay at today's level until 2020, then decline and become negative in 2100 – CO_2 concentrations peak around 2050, followed by a modest decline to around 400 ppm by 2100 (Van Vuuren *et al.*, 2011a; Van Vuuren *et al.*, 2011b)
RCP 4.5	Intermediate emissions and was developed by the GCAM modeling team at the Pacific Northwest National Laboratory's in the US. Stabilization without overshoot pathway to 4.5 W/m2 (~650 ppm CO_2 eq) at stabilization after 2100. It is consistent with a future with relatively ambitious emissions reductions. Comparable SRES scenario: B1. This future is consistent with: – Lower energy intensity – Strong reforestation programmes – Decreasing use of croplands and grasslands due to yield increases and dietary changes – Stringent climate policies – Stable methane emissions – CO_2 emissions increase only slightly before decline commences around 2040 (Thomson *et al.*, 2011; Van Vuuren *et al.*, 2011b).
RCP 8.5	High emissions and was developed using the MESSAGE model and the IIASA Integrated Assessment Framework by the International Institute for Applied Systems Analysis (IIASA), Austria. Rising radiative forcing pathway leading to 8.5 W/m2 (~1370 ppm CO_2 eq) by 2100. It is consistent with a future with no policy changes to reduce emissions which is comparable SRES scenario is A1F1. This future is consistent with: – Three times today's CO_2 emissions by 2100 – Rapid increase in methane emissions – Increased use of croplands and grassland which is driven by an increase in

	population – A world population of 12 billion by 2100 – Lower rate of technology development – Heavy reliance on fossil fuels – High energy intensity – No implementation of climate policies (Riahi *et al.*, 2011; Van Vuuren *et al.*, 2011b)